ScuDo

Scuola di Dottorato ~ Doctoral School

WHAT YOU ARE, TAKES YOU FAR

Doctoral Dissertation

Doctoral Program in Electronics and Telecommunications (29^{th}cycle)

Analysis of High Capacity Short Reach Optical Links

By

M. Shoaib Khaliq

******

Supervisor(s):

Prof. Vittorio Curri, Supervisor

Doctoral Examination Committee:

Prof. Pierpaolo Boffi, Referee, Politecnico di Milano, Italy

Prof. Cristian Antonelli, Referee, Università dell'Aquila, Italy

Politecnico di Torino

2017

Declaration

I hereby declare that, the contents and organization of this dissertation constitute my own original work and does not compromise in any way the rights of third parties, including those relating to the security of personal data.

M. Shoaib Khaliq
2017

* This dissertation is presented in partial fulfillment of the requirements for **Ph.D. degree** in the Graduate School of Politecnico di Torino (ScuDo).

I would like to dedicate this thesis to my loving parents and my family

Acknowledgements

"In the name of Allah the most Merciful and Beneficent"
I thank GOD almighty for all the blessing bestowed on me, for providing me the opportunities and the strength to achieve all this.
I express my heartfelt gratitude to my supervisor Prof. Vittorio Curri for all the encouragement, appreciation, trust and guidance. I appreciate all his contribution of time, ideas and untiring support.
I would also like to thank all the professors of Optcom group for the support and inspiration. Thanks to Dr. Stefano Straullu for the support and guidance for the conduction of experimental analysis. I am thank full to the people of AQUARIO for all the discussion, suggestions, help and the time we spent together, with a special mention to Mattia Cantono.
I would like to thank Prof. Pierpaolo Boffi, and Prof. Cristian Antonelli, for accepting the role of the reviewer of this thesis.
I owe special thanks to my family, my parents for all what they have done for me throughout the years, my siblings for all the support and love. Last but not the least thanks to my wife and kids for their love and understanding during these days.
Special thanks to my friend S.M. Bilal for his assistance. I am also thankful to all my friends in Italy who have been a family for me in Italy.
I would like to thank Higher Education Commission (HEC) Pakistan for providing me financial support during my PhD.

Abstract

Over the last few years, the global Internet traffic has grown exponentially due to the advent of the social networks, high definition streaming, online gaming, high performance computing and cloud services. The network is saturating, facing a challenge to provide enough capacity to such ever-demanding bandwidth expensive applications. Fiber optic communications is the only technology capable of dealing such high demands due to its advantages over the traditional electrical transmission technology.

The short haul transmissions currently rely on direct detection due to low cost, low power and low complexity as compared to the coherent detection schemes. In order to increase the bit rate, several advance modulation formats are under investigation for short reach transmissions. Such links mostly use intensity modulation direct detection (*IMDD*) schemes providing a simple system when compared with the coherent receivers.

In this thesis the performance of Multilevel Pulse Amplitude Modulation (*MPAM*) is studied using IMDD, providing good spectral efficiency as well as able to deal with the limited electronic devices bandwidth. MPAM can address the typical optical channel without the need to go with more complex and higher power modulation schemes. It provides a trade off between sensitivity and the complexity. So a simple communication system using MPAM is implemented using an external modulated laser transmitted over a distance of 2 km. In order to reduce the cost, single laser and single receiver technique is being adopted. The performance of the MPAM system in a bandwidth limited scenarios is studied with a possibility to use equalization techniques to improve the sensitivity. The utility of Forward Error Correction codes is also studied to improve the performance without increasing the latency.

By increasing the number of bits per symbol, the system becomes more sensitive to the impairments. Moreover, the components and the connectors in the transmission

system also introduces multipath interference (MPI) that is a key limitation to the use of advance modulation formats. Hence a detailed study is carried out to investigate the MPI effects. At the end, a novel idea based on reflective Mach-Zehnder modulator (MZM) is presented that reuses the modulated wavelength eliminating the need for a laser. As a consequent, the cost and power consumption specifically targeted for the optical interconnect environment is reduced.

In a nutshell, the thesis provides an overview of the direct detection system targeted to the short optical links. It includes the studies related to the optical transmission systems and provides an insight of the available advance modulation formats and the detection schemes. Finally, the simulations and laboratory results are provided showing that adoption of MPAM is a viable solution that should be employed in high capacity short reach optical links.

Contents

List of Figures

List of Tables

Nomenclature

Acronyms / Abbreviations

ADC Analog to Digital Converter

ADSL Asymmetric Digital Subscriber Line

BER Bit Error Rate

BPSK Binary Phase Shift Keying

BW Bandwidth

CAGR Compound Annual Growth Rate

CAP Carrier-less Amplitude and Phase Modulation

CD Chromatic Dispersion

CMOS Complementary Metal Oxide Semiconductor

CW Continuous Wave

*D*P Digital Signal Processing

DAC Digital to Analog Converter

DD Direct Detection

DFE Decision Feedback Equalizer

DL Double Link

DML Directly Modulated Laser

DMT Discrete Multitone

DRS Double Rayleigh Scattering

DS Down Stream

EAM Electro Absorption Modulation

EDFA Erbium Doped Fiber Amplifiers

EO Electro-Optic

ER Extinction Ratio

FEC Forward Error Correction

FFE Feed Forward Equalizer

FFT Fast Fourier Transform

FIR Finite Impulse Response

FWHM Full Width Half Maximum

ICI Inter Channel Interference

IEEE Institute of Electrical and Electronics Engineers

IF Intermediate Frequency

IL Insertion Loss

IMDD Intensity Modulation Direct Detection

IP Internet Protocol

ISI Inter Symbol Interference

LAN Local Area Network

LC Lucent Connector

LMS Least Mean Square

LO Local Oscillator

LSB Least Significant Bit

MAN Metropolitan Area Network

MD Modulation Depth

MPAM Multilevel Pulse Amplitude Modulation

MPI Multi Path Interference

MPO Multiple Fiber Push-On/ Pull-off

MSB Most Significant Bit

MZI Mach Zehnder Interferometer

MZM Mach-Zehnder Modulator

NBW Normalized Bandwidth

NRZ Non Return to Zero

OE Opto-Electrical

OFDM Orthogonal Frequency Division Multiplexing

OH Over Head

PAM Pulse Amplitude Modulation

PAPR Peak to Average Power Ratio

PBS Polarization Beam Splitter

PD Photo Detector

PIC Photonics Integrated Circuit

PMD Polarization Mode Dispersion

PRBS Pseudo Random Binary Sequences

PSK Phase Shift Keying

QAM Quadrature Amplitude Modulation

QPSK Quadrature Phase Shift Keying

RF Radio Frequency

RIN Relative Intensity Noise

RL Return Loss

ROSA Receiver Optical Sub-Assembly

RS Reed Solomon

SiP Silicon Photonics

SL Single Link

SMF Single Mode Fiber

SNR Signal to Noise Ratio

SOP State of Polarization

SpS Samples per Symbol

SRON Short Reach Optical Network

TIA Trans-Impedance Amplifier

TOSA Transmitter Optical Sub-Assembly

US Up Stream

WAN Wide Area Network

WDM Wavelength Division Multiplexing

ZB Zeta Byte

Chapter 1

Introduction

1.1 Background

The era we live in today is the information age. The paradigm has shifted from the industrial to the information revolution. Today the smart gadgets surround the society, where people are using social networks, online high definition video streaming, online games, video conferences, cloud computing and many other bandwidth intensive services as shown in Fig.1.1. These services will effectively increase the data rate enormously and the demand is increasing constantly. This is where optical communication comes to play its role by providing high capacity data links with reach up to thousands of kilometers.

Fiber optic communication is the basis of the modern network. The technology has migrated from the previously deployed copper cable to the fiber optics. Copper cables were easy to use and install but they have a high loss at high frequencies, on the other hand, fibers have low cost and low loss that make it the preferred choice to be used for the telecommunication networks. In the early years, for long haul transmission, the cost of repeaters (Re-time, Re-shape, and Re-amplification) made the transmission very expensive but the advent of Erbium Doped Fiber Amplifiers ($EDFAs$) has reduced the cost for the wavelength division multiplexing (WDM) systems.

According to CISCO global cloud index [1] the global data center traffic will increase from 4.3 Zeta Bytes (ZB) to 15.3 ZB during the years 2015 to 2020, showing an annual growth of 27% as shown in Fig.1.2. The report also shows that most data

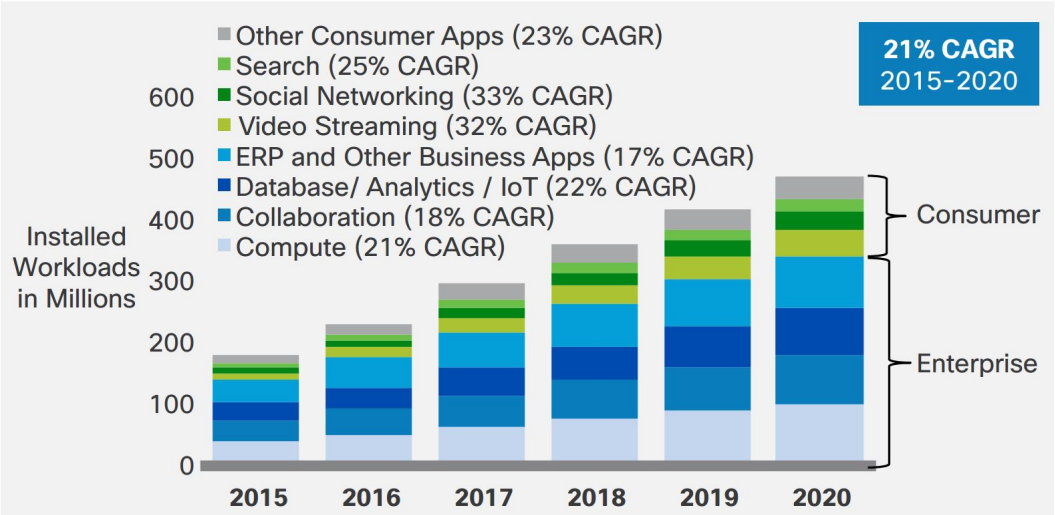

Fig. 1.1 Global Data Center workload by application[1]

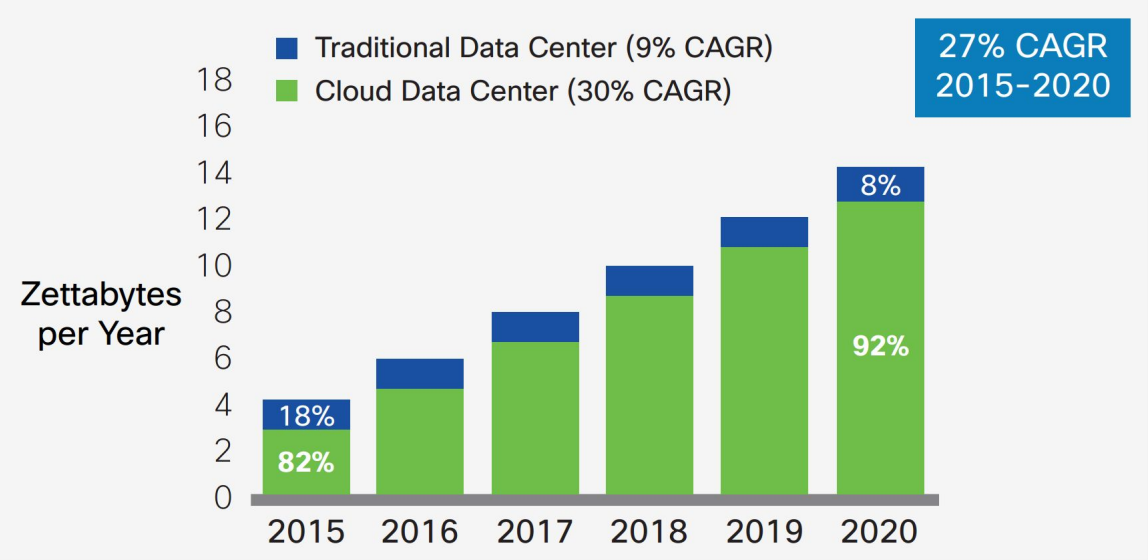

Fig. 1.2 Data Center Traffic growth [1]

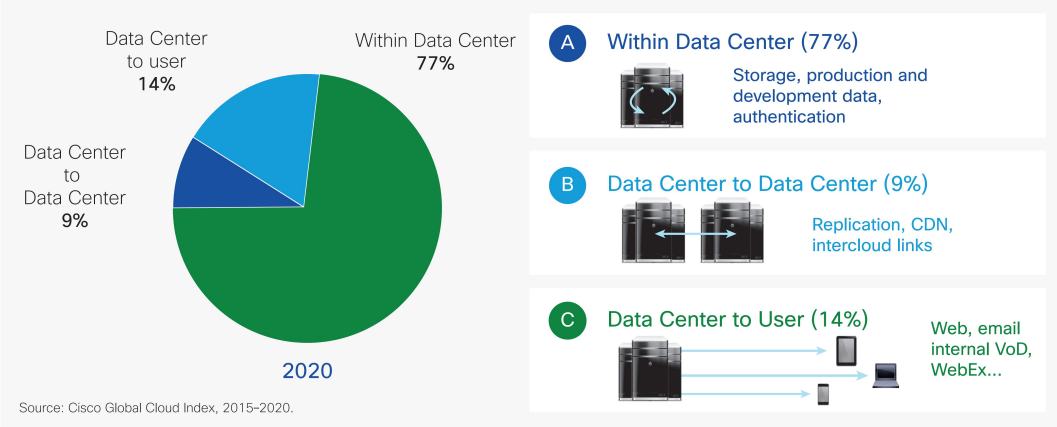

Fig. 1.3 Global Data Center Traffic distribution[1]

center traffic i.e. 77% remains within the data center while data center to data center will be 9% and 14% will be traffic between data center and the user by 2020 as depicted in Fig.1.3. This increase in data center to data center traffic is due to content distribution networks and due to services and data transport between the clouds.

To deal with this increased traffic demand not only the capacity needs to be increased but also the transmission medium needs to be upgraded even in the short-range links. Today the copper cable in the data center have been replaced by the optical fiber and optical interconnects because with the time copper and the fiber are becoming cheaper at almost the same rate. The high bit rate communication has forced the interconnects to be replaced by the optics in board to board and chip to chip transmission. The evolution of the optical network is shown in table. 1.1 . Today the elctro-optic (EO) conversion is moved close to the chip to achieve the advantage of interconnect density and power efficiency.

1.2 Short reach optics

Since optical fiber provides low losses and resilience to electro-magnetic interference, they are largely installed for the optical communication networks. The use of EDFAs and advanced modulation formats are utilized to achieve the spectral efficiency for the long haul transmission. While the requirements for short reach are very different from the long haul transmission. For short reach communication, optical interconnects are being developed and deployed in data centers (DC) and for high

Table 1.1 Optical Network Evolution [2]

Network Type	**MAN / WAN**	**LAN**	**System**	**Board**	**Chip**
	Metro / Long Haul	Campus / Enterprise	Intra / Inter Rack	Chip to Chip	On−Chip
Distance	Multi−Km	10−300m	0.3−10m	0.01−0.3m	<2cm
Adoption of Optics	Since 80s	Since 90s	Since late 00s	After 2012	After 2012
Connectivity type	All Optical	Point to Point & All Optical	Point to Point	Point to Point	Point to Point & All Optical

performance computing. With the increase in the data rate i.e. 100 Gbps and 400 Gbps use of optical interconnects is unavoidable even for the short reach optics.

Currently, the energy consumed by the data centers is about 3% of the overall energy usage that is the 12th largest energy consumption in the world [3]. Due to this the data centers growth cannot be increased proportional to the capacity requirements.

Other than the physical resources and equipment, for the growth of the data center, one can use the physical layer implementation techniques to expand and meet the capacity/ bandwidth requirements. The increasing requirements have steered the standardization of 100 Gbps and 400 Gbps as investigated by the IEEE 802.3bs 400GbE task force [4] with a possibility to use single or multiple channels (4 x 25 Gbps).

Considering the cost constraint the focus is to use advanced modulation formats along with digital signal processing. Different modulation schemes have been studied like Non return to zero (*NRZ*), a simple but spectrally less efficient technique. Multilevel Pulse amplitude modulation (*MPAM*) [5], better spectral efficiency as compared to NRZ but with a lower receiver sensitivity, Discrete multitone (*DMT*) spectrally efficient and resilient to the dispersion [6], carrier less amplitude and phase modulation (*CAP*) another spectrally efficient low power technique [7]. To meet the need for the low energy dissipation, the complexity, link power and power dissipation of the different modulation schemes have also been analyzed and compared [8–10].

1.3 Motivation

Today for the long haul transmission 100G coherent optical links are being employed with higher order modulation format. Modulation format such as Quadrature phase shift keying (*QPSK*), Quadrature amplitude modulation (*QAM*) etc are in use. Coherent detection was the reason to handle ever increasing data rate in optical transmission. Since using coherent detection both in phase and quadrature component can be detected. But coherent detection needs a laser source also at the receiver working at the same wavelength as the transmitter to recover entire field information. This will increase both cost and complexity of the system but are acceptable for the high capacity long haul transmission.

On the other hand for short reach optical communication coherent detection is not a feasible solution due to the cost and system complexity, so it must rely only on direct detection (*DD*). IMDD systems detects the intensity of the light only using a simple photodiode so the in phase and quadrature component is not considered. The system must provide

- Low cost
- Low complexity
- Low power consumption
- Small footprint
- High spectral efficiency

To achieve these goals, either we can increase the bit rate or we can use advanced modulation formats to reduce the number of wavelengths or the parallel transceiver. Using direct detection the simplest technique is to use multi-level PAM. MPAM provide a good spectral efficiency but as the number of bits per symbol increases the receiver sensitivity penalty increases, higher optical to signal noise ratio is required to achieve a specific bit error rate. With higher level the system become becomes more vulnerable to the channel losses, bandwidth limitations and chromatic dispersion (*CD*). For the considered scenario of a short link i.e. 2 km, the CD is negligible. The goal of this work is to provide a simple, low cost, power and spectrally efficient MPAM system using IMDD to provide high capacity links with propagation upto 2 km to be adopted in future data center transmission.

1.4 Organization of the thesis

This thesis presents a collection of the work done related to high capacity short reach optical communication. The thesis is organized in order to make it clear and concise for easy understanding. The chapters are briefly described as.

- **Chapter 1:** Introduction to the thesis
- **Chapter 2: Optical Communication** This chapter presents the basic theory related to the optical communication system at both the transmitter and the receiver end. Describing both direct and the external modulation, Mach-Zehnder modulator is also briefly explained. At the receiver side direct detection and coherent detection is explained.
- **Chapter 3: Advance Modulation Formats** Different modulation formats like pulse amplitude modulation, discrete multitone and carrier less amplitude and phase modulation are explained briefly. Pulse amplitude modulation is explained extensively that is selected and is used for the conducted study.
- **Chapter 4: Performance Analysis of M-PAM** Once PAM is selected as the choice for the modulation format to be adopted for the study, its performance is examined focusing on the effect of bandwidth limitations and the effect of the equalizer on the receiver sensitivity. The reasons for the signal degradation and the possible equalization is also presented.
- **Chapter 5: Multipath Interference effects on PAM4** Multi-path interference effect caused mainly due to the connector reflection is explained in this chapter. There effect on the bit error rate for different link lengths, relative intensity noise and fiber delay is studied in this chapter.
- **Chapter 6: Analysis of Forward Error Correction on PAM4** In this chapter the effect of the forward error correction (FEC) overhead and the consequently the introduced latency is investigated.
- **Chapter 7: Master Slave Architecture** This chapter presents a novel idea where the Reflective MZM is used to reuse the wavelength for the transmission without the need for a laser, providing a cost and efficient solution for the data center applications .

- **Chapter 8: Conclusions and Future Work** As suggested by the name, the final conclusion about the work will be presented in this chapter, along with the possible future directions for further investigation for the short reach communication system.

Chapter 2

Optical Communication

2.1 Introduction

The goal of optical communication is to transmit at a high data rate on the longest channel at a low cost. It is desired to have an error free communication between the two nodes. The optical link should be reliable achieving the specified target bit error rate. It is also required to have a higher signal to noise ratio (SNR) which in turn is related to the receiver sensitivity. Some of the other parameters that are effecting the optical transmission that needs to be taken care of during the design to achieve the above goal are extinction ratio, amplifier gain, responsivity, noise parameters, attenuation, losses, dispersion. A good design will provide a balance between all the parameters to provide a reliable communication link.

2.2 Optical Transmitter

The main function of an optical transmitter is to convert the input electrical signal to the optical signal. This conversion from high speed electrical signal to light is done by a modulator through the process of modulation. The possible modulation schemes are

- Intensity modulation
- Phase modulation

- Frequency modulation

In *intensity modulation* the intensity or power of light is varied according to the transmitted data, at the detector a simple photodiode is used, the optical power is measured using the received photocurrent. In *Phase modulation*, the amplitude of signal remains constant while the phase of the signal is varied with respect to the input signal. Some forms of phase modulation are Phase Shift Keying *PSK*, Binary Phase Shift Keying *BPSK*, Quadrature Phase Shift Keying *QPSK*. Another form is Quadrature Amplitude Modulation *QAM* that used both phase and amplitude modulation. *Frequency modulation* is similar to phase modulation, in frequency modulation with the variation in input signal the carrier frequency is varied.

There are two techniques for the intensity modulation.

- Direct modulation
- External modulation

Fig. 2.1 show the transmission distance and achievable modulation speed for different modulation laser. It can be observed that for short reach, low data rate applications direct modulation can be used. On the other hand, external modulation is used for high speed long distance transmission. Direct modulation is simple and less expensive while external modulation is faster but expensive using complex circuitry.

2.2.1 Modulation Parameters

There are three main modulation parameters that needs to be taken into consideration namely as

- Operation Speed
- Extinction Ratio
- Frequency Chirping

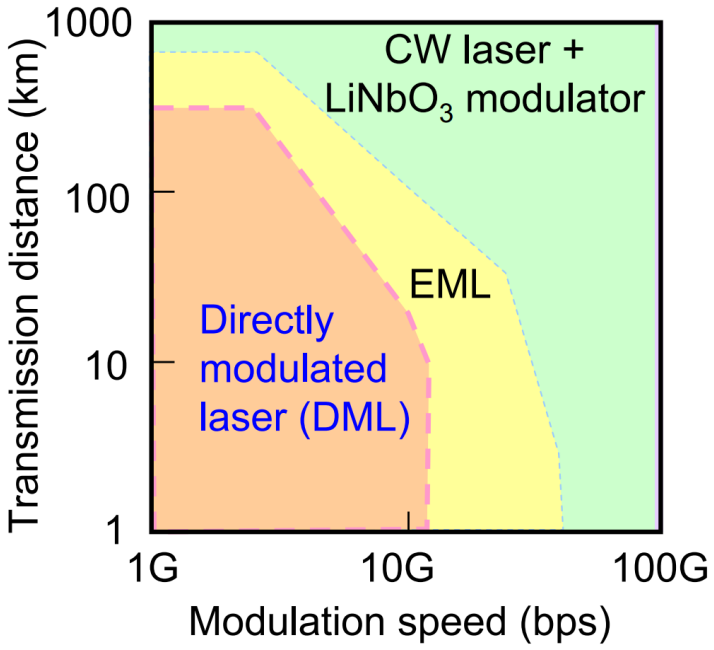

Fig. 2.1 Transmitters for optical communication [11]

Operation Speed

Since the data is transferred in the form of trains of 1s and 0s, it is desired that the transmitter should be fast enough to switch between the two states. For the current high data rates i.e. multiple of Gbps, the corresponding bit period is in fractions of a picosecond, so the transmitter should be able to switch at this speed for a proper operation.

Extinction Ratio

The extinction ratio (ER) of the optical signal is the ratio of optical power level when the source is on and the power level when the source is off.

$$ER = \frac{P_1}{P_0} \tag{2.1}$$

$$ER[dB] = 10log_{10}\frac{P1}{P0} \quad ER\ in\ Logrithmic\ scale \tag{2.2}$$

where P_1 represent the power for a zero and P_0 represent the power for a one. Ideally, the ER should be infinite. Higher the ER, larger is the separation between the two level ensuring a minimum power for the lower level. Higher the ER better is the bit error rate, lower is the power requirement to achieve the target BER, On the other hand lower ER results to a closed eye diagram, worse BER and increased power penalty. The power penalty for a receiver limited by thermal noise only is given by [12, 13]

$$PP[dB] = 10log_{10}\left(\frac{ER-1}{ER+1}\right) \tag{2.3}$$

The proper value of the extinction ratio depends on the transmission distance. For short reach optics using a silicon phonics device the values of the ER is used to be 6 dB [14].

Since extinction ratio provides the difference between the two power level that means for a higher difference we can use low power to achieve the same BER and vice versa. So there is a flexible trade off between the power and the ER value.

Frequency Chirping

The electric field of the optical carrier is given by [15]

$$E(t) = \left[|A(t)|e^{i\phi(t)t}e^{i\omega_0 t}\right] \tag{2.4}$$

$$= \sqrt{P(t)}e^{i\phi(t)t}e^{i\omega_0 t}$$

$$E(t) = \sqrt{P(t)}e^{it(\phi(t)+\omega_0)} \tag{2.5}$$

where ω_0 is angular frequency of the carrier, A(t) is the signal with phase ϕ and $P(t) = |A(t)|^2$ is the power of the signal.

In intensity modulation with the variation in the modulating signal the power P(t) is varied, it modulate the phase also, so both power P(t) and phase $\phi(t)$ becomes function of time. The optical carrier frequency becomes as

$$\omega = \omega_0 + \frac{d\phi}{dt} \tag{2.6}$$

This phase variation with time is equivalent to a change in the signal instantaneous frequency and the modulation is known as *frequency chirping*. Since different frequency components travels at different speeds causing the pulse broadening at the receiver leading to intersymbol interference degrading the system performance. Considering a chirped Gaussian pulse propagating in the optical fiber given by [16]

$$A(t) = A_0 exp\left[-\frac{1-iC}{2}\frac{t}{T_0}^2\right] \tag{2.7}$$

where C represent the frequency chirp and T_0 is the half width at $1/e$ intensity point and the relation with the full width half maximum ($FWHM$)is given by

$$T_{FWHM} = 2\sqrt{ln2}T_0 \approx 1.665T_0 \tag{2.8}$$

Therefore the instantaneous frequency becomes

$$\omega(t) = \omega_0 + \frac{C}{T_0^2}t \tag{2.9}$$

that is dependent on time t. The product of the dispersion induced, described by β_2 and the chirp factor C will define the broadening or compression of the pulse. If $C\beta_2 > 0$, the pulse will broaden faster compared to the case of an unchirped signal. For $C\beta_2 < 0$, the pulse will initially compress at a faster rate than for an unchirped pulse before broadening.

2.2.2 Direct Modulation

In digital system, the two "ON" and "OFF" states are represented by logical "1" and "0". During the on state the laser will emit a "1", while in the off state laser will transmit a "0". Initially the laser diode is in the off state for the input current below the threshold current, once the threshold value is exceeded, population inversion is achieved the laser will be in the on state. Increasing the input current will increase the laser output power until the saturation is achieved. This dependence of laser

output power on the input current is used for the conversion from electrical to the optical domain as the input current is varied with respect to the input data as shown in Fig. 2.2.

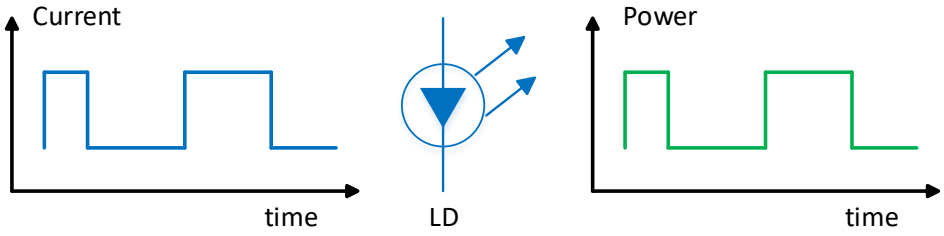

Fig. 2.2 Direct Modulation.

By driving the laser below the threshold, generating a "0" and above the threshold to generate a "1", high extinction ratio can be achieved. Doing so the laser will switch from the off state to on state but this requires some time for the accumulation of sufficient number of carriers to achieve the population inversion. This time delay is known as the *turn on delay* and is given by

$$t_d = \tau_c ln\left(\frac{I_1 - I_0}{I_1 - I_{th}}\right) \tag{2.10}$$

where τ_c is the carrier lifetime, I_1 and I_0 are the driving currents for “1s” and “0s”, respectively. This delay is not suitable for high speed operation as the bit period is in picoseconds. To mitigate this turn on delay, the laser must operate at a value higher than the threshold. This will reduce the current swing, as a result, limits the maximum achievable extinction ratio. During the switching between the two states, there is always the transient current in the laser creating a damped oscillation at the output known as *relaxation oscillations*. The oscillation is due to the mixing of the induced and the emitted photon and depends on the input driving current. The change in the bias current changes the carrier density resulting into the change in the refractive index of the material. Due to the change in the refractive index, the feedback condition is changed and the lasing wavelength is changed. So the instantaneous frequency of the signal will change with time leading to the frequency chirping. This chirp is mainly due to the contribution of transient chirp and the adiabatic chirp. Transient chirp exist during the variation in the power while

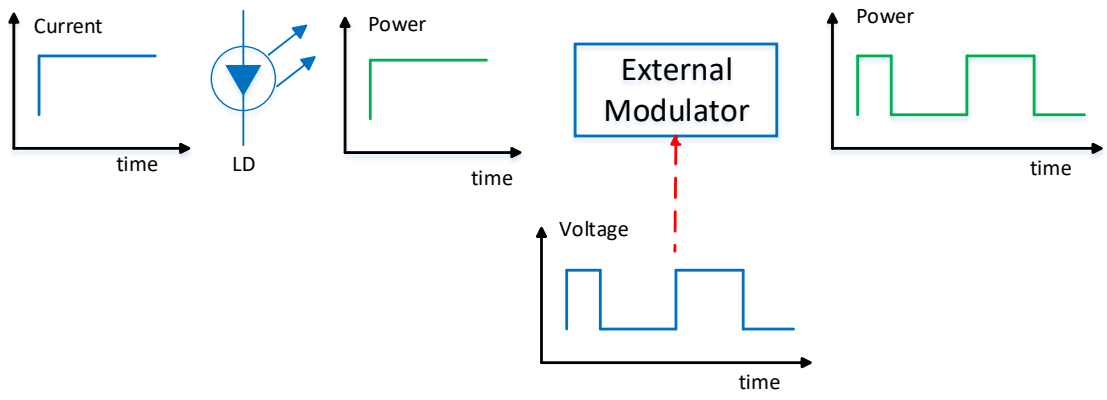

Fig. 2.3 External Modulation.

adiabatic occurs due to emission of different frequencies under steady state condition. Direct modulation is simple and cost effective but is limited to short reach only.

2.2.3 External Modulation

For direct modulation at a bit rate of 10 Gbps and higher the frequency chirping become so larger that direct modulation is rarely used [16]. So for high data rates transmission the laser is always in the "on" state so has the name continuous wave (*CW*) laser, acts as a carrier and an optical modulator is used to turn on or off the the optical power according to the input signal and the process is known as the external modulation and is shown in Fig.2.3. External modulation has the advantage of extended reach and high bit rate. There are two main types external modulation

- Electro-Absorption modulation
- Electro-Optic modulation

When an external electric field is applied the absorption coefficient of the material is change for the electro-absorption modulators while the refractive index is changed for the electro-optic modulators.

Electro-Absorption modulation

The Electro absorption modulators normally works on *Franz-Keldysh effect*. Which states that the optical absorption property of semiconductor is change under the effect of electric field i.e. with the increasing electric field the effective bandgap decreases. If the energy of the wavelength $E = hv$ is smaller than the bandgap energy, the light will not be absorbed but as the electric field is increased the bandgap is reduced and the light starts being absorbed.

Electro-Absorption modulator and a CW laser are made up of the same material so are normally integrated on the same substrate chip leading to a small compact design with low coupling losses. Such modulators operate at bit rates up to 100 Gbps [17].

The optical modulation due to the application of an electrical field is possible by the proper selection of the operating signal wavelength that experiences a significant change in absorption when the electric field is applied. This change in the absorption will also change the refractive index of the material, resulting in a change of the phase or instantaneous frequency of the signal. So some frequency chirping will be introduced but is usually smaller as compared to the chirp when direct modulation is used.

Electro-Optic modulation

The second type of external modulators is the electro-optic modulator. The device mainly used is the Mach-Zehnder Modulator (MZM). It can be made up of silicon (Si), indium phosphate (InP) or lithium niobate ($LiNbO_3$). For $LiNbO_3$ modulators, there is a linear phase dependence on the driving voltage, it also provides larger operating bandwidth with small driving voltage but with a drawback of the size that is difficult to integrate with the transmitter.

To achieve the Intensity modulation, the phase modulation is transformed to intensity modulation using an interferometer. The refractive index of these materials is changed when an external electric field is applied, consequently, there is a change in the phase. The phase variation experienced by light having wavelength λ traveling through a medium of length L and refractive index n is given by

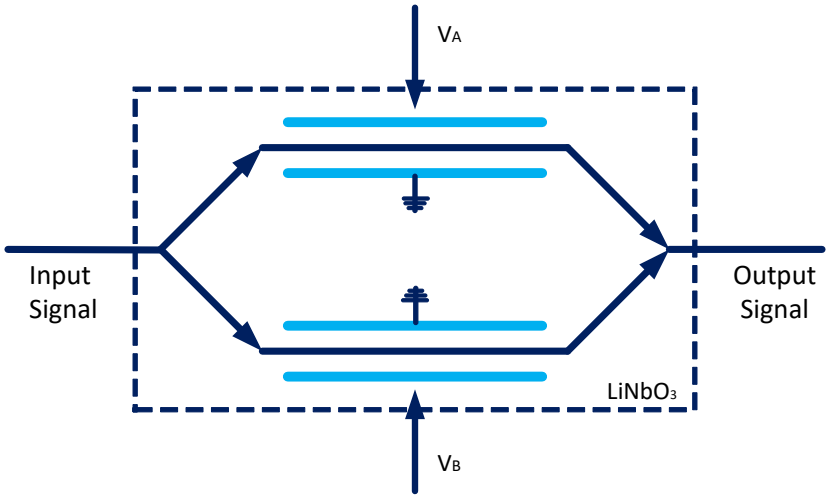

Fig. 2.4 Dual Drive Mach-Zehnder Modulator

$$\phi = \frac{2\pi}{\lambda} nL \tag{2.11}$$

Consider a dual arm, dual drive $LiNbO_3$ modulator where the phase modulators in both the arms can be derived independently as shown in Fig. 2.4. The dual drive modulator is used to generate the intensity modulation. Assume the power is split equally to both arms. After passing through the phase modulators light is combined again. The driving voltage will introduce the phase shift in the arms. Depending on the phase shift it can be constructive or destructive interference. The relation between the input and the phase modulated output optical field is given by

$$E_{out}(t) = E_{in}(t) e^{j\phi(t)} \tag{2.12}$$

where

$$\phi(t) = \pi \frac{V(t)}{V_\pi} \tag{2.13}$$

so we have

$$E_{out}(t) = E_{in}(t) e^{j\pi \frac{V(t)}{V_\pi}} \tag{2.14}$$

Where $\phi(t)$ is the phase shift in the arm, V_π is the voltage required to have a phase shifts of π and $V(t)$ is the driving voltage. The transfer function of the MZM ignoring the insertion loss is given by

$$TF_{MZM} = \frac{E_{out}(t)}{E_{in}(t)} = 1/2 \cdot \left(e^{j\phi_A(t)} + e^{j\phi_B(t)}\right) \tag{2.15}$$

Mach-Zehnder modulator can operate in either dual drive or single drive modulator. In single drive configuration, the driving voltage is applied to one arm only while in dual drive the voltage is applied to both arms. In absence of any external voltage, the optical field in the two arms will have similar phase shift, constructive interference will take place. On the other hand application of voltage on one arm will result in a phase variation and a destructive interference. If the phase difference is π because of destructive interference no light will be transmitted.

For a perfect symmetric condition i.e. $\phi_A(t) = \phi_B(t) = \phi(t)$, $V_A = V_B = V$ and $V_{\pi_A} = V_{\pi_B} = V_\pi$, a phase modulation is achieved as given by equation 2.14. While in push pull configuration where $V_A = -V_B = V/2$, $\phi_A(t) = -\phi_B(t)$ and $V_{\pi_A} = V_{\pi_B} = V_\pi$ chirp free modulation is achieved.The transfer function is given by

$$\frac{E_{out}(t)}{E_{in}(t)} = cos\left(\frac{V(t)}{2V_\pi}\pi\right) \tag{2.16}$$

and the power transfer function is given by

$$\frac{P_{out}(t)}{P_{in}(t)} = \frac{1}{2} + \frac{1}{2} \cdot cos\left(\frac{V(t)}{2V_\pi}\pi\right) \tag{2.17}$$

Mach-Zenhder modulator is normally used on two bias point as shown in Fig. 2.5

- At the quadrature point, with a bias voltage $V_{bias} = \frac{-V_\pi}{2}$ and a peak-to-peak modulation of V_π, where intensity response is maximally linear.
- At the null point, with a bias voltage $V_{bias} = -V_\pi$ and a peak-to-peak modulation of $2V_\pi$, where amplitude response is maximally linear.

Depending on the modulation scheme (field or intensity) the modulator is biased at the quadrature or the null.

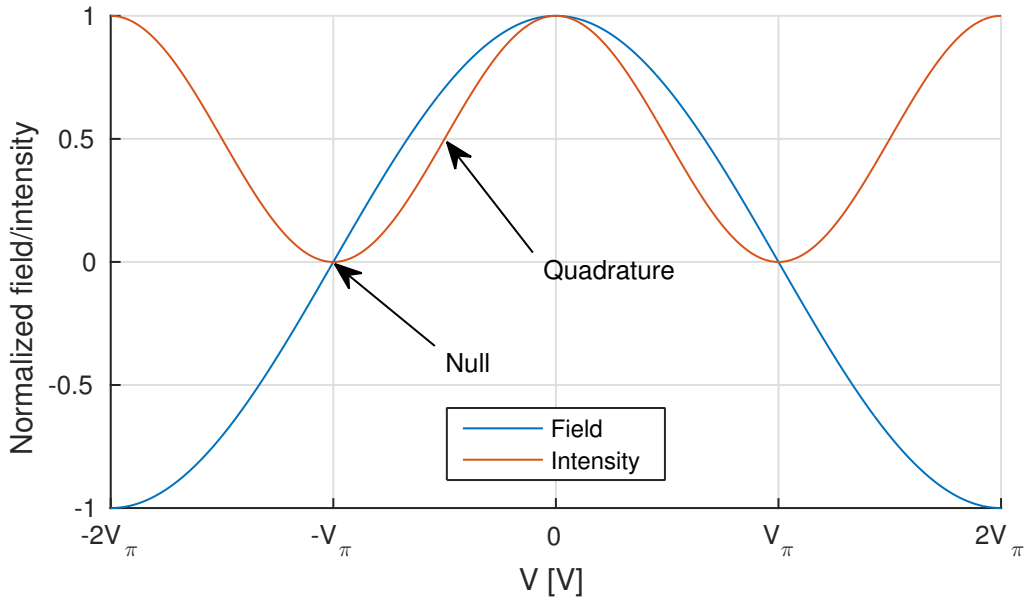

Fig. 2.5 Mach-Zehnder Modulator operating points [18]

2.3 Optical receiver

The main purpose of the receiver is to convert the incoming signal from optical to electrical domain. This electrical data is then processed to recover the transmitted data. The receiver may have amplifiers, equalizer and the decision circuit providing the binary data at the output. Based on the transmission techniques used, the receiver can use a direct detection or a coherent detection scheme. The detection techniques are explain briefly here.

2.3.1 Direct Detection

The earlier optical communication system was based on a less complex simple scheme, where the input electrical bits trains was used to modulate the intensity of the laser, this modulated signal is transmitted through the fiber. At the receiver a simple photodiode is used to receive the signal and is converted back to the electrical signal. The process is known as intensity modulation with direct detection (IMDD) scheme. In this simplest scheme as shown in Fig. 2.6, the information is only in the amplitude / power of the optical signal, so the receiver sensitivity is independent of phase and state of polarization (*SOP*). Since IMDD is not using the phase information

so we have a single degree of freedom only that reduces the power and the spectral efficiency. Since the phase information is not used/recovered lowering the tolerance and electrical compensation of fiber impairments like chromatic dispersion (*CD*) and polarization mode dispersion (*PMD*) [19]. In earlier days due to the simple, low cost hardware and the employment of EDFAs in the long-haul networks increasing the transmission capacity of a single fiber, direct detection was preferred. Nowadays, the Interest in direct detection has decreased due to the usage of higher order modulation formats for increasing the transmission bit rate [16].

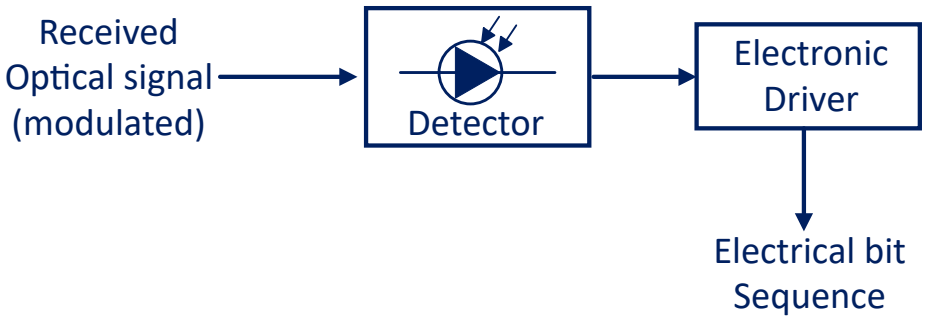

Fig. 2.6 Direct-Detection scheme

A photodetector is used to demodulate the received optical signal. It converts the incident light to current and convert the electrical current to the output optical power by taking it's square so is known as square law detector. The received electric field of the modulated signal is given by

$$Incoming\,signal \quad E_s = A_s exp[-j(\omega_0 t + \Phi_s)] \tag{2.18}$$

In a direct detection scheme, the detected photocurrent I_p is given by:

$$I_p = \Re \cdot P_{in} \tag{2.19}$$

The electrical power, P_{el} generated in the detector with the Ohmic resistor is then given by

$$P_{el} = R \cdot I_p^2 = R \cdot (\Re P_{in})^2 \tag{2.20}$$

where R is the resistance and $\Re$ is the *responsivity* that defines the ratio of photo current generated for each watt of incident light expressed in ampere/watt.

$$\Re = \frac{q\eta\lambda}{hc} = \frac{\eta\lambda}{1 \cdot 24 \cdot 10^{-6}} A/W \tag{2.21}$$

where c is the speed of light q is the charge of an electron λ is the wavelength of the photons being detected.

2.3.2 Coherent Detection

Since the direct detection is using only the amplitude reducing the power and the spectral efficiency. Coherent detection scheme uses both amplitude and the phase of the optical carrier. Since the phase information is restored, the impairments like chromatic dispersion and polarization mode dispersion can be compensated in the post processing. Using coherent detection, the receiver sensitivity can be improved up to 20 dB permitting a longer transmission distance [16], it also allows efficient use of fiber bandwidth by simultaneous transmission using frequency division multiplexing consequently increasing the spectral efficiency when compared to the direct detection scheme. At the same time, the coherent receivers are complex and are sensitive to the phase and the state of polarization of the incoming signal.

With the increased transmission capacity demand, exploiting multilevel modulation formats using coherent technologies is the viable solution [20]. On the other hand using digital signal processing (*DSP*) at the transmitter and the receiver it is possible to process and retrieve phase and amplitude information. It is also possible to post process the data for the compensation of the fiber impairments. Due to coherent receiver many kinds of multi-level modulation formats can be introduced, increasing the spectral efficiency from 1 bit/s/Hz/polarization to M bit/s/Hz/polarization using multilevel modulation format with M bits information per symbol [21]

The basic difference between direct detection and Coherent detection is the addition of a continuous wave optical field with the received optical signal having the same frequency at the receiver. These mixed signals are then received by the photo detector. Since the CW field is generated by a narrow line width laser at the receiver so is known as the local oscillator (*LO*) as seen in Fig. 2.7. The mixing of the two signals improves the performance as will be discussed below.

The optical field associated with the signal and the local oscillator is given by

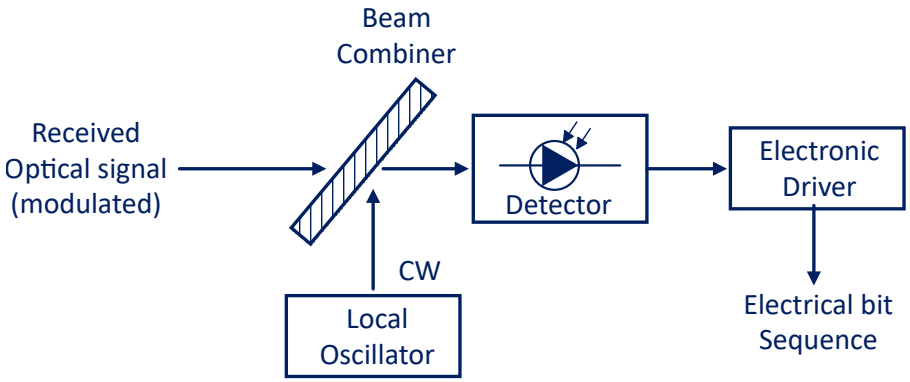

Fig. 2.7 Coherent-Detection scheme

$$Receved\,optical\,signal \quad E_S = A_S exp[-j(\omega_0 t + \Phi_S)] \tag{2.22}$$

$$Local\,oscillator \quad E_{LO} = A_{LO} exp[-j(\omega_{LO} t + \Phi_{LO})] \tag{2.23}$$

where A_s, ω_0 and Φ_s represent the amplitude, frequency and phase of the received signal and A_{LO}, ω_{LO} and Φ_{LO} represent the amplitude, frequency and phase of the local oscillator signal.

Since the optical power is equal to the square of the electrical field, solving equation 2.22 and 2.23 we have

$$P = K|E_S + E_{LO}|^2 \tag{2.24}$$

$$P(t) = P_s + P_{LO} + 2\sqrt{P_s P_{LO}} cos(\omega_{IF} t + \Phi_s + \Phi_{LO}) \tag{2.25}$$

where

$$P_s = KA_s^2$$

$$P_{LO} = KA_{LO}^2$$

$$\omega_{IF} = \omega_0 - \omega_{LO} \tag{2.26}$$

where K is the constant of proportionality. $\omega_{IF}/2\pi$ is known as the intermediate frequency (IF). Depending on the value of ω_{IF} the coherent detection can be defined as,

- homodyne detection if $\omega_{IF} = 0$
- heterodyne detection if $\omega_{IF} \neq 0$

Homodyne detection

When the local oscillator frequency is equals to optical carrier frequency, i.e. it coincide with the carrier frequency $\omega_{IF} = \omega_0 - \omega_{LO}$

The photocurrent generated by the optical detector is proportional to the optical power (or optical intensity) i.e. $I = P\Re$, so equation 2.25 becomes

$$I(t) = \Re(P_s + P_{LO}) + 2\Re\sqrt{P_s P_{LO}}cos(\Phi_s + \Phi_{LO}) \tag{2.27}$$

Normally $P_{LO} \gg P_s$ so we have $P_s + P_{LO} \approx P_{LO}$. When the local oscillator phase is equal to the signal phase ($\Phi_s = \Phi_{LO}$), equation 2.27 becomes

$$I(t) = 2\Re\sqrt{P_s P_{LO}}cos(\Phi_s + \Phi_{LO}) \tag{2.28}$$

Since $P_{LO} \gg P_s$, when compared with the direct detection scheme there is an improvement of SNR.

$$\left(\frac{I_{HomodyneDetect}}{I_{DirectDetect}}\right)^2 = \left(\frac{2\Re\sqrt{P_s P_{LO}}}{\Re P_s}\right)^2 \Rightarrow \frac{4P_{LO}}{P_s} \gg 1 \tag{2.29}$$

So using a homodyne receiver the average power is increased by a factor of $\frac{4P_{LO}}{P_s}$. It can also be observed that since P_{LO} can be much larger than P_s, so we can have an improvement exceeding 20 dB [16].

The Main disadvantage of using homodyne receivers are there sensitivity to the phase variations. Φ_{LO} and Φ_S should remain constant, there fluctuation can be controlled be using a phase locked-loops making the receiver complicated.

heterodyne detection

In heterodyne detection the local oscillator frequency is not equal to the carrier frequency. So equation 2.26 is not 0 and intermediate frequency ω_{IF} is in the range of 0.1 to 5Ghz. So the photo-current using equation 2.25 we have

$$I(t) = \Re(P_s + P_{LO}) + 2\Re\sqrt{P_s P_{LO}}cos(\omega_{IF} + \Phi_s - \Phi_{LO}) \tag{2.30}$$

following the same considerations we made in homodyne detection

$$I(t) = 2\Re\sqrt{P_s P_{LO}}cos(\omega_{IF} + \Phi_s - \Phi_{LO}) \tag{2.31}$$

There is an improvement in this case also when compared with the direct detection case. However, the improvement is lowered by 2-3 dB as compared to the homodyne detection. Since no phase locked loop circuit is used in this case the receiver is simpler than the homodyne receiver and is suitable for the optical communications systems.

Signal to Noise ratio

By considering the signal to noise ratio of the received signal we can find the advantage of using coherent detection. Due to the shot and thermal noise the current fluctuates at the receiver. Considering the noise variance we have

$$\sigma^2 = {\sigma_S}^2 + \sigma_T^2 \tag{2.32}$$

where

$${\sigma_s}^2 = 2q(I + I_q)\triangle f$$

and

$$\sigma_T{}^2 = (\frac{4K_bT}{R_L})F_n\triangle f$$

Considering the fact that $P_{LO} \gg P_s$, the current is mainly due to the term RP_{LO}. The SNR for the heterodyne case is given by

$$SNR = \frac{\bar{I}^2}{\sigma^2} = \frac{2\Re^2 P_S P_{LO}}{2e(\Re P_{LO} + I_d)\triangle f + \sigma_T^2} \tag{2.33}$$

if $\Phi_s = \Phi_{LO}$ in equation 2.27, the SNR is improved by a factor of 2 for a homodyne receiver. Photocurrent I depends on the detection process (homodyne or heterodyne). Since at the receiver, we can control the P_{LO} making it large enough that the receiver noise is overcome by the shot noise i.e. $\sigma_S{}^2 \gg \sigma_T^2$ when

$$P_{LO} \gg \sigma_T^2 \gg \sigma_T^2/2e\Re\triangle f \tag{2.34}$$

so the dark current become negligible as compared to the shot noise $I_d \ll 2e\Re P_{LO}$, The overall SNR becomes

$$\Rightarrow SNR = \frac{\Re P_s}{e\triangle f} = \frac{\eta P_S}{h\nu\triangle f} \tag{2.35}$$

Representing the SNR in terms of number of photons we have

$$\Rightarrow SNR = 2\eta N_p \tag{2.36}$$

Since for the case of homodyne detection the SNR is improved by a factor of 2 so the SNR in terms of number of photons is given by

$$\Rightarrow SNR = 4\eta N_p \tag{2.37}$$

Chapter 3

Modulation Formats for Short Reach Optics

3.1 Introduction

The optical network is mainly divided into core, metro and access networks. Core networks are the long haul high capacity optical links that can link different cities with a distance covering 1000s of km, while metro network lies between the core and the access network connecting enterprises, residential customers etc., the network ranges from 10 to 100 km. Access network also known as the last mile access is connecting the end users to the network. The aggregated data of all the end users is transported through the metro to the core network.

Over the last few years due to the social media, video applications, data center and cloud traffic, the overall network traffics has increased a lot. According to Cisco global cloud index, the global data center IP traffic will increase 3 times over next 5 years i.e. from 4.7 ZB to 15.3 ZB during 2015 to 2020. The overall compound annual growth rate (*CAGR*) of the data center IP traffic will be 27 percent from 2015 to 2020 [1].

Since most of the internet traffic terminates at the metro network, the cost and the power consumption has increased significantly [22]. Beside this, due to a large number of users and high power consumption at optical nodes in the network, the cost and the power consumption of short reach optical networks (*SRON*) has increased and become a key consideration along with the transmission performance [8].

In short reach optical networks a larger number of transceivers are deployed for a wide area coverage increasing the overall component cost. Due to the cost constrain coherent transceiver enabling two dimensional signal constellation cannot be used in short reach optics, consequently, modulation format must rely on Direct Detection (*DD*) having a simpler and low power transceiver design [23]. The transmission distance in direct detection is limited to few kms due to the chromatic dispersion along with low spectral efficiency. Digital signal processing techniques are required to compensate the impairments like clipping, chirp effect, low bandwidth limitations etc. To increase the optical data rate there the following techniques can be used as shown in Fig. 3.1

- increase wavelengths
- increase fibers
- increase data rate
- increase bits per symbol
- Number of polarization state

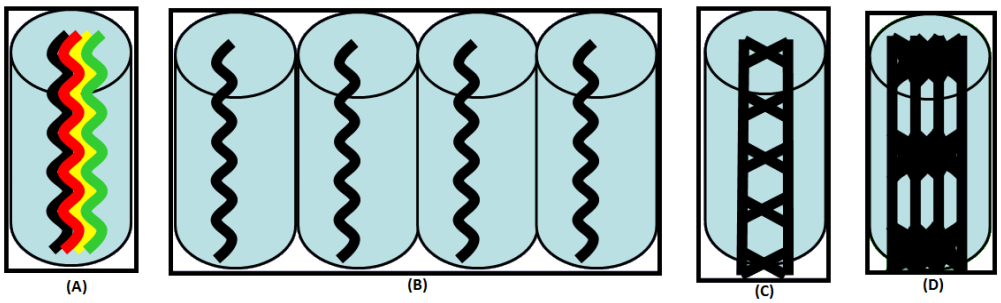

Fig. 3.1 Improving the optical data rate[24] (a) increase wavelengths (b) increase fibers (c) increase data rate and (d) increase bits per symbol

For short reach optical communication links considering the cost constraint, increasing the wavelengths i.e. adding more lasers or increasing the fiber is not a feasible solution. But, the spectral efficiency can be improved using advanced modulation formats. Instead of using only 2 states to transmit the information, a higher number of states can be transmitted (each with a unique phase and magnitude). A higher number of states means higher number of bits in each symbol. Increasing

the number of states make the signal more like an analog signal but at the same time it will become difficult for the receiver to detect the symbol correctly. An example of pulse amplitude modulation (PAM) 4 is shown in Fig. 3.1(d) using 2 bits per symbol so having a total of 4 states instead of only 2 states. A number of advanced modulation schemes are available, here we are discussing only pulse amplitude modulation, Discrete multi-tone and Carrierless Amplitude and Phase Modulation.

3.2 Basic Relations

In digital communication system, the modulator maps a k binary symbols to a corresponding signal $s_m(t)$, $1 \leq m \leq M$, where the possible combinations $M = 2^k$ or $k = log_2 M$. If the *symbol interval or duration time* i.e. the interval at which the signals are transmitted is T_s seconds, the total symbols transmitted in a second are given by

$$R_s = \frac{1}{T_s} \tag{3.1}$$

where R_s is known as the *symbol rate*. Since each signal carries k bits of information, the time to transmit 1 bit of information i.e. *bit interval* T_b is given by

$$T_b = \frac{T_s}{k} = \frac{T}{log_2 M} \tag{3.2}$$

and the *bit rate* R is given by

$$R = kR_s = R_s log_2 M \tag{3.3}$$

The *average signal energy* of the signal $s_m(t)$ is given by

$$\varepsilon_{avg} = \sum_{m=1}^{M} p_m \varepsilon_m$$

where p_m is the probability of the *mth* signal, for the equiprobable case, $p_m = 1/M$, and the average energy is given by,

$$\varepsilon_{avg} = \frac{1}{M}\sum_{m=1}^{M}\varepsilon_m$$

if all signals are equiprobable and have the same energy, then $\varepsilon_m = \varepsilon$ and $\varepsilon_{avg} = \varepsilon$ and the *average energy per bit* is given by

$$\varepsilon_{bavg} = \frac{\varepsilon_{avg}}{k} = \frac{\varepsilon_{avg}}{log_2 M} \tag{3.4}$$

or

$$\varepsilon_b = \frac{\varepsilon}{k} = \frac{\varepsilon}{log_2 M} \tag{3.5}$$

The average power to transmitter energy of ε per bit in T_b seconds is

$$P_b = \frac{\varepsilon_b}{T_b} = R\varepsilon_b \tag{3.6}$$

3.3 Pulse Amplitude Modulation basic

Pulse amplitude modulation (*PAM*) is the simplest scheme, transmit data by changing the voltage or the power amplitude of the signal [25–27]. The transmitted data is encoded in the amplitude of the signal. Not strictly but PAM is considered as the intensity modulation scheme. Unlike NRZ scheme PAM uses more than two levels. As described in the previous section with k bits symbols we can have $M = 2^k$ different amplitude levels. Pam can be used to increase the data rate for bandwidth limited components. Increasing the levels will increase the bit rate, using equation 3.3 for possible M combinations, the data rate R is increased by a factor of $R = R_s log_2 M$. At the same time increasing the levels will make the signal more like an analog signal consequently increasing the impairments reducing the receiver sensitivity. By doubling the level the receiver sensitivity is reduced by 3dB [9]. On the other hand working at a lower level will reduce the noise but it requires operating at higher baud rate, requiring the equalizer (feed forward and/or decision feedback) at the receiver to enhance receiver sensitivity.

PAM is the simplest technique for short reach optical communication using intensity modulation and direct detection technique.

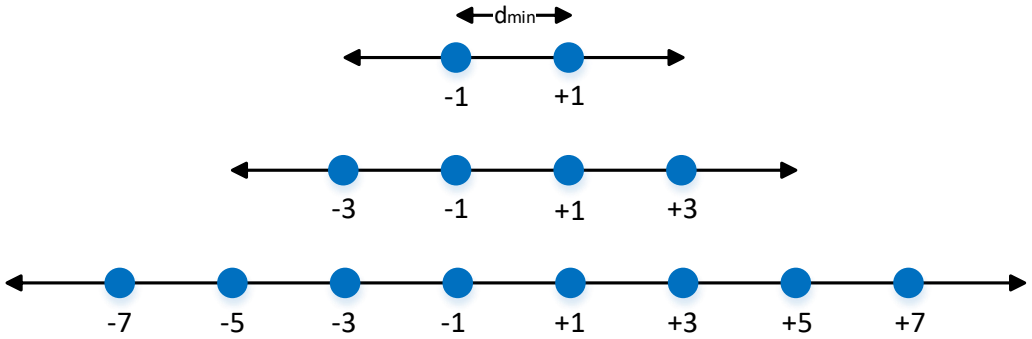

Fig. 3.2 PAM constellation for M=2,4 and 8

The PAM signal waveform can be represented as

$$s_m(t) = A_m p(t), \quad m = 1 \leq m \leq M \tag{3.7}$$

where $p(t)$ is a pulse of duration T. For k number of bits in the symbol with total combination equal to $M = 2^k$ the corresponding set of amplitudes are $\{A_m, \quad m = 1 \leq m \leq M\}$. The discrete signal amplitudes A_m are

$$A_m = 2m - 1 - M, \quad m = 1, 2, \cdots, M \tag{3.8}$$

i.e. $A_m = \pm 1, \pm 3, \pm 5, \ldots, \pm(M\text{-}1)$. The energy in signal $s_m(t)$ is given by

$$\varepsilon_m = \int_{-\infty}^{\infty} A_m^2 p^2(t) dt \tag{3.9}$$

$$= A_m^2 \varepsilon_p \tag{3.10}$$

where ε_p is the energy in $p(t)$. The average energy is given by

$$\varepsilon_{avg} = \frac{\varepsilon_{avg}}{M} \sum_{m=1}^{M} A_m^2$$

$$= \frac{(M^2 - 1)\varepsilon_p}{3} \tag{3.11}$$

and the average energy per bit is given by

$$\varepsilon_{bavg} = \frac{(M^2-1)\varepsilon_p}{3log_2 M} \tag{3.12}$$

Normally the carrier-modulated bandpass PAM signals with low pass equivalents of form $A_m g(t)$ with the carrier frequency fc is represented as,

$$s_m(t) = A_m p(t) = A_m g(t) cos(2\pi f_c t) \tag{3.13}$$

The energy for the bandpass PAM is

$$\varepsilon_{bavg} = \frac{(M^2-1)\varepsilon_p}{6log_2 M} \tag{3.14}$$

The minimum distance between any two constellation points in M-ary PAM system is given by

$$d_{min} = \sqrt{\frac{12log_2 M}{M^2-1}\varepsilon_{bavg}} \tag{3.15}$$

3.3.1 BER calculation

Fig. 3.2 shows the constellation diagram for PAM 2,4 and 8. The minimum distance between any two points is d_min and is given by equation 3.15 i.e.

$$d_{min} = \sqrt{\frac{12log_2 M}{M^2-1}\varepsilon_{bavg}} \tag{3.16}$$

The constellation points are located at $\{\pm\frac{1}{2}d_{min}, \pm\frac{3}{2}d_{min}, \ldots, \pm\frac{M-1}{2}d_{min}\}$.

The symbol error probability is given by

$$P_e = \frac{1}{M}\sum_{m=1}^{M} P[error \mid m sent]$$

$$= \frac{2(M-1)}{M} 2Q\Big(\frac{d_{min}}{\sqrt{2N_0}}\Big) \tag{3.17}$$

Substituting for d_{min} from equation 3.15we have

$$P_e = 2\Big(1-\frac{1}{M}\Big)Q\Big(\sqrt{\frac{6log_2M}{M^2-1}\frac{\varepsilon_{bavg}}{N_0}}\Big) \tag{3.18}$$

$$\approx 2Q\Big(\sqrt{\frac{6log_2M}{M^2-1}\frac{\varepsilon_{bavg}}{N_0}}\Big) \quad for large M \tag{3.19}$$

Equation 3.18 can be also represented in $erfc$ as

$$P_e = \Big(\frac{M-1}{M}\Big)erfc\Big(\sqrt{\frac{3log_2M}{M^2-1}\frac{\varepsilon_{bavg}}{N_0}}\Big) \tag{3.20}$$

From equation 3.18 it can be observed that the average SNR/bit $\frac{\varepsilon_{bavg}}{N_0}$ is scaled by the factor $\frac{6log_2M}{M^2-1}$. So, to keep the error probability constant the SNR/bit must be increased with the increase in M. 6 dB extra power is required for the addition of each additional bit in the transmission.

3.3.2 Effect of RIN

Relative Intensity Noise (RIN) describes the fluctuation of the laser output power. The fluctuation can be in intensity, phase or the frequency. The cause for the fluctuation is spontaneous emission and shot noise. The spontaneous emission generates photon with a random phase that will be added in the coherent field generated due to the stimulated emission causing fluctuation both in phase and amplitude. On the other hand the shot noise i.e. the recombination of electron and holes occurs randomly, even at a constant bias condition causing a change in the signal current. Since the laser is not able to respond at high frequencies the RIN is enhanced near the relaxation oscillation frequency.

Fig. 3.3 shows the power penalty as a function of RIN. It can be observed that for a BER target of $1e-4$ with an acceptable penalty of 0.5 dB the RIN should be lower than -125 dB/Hz, -134 dB/Hz and -142 dB/Hz for PAM 2, 4 and 8 respectively

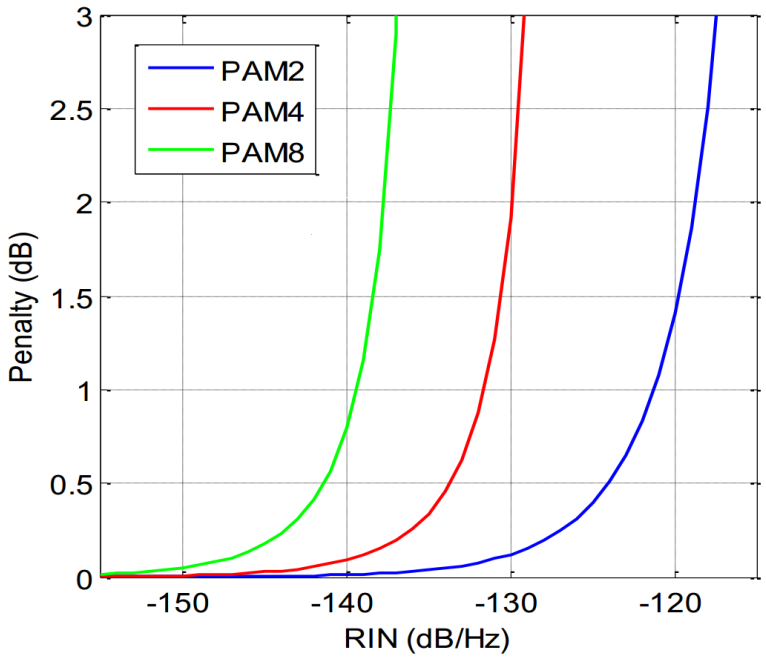

Fig. 3.3 Effect of laser RIN for PAM 2,4 and 8 [28]

as listed in the Table. 3.1. It is also observed that the required RIN increases with increasing PAM-M order. For each bandwidth doubling, RIN has to be reduced 3 dB and for increasing PAM level at least 6 dB increment is required[25].

Table 3.1 Power Penalty due to RIN for PAM-N @target BER 1e-4 [28]

PAM-N	RIN
PAM 2	$\leq$-125 dB/Hz
PAM 4	$\leq$-134 dB/Hz
PAM 8	$\leq$-142 dB/Hz

3.3.3 InterSymbol Interference

The PAM symbols train is transmitted separated with sufficient time duration. Due to the filtering effect of the transmitter, receiver and the channel the symbols spread out. So if the pulse is wider than the time separation between the symbols they overlap causing intersybmol interference (ISI). Due to this intersymbol interference the eye opening is reduced, vertical closure causing the power penalty and the horizontal closure cause the timing penalty. The ISI penalty for PAM is given by [29]

$$P_{ISI} = 10log_{10}\Big(\frac{1}{1-E_M}\Big) \tag{3.21}$$

where E_m is the worst case eye closure. E_m for the PAM 2, 4 and 8 is approximated as

$$E_{mPAM2} = 1.425exp\Big(-1.28\Big(\frac{T_s}{T_C}\Big)^2\Big) \tag{3.22}$$

$$E_{mPAM4} = 2.85exp\Big(-1.28\Big(\frac{T_s}{T_C}\Big)^2\Big) \tag{3.23}$$

$$E_{mPAM8} = 5.7exp\Big(-1.28\Big(\frac{T_s}{T_C}\Big)^2\Big) \tag{3.24}$$

Generalizing for MPAM we have

$$E_{mPAMM} = \frac{M}{2}1.425exp\Big(-1.28\Big(\frac{T_s}{T_C}\Big)^2\Big) \tag{3.25}$$

where T_s is the bit period and T_C is the channel $10\%-90\%$ rise time and the relation is valid for a channel having a Gaussian response with rectangular input. It can be observed that the eye closure for PAM 4 is double as of PAM 2 and the same applies to the eye closure for PAM 8 and PAM 4 eye closure. So by increasing the modulation level we can increase the spectral efficiency.

3.4 Discrete Multitone

Discrete multitone (*DMT*) scheme is multicarrier modulation scheme similar to orthogonal frequency division multiplexing (*OFDM*) with high spectral efficiency, flexible multi-level coding and tolerance to intersymbol interference for low-cost and short reach communication [30]. In DMT the size of the constellation can be adjusted depending on the Signal to Noise ratio (SNR) and the process is known as bit loading [31–33].

The constellation order and power of each subcarrier is adapted to channel conditions e.g assigning the larger number of bits to the sub-channels with the

highest sub channel SNR and vice versa, which either maximizes the bit-rate (for a given margin as in the case of ADSL) or maximizes the margin (for a given bit-rate as in the case of e.g. 100G Ethernet). A larger number of subcarriers allows an easy adaptation to channel conditions but a lower number of subcarriers is preferred considering the power consumption

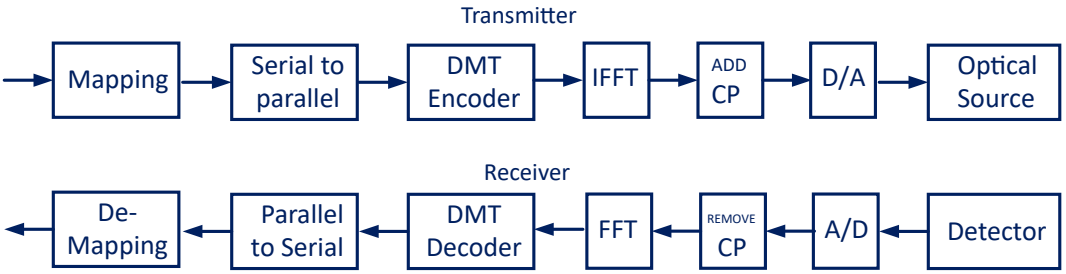

Fig. 3.4 Discrete Multitone schematic Diagram

Fig. 3.4 shows the schematic diagram of the DMT system. The encoder maps the input bits sequence to complex symbols. The serial data is converted to parallel streams and each stream is modulated on N sub carriers. Another N points that are the conjugate of the signal are used to generate the real output. The cyclic prefix is added to avoid ISI and intercarrier interference (*ICI*)[34]

Using Digital to analog converter (*DAC*) the DMT signal is converted to an analog signal to modulate the light source. At the receiver after detection, analog-to-digital converter (*ADC*) converts the signal to digital signal, cyclic prefix is removed and fast FFT is performed. Out of the 2N signals, only first half is used for signal decoding. Due to the lack of synchronization between transmitter and receiver, an equalizer is required at the receiver.

One of the drawbacks is high peak to average power ratio (*PAPR*), limiting this power will reduce the range of the of multicarrier transmission [35], this requires clipping and higher average optical power [6]. New DSP techniques reducing the PAPR, ICI and improving dispersion tolerance are required.

3.5 Carrierless Amplitude and Phase Modulation

Carrierless Amplitude and Phase (*CAP*) modulation is a variation of Quadrature amplitude modulation. It allows high data rate using bandwidth limited optical com-

ponents with a simpler implementation. The carrier is suppressed at the transmitter before the transmission and generated again at the receiver so is called carrier less.

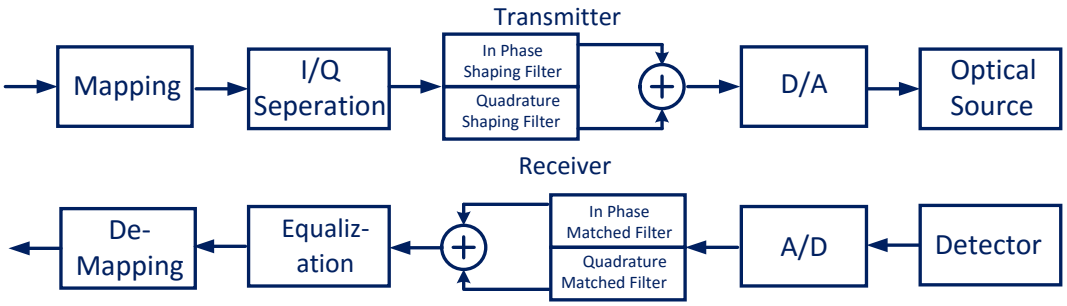

Fig. 3.5 Carrierless Amplitude and Phase Modulation schematic Diagram

Fig. 3.5 shows the schematic diagram of CAP modulation. The encoder maps the input bit sequence to complex symbols. Using finite response filter, in phase and quadrature components are generated and up sampled and passed through the shaping filter. Using Digital to analog (*DA*) converter the CAP signal is converted into an analog signal to modulate the light source. At the receiver after detection, analog-to-digital (*AD*) converter converts the signal back to digital and is fed to two matched filters to separate the in-phase and quadrature component. The signals are down sampled to the symbol rate, equalized and converted back to original sequence using the decoder. The AD and DA converters and the filters at both transmitter and receiver are operating at the same rate. The generated signal is given by

$$s(t) = a(t) \otimes g_i(t) - b(t) \otimes g_q(t) \tag{3.26}$$

where $a(t)$ and $b(t)$ are the in-phase and quadrature components of the transmitted sequence respectively, and

$$g_i(t) = g(t)(2\pi f_c t) \tag{3.27}$$

$$g_q(t) = g(t)(2\pi f_c t) \tag{3.28}$$

are the corresponding impulse response of the filters forming the Hilbert pair [7], $g(t)$ is the square-root raised-cosine function filter. Since sampling at a proper instant is difficult so any sampling time offset will lead to ISI and the cross talk between

the in-phase and quadrature components. This distortion due to ISI and cross talk is linear, an adaptive equalizer is required to recover the output signal. CAP is highly sensitivity to non flat channel frequency responses, to mitigate the requirement of a flat frequency response, multiband CAP was proposed [36], in which multiple independent sub-bands with tailored modulation order and signal power are created.

3.6 Conclusions

Higher-order amplitude, phase, and multi carrier modulation are under investigation for high data rate (e.g. 400G) applications. Different modulation schemes as discussed are available for short reach optical communication using direct detection. PAM using IMDD is the simplest to be used for a short distance communication. For longer distance with higher data rates, DMT or CAP can be used. Compared to DMT, CAP provides a simple implementation with direct detection. In terms computational complexity, PAM requires an equalizer (FFE/DFE) for channel equalization, CAP requires filters for symbol generation and DMT uses fourier and inverse fourier transform for sub carrier multiplexing [37]. Table. 3.2 explains some of the main performance parameters for the different modulation formats.

For PAM 2, the bit rate R = Symbol rate R_s, with the $BW = R$ so the spectral efficiency is of $1b/s/Hz$. PAM 4 modulation for 2 bit per symbol, the spectral efficiency is doubled to $2b/s/Hz$ and $3b/s/Hz$ for PAM 8 [20]. For a complex CAP modulation and the bit rate and spectral efficiency are similar to PAM-M. with the negligible effect of cyclic prefix, DMT has the same bandwidth and spectral efficiency as CAP for the same bit rate and subcarrier modulation. The Performances of different modulation formats have been extensively investigated and are presented in [38, 8, 9, 39, 10]

Table 3.2 Summary of Different Modulation Formats[40]

Modulation Format	Symbol Rate	Bandwidth	Spectral Efficiency
	Baud	BW (Hz)	(b/s/Hz)
PAM 2	R	R	1
PAM 4	R/2	R/2	2
PAM 8	R/3	R/3	3
CAP 16	R/4	R/2	2
DMT 16	N.A.	R/2	2

Chapter 4

Performance Analysis of M-PAM

4.1 Introduction

To meet the high data rate short reach optical links requirement, the possible solutions are to increase the wavelengths, increasing the number of fibers or bits per symbol etc. as discussed in chapter 3. Increasing the number of fibers or the lasers at the transmitters will not only increasing the cost but also the size and the power. Increasing the bits in each line using advance modulation formats is the feasible solution providing high spectral efficiency and low complexity without increasing the fiber, lasers, detectors and other components. In this chapter, we have investigated Pulse amplitude modulation as a possible candidate for the short reach communication link with a good spectral efficiency and low complexity, catering the cost and power constraint. The performance of PAM-n (n= 2, 4, 8), for short reach applications with transmission distance up to 2 km using standard single mode fiber is studied. We rely on silicon-photonics modulators characterized by limited extinction ratio. For all three modulation levels, the same bit-rate of 25 Gbps and the same symbol rate of 25 Gbaud is used for the operation with forward error correction overhead of 3.125 % [41] and target bit error rate of 10^{-4}. Digital signal processing is used and analyzed at the transmitters (Tx) and the receivers (Rx), that includes a training-driven finite impulse response (*FIR*) filter equalizer established by the least mean square (*LMS*) algorithm. Since the increase in the data rate in short-range optics is limited by the component bandwidth and dispersion consequently reducing the maximum distance. The sensitivity impairments due to the limited Tx/Rx electrical bandwidth is studied

along with the number of filter taps to achieve sensitivity benefits without increasing the latency of the system. Since low-latency is the main constraint for distributed and high performance computing in pursuance to enable distributed big-data processing [42]. The analysis is primarily targeted for intra-data-center networking, where component cost is certainly a constraint. Therefore, modulation formats must depend only on direct-detection, keeping apart for the time being the possibility of using coherent receivers. The chapter is organized as follows. In Sec. 4.2 basic concept of interference and equalization is described. In Sec. 4.3 the considered setup and the simulative analyses is explained. For the reference case, large Tx/Rx bandwidth and large N_{taps} is used to show the bit error rate (BER) vs. optical SNR ($OSNR$) curves for the considered PAM configurations. In Sec. 4.4, The sensitivity penalty due to the reduction in electrical bandwidth is presented. Sec. 4.5 shows the effect on performances with respect to the number of FIR equalizer taps.

4.2 Intersymbol Interference and Equalization

For the efficient sharing of the frequency resources, the transmitted signals are filtered to limit its bandwidth. In pulse amplitude modulation (PAM), the symbols are represented by their amplitudes. When a pulse is transmitted, the channel act as a low pass filter spreading symbols beyond the time interval used to represent them, spreading the shape and overlapping with the neighboring symbols causing interference known as intersymbol interference. The channel also converts the original discrete signal to a continuous signal, degrading the overall system performance.

If x(t) is the input train, that consists of periodically transmitted impulses of varying amplitudes, we have

$$x = \begin{cases} 0 & for\, t \neq kT \\ X_k & for\, t = kT \end{cases} \tag{4.1}$$

where T is the symbol period. The only significant value is for $\tau = kT$, any other value of τ is a multiplication by “0”, so It can be represented as the superposition of many scaled and shifted signals represented as

$$r(t) = \sum_{k=-\infty}^{\infty} x_k h(t - kT) + n(t) \tag{4.2}$$

Where $h(t)$ is the channel impulse response and $n(t)$ is the noise. The received signals $r(t)$ are sampled periodically, so replacing t with nT, we have

$$r(nt) = x_n h(0) + \sum_{k=-\infty} x_k h(nt - kT) + n(nt) \tag{4.3}$$

If the receiver and transmitter sampling frequency is not synchronized there will be a channel delay and offset phase, so an offset t_0 will be added to the time index making the equation as

$$r(nt) = x_n h(t_0) + \sum_{k=-\infty} x_k h(t_0 + nt - kT) + n(t_0 + nt) \tag{4.4}$$

The first term on the right is the component of $r(t)$ and is the desired signal multiplied by the channel-impulse response. It is used to identify the transmitted amplitude level. The last term is the additive noise, while the middle term is the contribution due to the interference from neighboring symbols. These unwanted contributions from other symbols are the intersymbol interference terms.

There are two major ways to cancel the effect of ISI

- Design of band limited signal
  design of bandlimited channels to generate ISI free pulse i.e. Nyquist pulses
- Equalization
  filter the received signal to cancel the ISI introduced by the channel impulse response.

4.2.1 Nyquist Pulse

It is possible to have no ISI if the signal/ channel is bandlimited. There is no ISI if the Nyquist condition is satisfied

$$x(nT) = \begin{cases} c & for\ n = 0 \\ 0 & for\ n \neq 0 \end{cases} \tag{4.5}$$

where c some constant. The condition in frequency domain is given by

$$\sum_{n=-\infty}^{\infty} = X(f - \frac{n}{T}) = T \tag{4.6}$$

In the above condition, there will be no ISI. When the channel is bandlimited to W Hz, i.e. $x(f) = 0$ for $f > 0$, we can have the following conditions.

- the symbol rate is so high that 1/T > 2w, there will signal overlapping causing ISI as shown in Fig.4.2
- the symbol rate is slower so 1/T = 2w, there signals can touch the neighbor but does not overlap. This is the critical rate (1/T = 2w) known as Nyquist criteria above which there is ISI
- the symbol rate is so slower that 1/T < 2w, there will signal no overlapping as shown in Fig.4.1

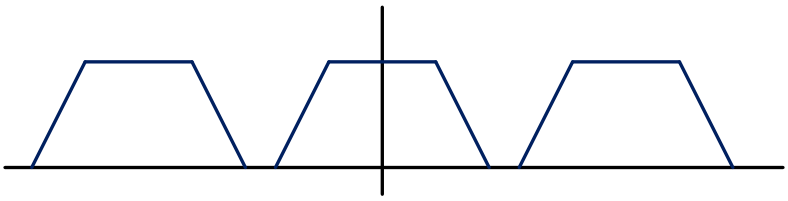

Fig. 4.1 Non Overlapping Spectrum

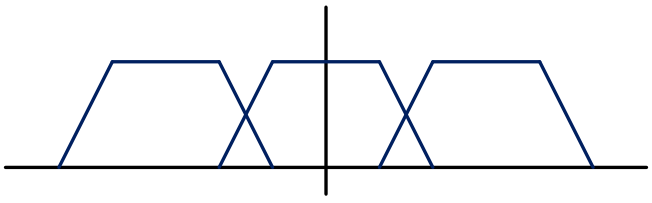

Fig. 4.2 Overlapping Spectrum

4.2.2 Equalization

A properly shaped transmitted pulse resembles a sinc function, when the signal is placed properly at selected sample points there will be no ISI. Practically during the transmission, the signals are distorted due non flat frequency response or multipath reception of the channel and due to addition of noise from the channel. The distortion can be removed by using a filter that is the inverse of the channel frequency response, and the process is known as *equalization*. These filters are easy to build, can be modified easily for different equalization schemes and channel conditions. There are two main techniques employed to formulate the filter coefficients:

Automatic Synthesis

Before the normal transmission, a known pre-stored signals at the receiver is used to find the error signal to have the knowledge of the channel characteristic and is used to adjust the equalizer coefficient to minimize the errors. The tap gain is adjusted during each symbol interval. For proper equalization, the training sequence must be at least as long as the length of equalizer. The direction of the taps gain is opposite to the error estimate to make it converge to the optimum value.

Adaptive Equalization

During the decision directed mode, the coefficients of the equalizer are adjusted continuously. The receiver decisions are highly probable, resulting to an error estimation correct enough to allow the adaptive equalizer to maintain precise equalization. Beside this, even in the decision directed mode the equalizer can track slow variations.

For a larger step size the convergence will be fast but with some excess mean-square error of the equalizer and is directly proportional to the number of equalizer coefficients, the step size and the channel noise power. During the training mode larger step size is used for fast convergence and is reduced in the decision directed mode for a fine tuning.

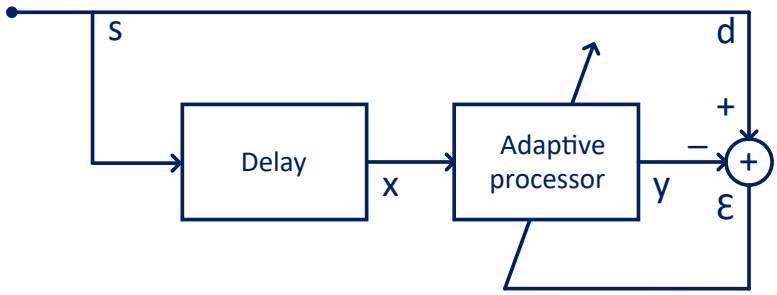

Fig. 4.3 Adaptive filter block diagram

4.2.3 LMS Equalization

The least mean square (LMS) algorithm tries to adjust the filter coefficients such that to minimize the error between pre-stored signal and the signal generated by the equalizer [43, 44]. During an iterative process, using the training sequence the filters coefficient are adjusted such that a minimum of mean square of error is achieved between the stored signal and the equalized signal. The value of the step size μ is a trade off between convergence and residual steady-state error. With a larger μ the equalizer converges faster but with some residual steady state error. The change in the weights also depends on μ , so for larger μ the change in weights will also be large, it will keep oscillating to reach the optimum value. The coefficients are updated according to the following equations

$$y(n) = (X(n) * W(n)) \tag{4.7}$$

$$W(n+1) = W(n) - \mu * e(n) * X(n) \tag{4.8}$$

where

$$e(n) = d(n) - y(n) \tag{4.9}$$

where

$W(n) =$ filter weight at time n

$d(n) =$ desired signal at receiver

$X(n) =$ Received signal at receiver

$y(n)$ = equalized signal at receiver

From equation 4.8 the next weight is equal to the current weight minus the correction factor. From 4.9 if the sample output is much smaller than the training signal, the error will be large. So the received sample values are scaled by this large difference. Similarly, if the error is small the adjustment to be made to equation 4.7 will also be very small. So the overall effect is to use filter weights to converge and to minimize the mean square error. It is also possible to use a decision device, depending on the output of the filter it estimates the most likely transmitted symbol value. Using the filter coefficients (tap weights) the error due to the difference between the decision device input and output can be adjusted.

4.3 Analyzed setup and simulative analyses

The block diagram for the considered PAM-n setup is shown in Fig. 4.4. The transmitter is made of a DSP block followed by a digital-to-analog converter, filter, RF driver amplifier whose output is driving the Mach-Zehnder modulator shaping the optical signal generated by a continuous wave laser.

The logical data is feed to the DSP unit that properly shapes the modulated signal to be used by the DAC. A pseudo-random binary sequences (*PRBS*) generator with degree 17 is used for the generation of the logical data, generating a total of $2^{17}-1 = 131071$ bits. Depending on the PAM level k streams of PRBS are generated where $k = 1,2,3$ for PAM-2, PAM-4 and PAM-8 respectively. The total number of symbols used for the simulation are 400000, that are sufficiently large enough to get reliable results down to the target bit error rate of 10^{-4}. The Bit error rate is calculated through error counting.

The DSP unit is working at 2 sample-per-symbol (SpS). A pre-emphasis filtering is included in the DSP unit that selectively enhances higher frequencies to counteract the unwanted effect due to the DAC induced signal distortion. Theses unwanted effects can be the low-pass response of the DAC and the limited resolution inducing the ISI and noise enhancement [45]. The impairments due to the DAC can be compensated using an equalizer at the receiver, since the channel noise is also added to the transmitted signal, post emphasis at the receiver will further add digitally enhanced noise[46]. At the transmitter, the *ArcSin* function expressed in equation

4.10 is used to mitigate the non linear, sinusoidal electro-optic transfer function of the MZM further improving the performance.

$$V(t) = \frac{4}{\pi} sin^{-1} \sqrt{1 + \frac{MD}{100} s(t)} \tag{4.10}$$

where V(t) is the adjusted output, MD is the Modulation Depth and s(t) is signal to be compensated.

To study and focus on bandwidth limitations effects, the number of quantizing bits used for the DAC are set to 10, that are sufficient enough to ignore the impairments due to quantizing noise. Since output voltage swing of the commercially available DACs are usually of few hundred mV, there is a need of RF driver/amplifier that matches the DAC output swing to the switching voltage of a typical MZM.

We used 5th order Bessel filter at the transmitter and receiver to consider electrical bandwidth limitations as shown in Fig. 4.4. The 3 dB bandwidth of the filter defines the Tx/Rx bandwidth limit for the system. The bandwidth limited electrical signal at the Tx will drive the modulator. For the MZM modulator, we suppose a value for the extinction ratio ER = 6 dB that is typical for silicon-photonics devices [14]. The optical PAM modulated signals generated after the electro-optical conversion operated by the MZM are transmitted through 2 km of standard single mode fiber.

For the considered scenarios of a short link i.e. 2 km, fiber propagation effects are negligible, except for the possible lumped reflections [47]. Since the penalties for PAM-2 and PAM-4 are smaller than 1 dBo [48], that are low enough to be ignored for the analysis performed. However detailed analysis on the lumped reflections has been performed and discussed in chapter 5 Assuming the receiver to be noise-limited, we have also neglected the effect of relative intensity noise. The acceptable maximum RIN to satisfy such assumption is around -134 dB/Hz and -142 dB/Hz for PAM 4 and PAM 8 respectively [28].

The receiver comprises of a photodetector, trans-impedance amplifier (TIA) followed by the ADC and the receiver DSP block.

At the receiver, a PIN photodetector followed by a TIA amplifier is used for the opto-electrical (OE) conversion. The responsivity R of the photodetector is supposed to be 0.7 A/W, while the TIA is characterized by a trans-impedance R_t = 285 Ω and by an input-referred noise factor of 32 pA/$\sqrt{\text{Hz}}$. The main source of noise

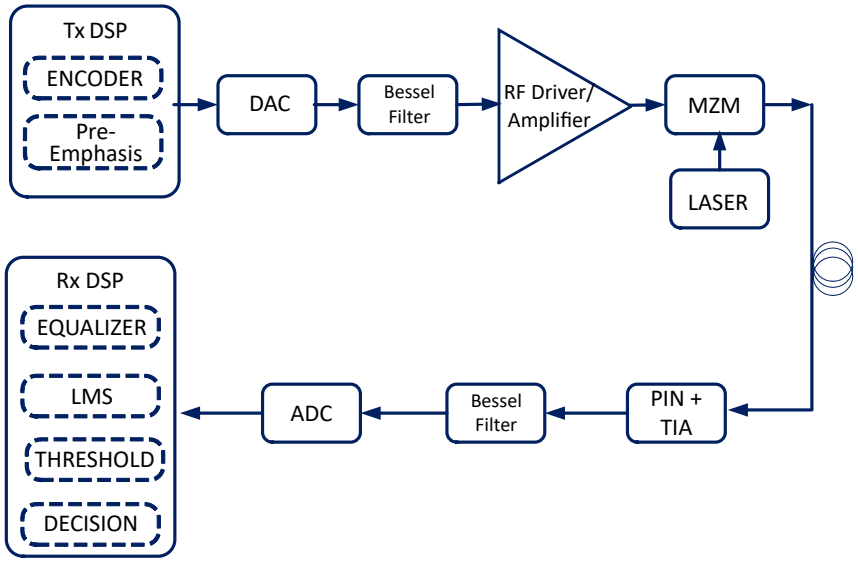

Fig. 4.4 Block diagram of the setup used for the presented simulative analyses.

impairments is due to the OE conversion, during the photodetection, random arrival of photons causing the shot noise and thermal motion causing the thermal noise generated by the amplification add noise in the system.

The bandwidth limitation for the OE conversion is equal to the symbol rate, eliminating the need for the use of a cascaded anti-aliasing electric filter. The filter after OE conversion is used for bandwidth-limiting the electrical signal. The signal is then converted to digital and is received by the receiver DSP block. The 3 dB bandwidth BW of the bandwidth-limiting Bessel filter at receiver is the same as the bandwidth of the filter at transmitter. After filtering, analog to digital converter converts the received electrical signal to a digital format, for the digital signal processing. Analogous to the Tx DAC, the number of ADC bits at the Rx ADC are also set to a large number sufficiently enough allowing to neglect the quantizing noise. The number of bits for analog to digital converter was set to 10 and is operating at 2 Sample per Symbol (SpS). The digital signal provided by the ADC is processed by a DSP unit including the training-driven FIR equalizer, the adaptive algorithm defining thresholds and the decision unit returning the detected data sequence. The pre-FEC BER is calculated using bit by bit comparison of the transmitted and the received data-sequence performing error-counting. We simulated a total of 400000 symbols, that are sufficiently large and accurate enough to have a BER estimation down below

to the target BER = 10^{-4}. Using equation 4.12, the total number of errors that can be observed are 40, 80 and 120 for PAM-2, PAM-4 and PAM-8 respectively.

$$BER_T = \frac{Total\,Errors}{N_{Symb} \cdot k} \tag{4.11}$$

$$Total\,Errors = N_{Symb} \cdot k \cdot BER_T \tag{4.12}$$

When using the training sequence, total errors that can be calculated are given by

$$Total\,Errors = (N_{Symb} - N_{Trai}) \cdot k \cdot BER_T \tag{4.13}$$

where
BER_T is the required target BER
N_{Symb} total number of symbols simulated
N_{Trai} total number of training symbols
and
k is the bits per symbol
With training sequence set to 45000 symbols, total errors that can be calculated are 35, 71 and 106 for PAM-2, PAM-4 and PAM-8 respectively.

Since at higher data rates, inter-symbol interference becomes a significant problem than at the lower data rates. To eliminate the noise and ISI, a fractionally spaced Feed Forward Equalizer (FFE) is used. It is a FIR based equalizer. Depending on the bit-rate or the symbol rate scenario i.e. the spacing between the taps is one DSP sample period i.e.: $T_b/2$ or $T_s/2$ respectively. FFE is simple to implement, can provide high speed, requires less power and cost as compared to a Decision Feedback Equalizer (DFE). During the training sequence, using the LMS algorithm the filtering coefficients of the FIR filter are calculated [43]. To ensure proper convergence of tap weights to the optimal values, the training sequence N_{Trai} is set to 45000 symbols and the LMS converge factor is set to 10^{-3}. During the training mode, equalizers taps are updated through the LMS, once convergence is achieved and the optimal values have calculated, it is switched from the training mode to the decision-directed mode. The algorithm introduces latency due to equalizer taps, if N_{taps} is the number of equalizer taps, the latency is given by

$$T_L = \frac{1}{SpS} \cdot (N_{taps} - 1) \cdot T_s \tag{4.14}$$

where T_s is the symbol duration. Since the DSP is working at 2 sample per symbol, we have

$$T_L = 1/2 \cdot (N_{taps} - 1) \cdot T_s \tag{4.15}$$

Along with the LMS equalizer, an adaptive decision threshold algorithm calculating the thresholds is part of the DSP unit. It uses the training sequence and calculates the thresholds traversing from the most-significant bit (*MSB*) to the least-significant bit (*LSB*). The training sample of the received sequence is distributed between "N" threshold values between the extreme values. Using error counting, the BER is calculated for each threshold value. The threshold value corresponding to the minimum BER is used for the rest of data. Finally, the Rx DSP Decision block operates by comparing the calculated threshold with the equalized signal.

The setup used for the presented simulative analyses is described in Fig. 4.4. The considered modulation formats are PAM-2, PAM-4 and PAM-8 with increasing number of bit-per-symbol (*BpS*) i.e. $BpS = 1$, $BpS = 2$ and $BpS = 3$ respectively. Two different data-rate scenarios are considered, case (i) the bit-rate R_b = 25 Gbps and in case (ii) the symbol rate R_s = 25 Gbaud.

The required DSP speed for the symbol rate case is $R_{DSP} = 2 \cdot R_s$, where R_s is scaled with BpS as $R_s = R_b/BpS$, while for the bit-rate case the DSP speed used is scale by the bit rate as $R_b = R_s \cdot BpS$. For all the analyzed cases, forward error-correction code was adopted and characterized by an overhead OH = 3.125 % [41] and target pre-FEC BER = 10^{-4} was used. The simulated line-rates ($R_{s,l}$) are enlarged accordingly, i.e.,

$$R_{s,l} = R_s \cdot (1 + \frac{OH}{100}) \tag{4.16}$$

The performance impairments was analyzed assuming the DSP bandwidth of Tx and Rx to be the same and equal to BW, that is represented as percentage of the symbol rate, i.e. as normalized bandwidth $NBW = BW/R_s \cdot 100$ that is varied between the range [50%; 100%]. 5^{th} order Bessel filters are used to imitate electrical bandwidth limitations at Tx/Rx. It represents the 3 dB bandwidth of the filters. The bandwidth is varied by changing the bandwidth of the Bessel filter and is

normalized (NBW) to the symbol rate. For the reference case considered bandwidth $NBW = 100\%$.

All analysis and results are represented as sensitivity, i.e. the minimum received power level required to ensure the target BER = 10^{-4}. As a starting point, a reference sensitivity P_{ref} for each scenario is established. For the reference case simulations, the impairments are minimized and the equalizer strength are maximized by setting NBW = 100% and N_{taps} = 39. For all the three modulation formats, reference analyses results are displayed as BER vs. P_{Rx} and are shown in Fig. 4.5a and Fig. 4.5b for the case of the same bit-rate of 25 Gbps and of the same symbol-rate of 25 Gbaud, respectively. P_{ref} for R_b = 25 Gbps is -6.5 dBm, -4.5 dBm and -1.75 dBm for PAM-2, PAM-4 and PAM-8, respectively. While, P_{ref} for R_s = 25 Gbaud, is -6.5 dBm, -1.8 dBm and 3.2 dBm for PAM-2, PAM-4 and PAM-8, respectively.

Note that for the case of PAM-2, 1 bit per symbol is being transmitted so the symbol rate is equal to the bit rate and the two scenarios coincide.

4.4 Results on performance impairments of Tx/Rx electrical bandwidth

Once the reference sensitivity for each PAM-n scenario is established, the analysis is performed aiming to find the sensitivity penalty because of the electrical bandwidth reduction of the Tx and Rx DSP units. Since the analysis is to demonstrate penalties induced by the lack of bandwidth only, the bandwidth percentage NBW is varied from the 50% to the reference value of 100%, however, the number of equalizer taps is set to the reference value of $N_{taps} = 39$. The evaluated BER vs. received power for the case of given bit-rate $R_b = 25$ Gbps and of given symbol rate $R_s = 25$ Gbaud for the three considered PAM-n cases are shown in Figs. 4.6, 4.7 and 4.8. For each value of NBW ranging from 50 % to 100 % a separate curve is shown. As discussed previously for PAM-2, symbol rate is equal to the bit rate so the two scenarios overlap and is displayed only in Fig. 4.6.

The same general behavior is observed for all the considered scenarios, as the NBW is decreased the BER curves start stretching away from the reference optimal ones are shown in Fig. 4.5 displaying an increased power penalty. The same occurs also with the use of the equalizer, as it recovers for the lack of bandwidth, but

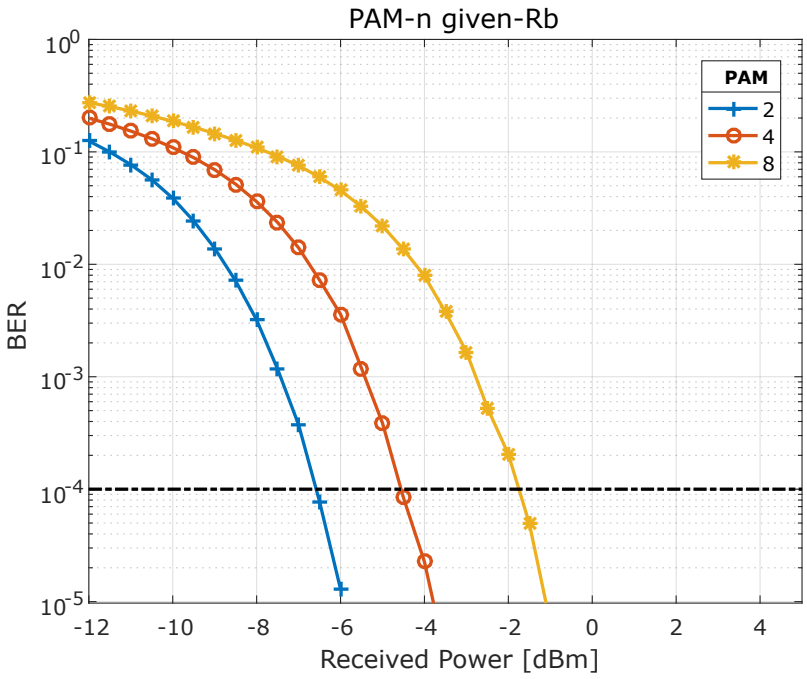

(a) same bit-rate of 25 Gbps

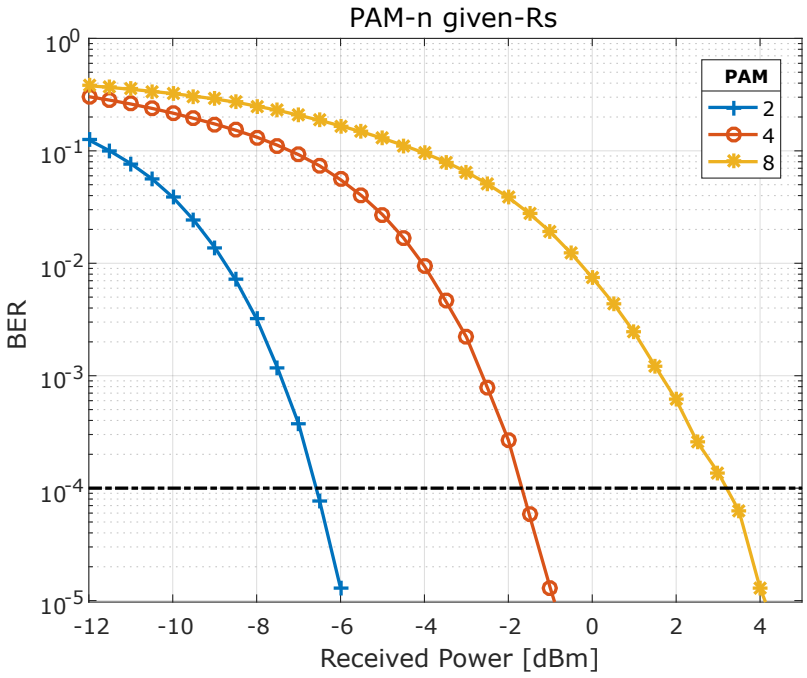

(b) same baud-rate of 25 Gbaud

Fig. 4.5 BER vs. the received power.

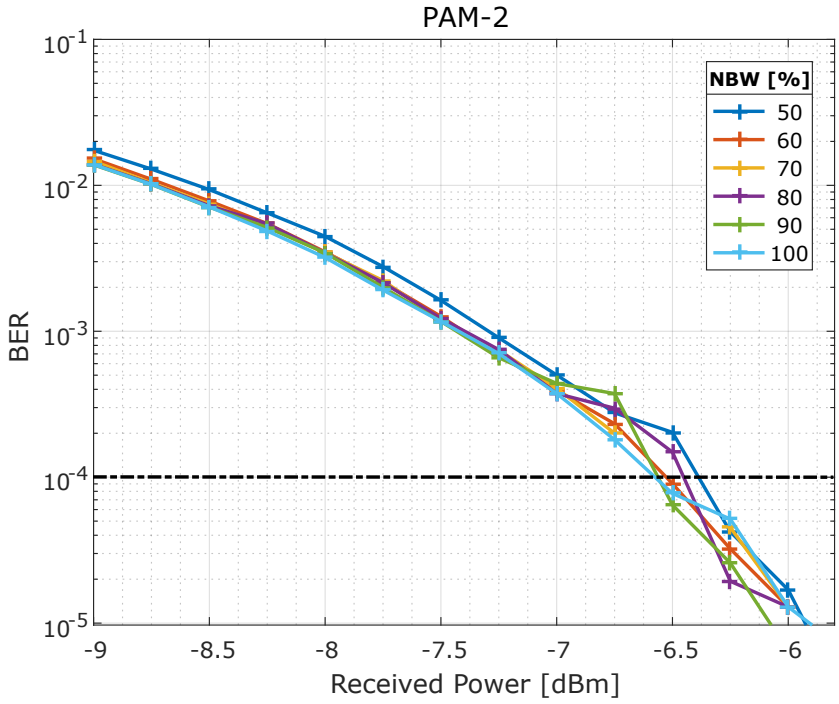

Fig. 4.6 BER vs. the received power for different value of normalized Tx/Rx electric bandwidth, for PAM-2 with $R_b = R_b = 25$

it boosts higher frequency noise components. For PAM-2 this penalty is almost insignificant (Fig. 4.6) But with the increase in number of PAM levels, the penalty increases due to the greater sensitivity of multilevel modulation formats to the noise.

The described behavior is observed in both the given-R_b and the given-R_s cases, but for the given-R_b scenario (Figs. 4.6, 4.7a, 4.8a) as with the decrease of the number of PAM levels $n = 2^{BpS}$, the occupied bandwidth determined by $R_s = R_b/BpS$ also scales down, so the effect is reduced a lot. For the given-R_s scenario, impairments are much more significant. A flooring effect is observed for PAM-8 for $NBW < 70$ %, that prevents to achieve the target BER (see Fig. 4.8b). The summary of the power penalty due to the reduction of Tx/Rx electric bandwidth with respect to the ideal scenarios whose performances are displayed in Fig. 4.5 at the target BER = 10^{-4} is shown in Figs. 4.9.

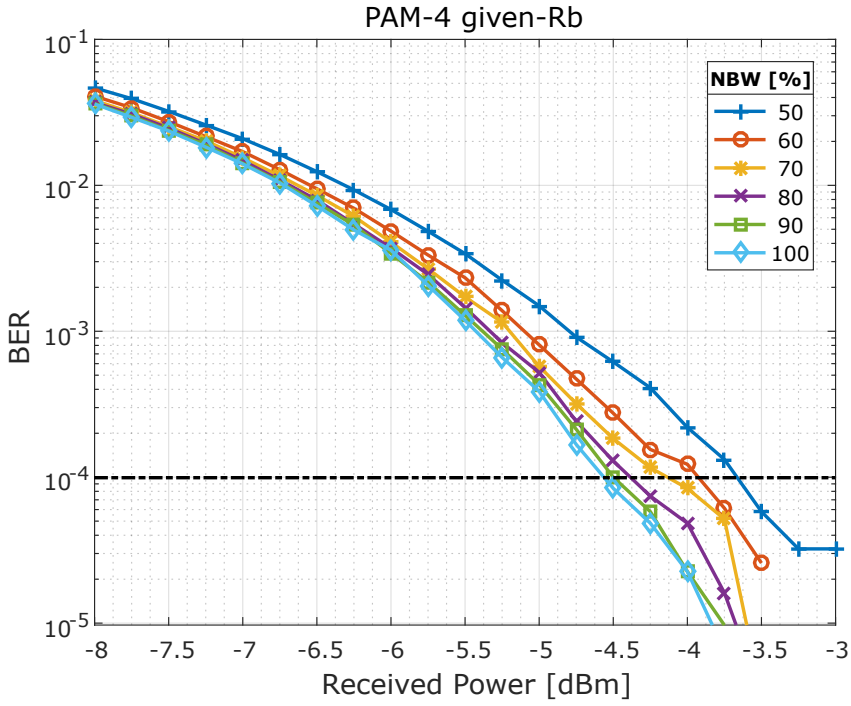

(a) $R_b = 25$ Gbps

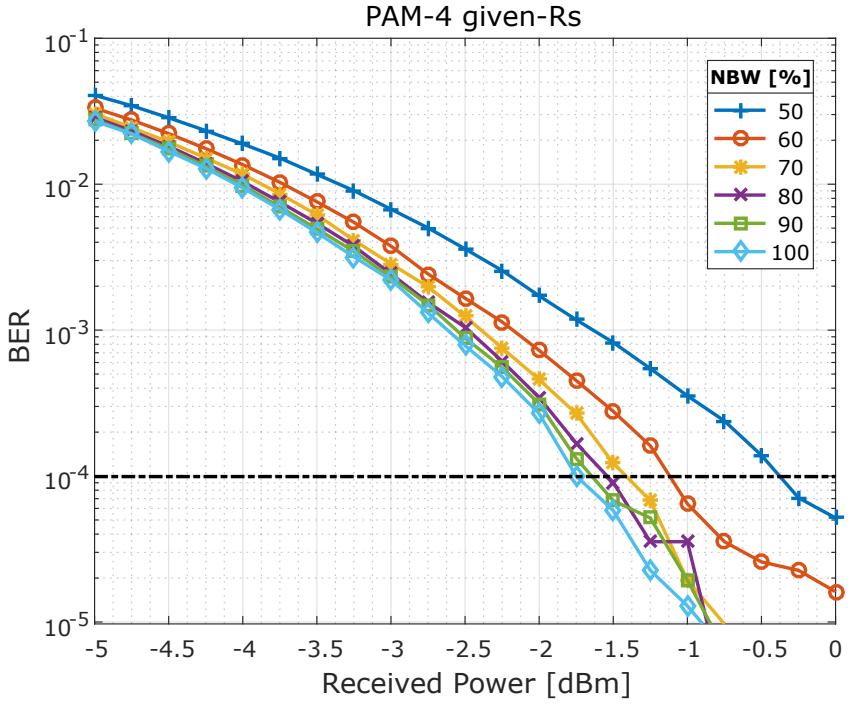

(b) $R_s = 25$ Gbaud

Fig. 4.7 BER vs. the received power for different value of normalized Tx/Rx electric bandwidth for PAM-4

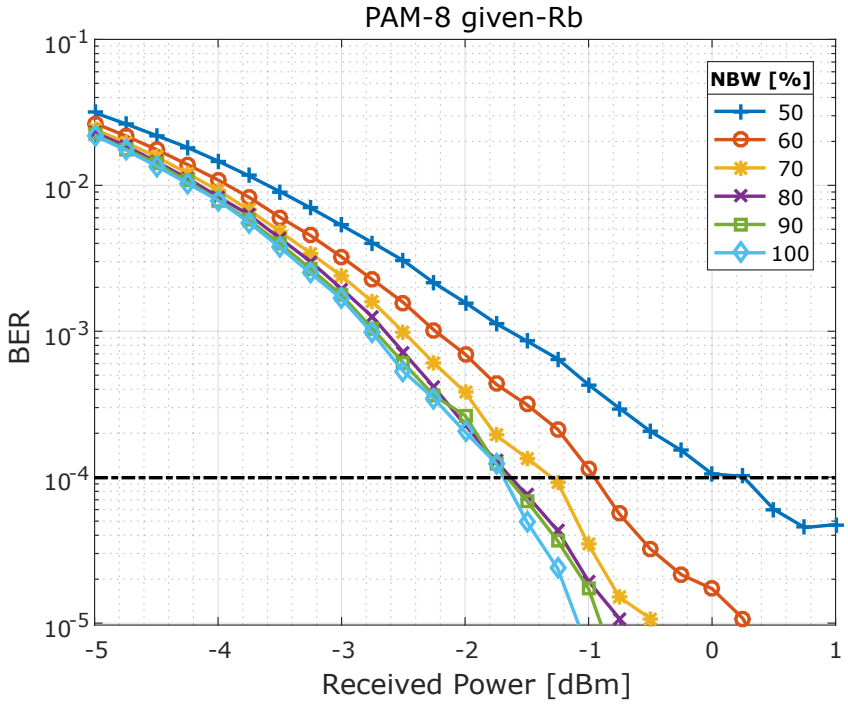

(a) $R_b = 25$ Gbps

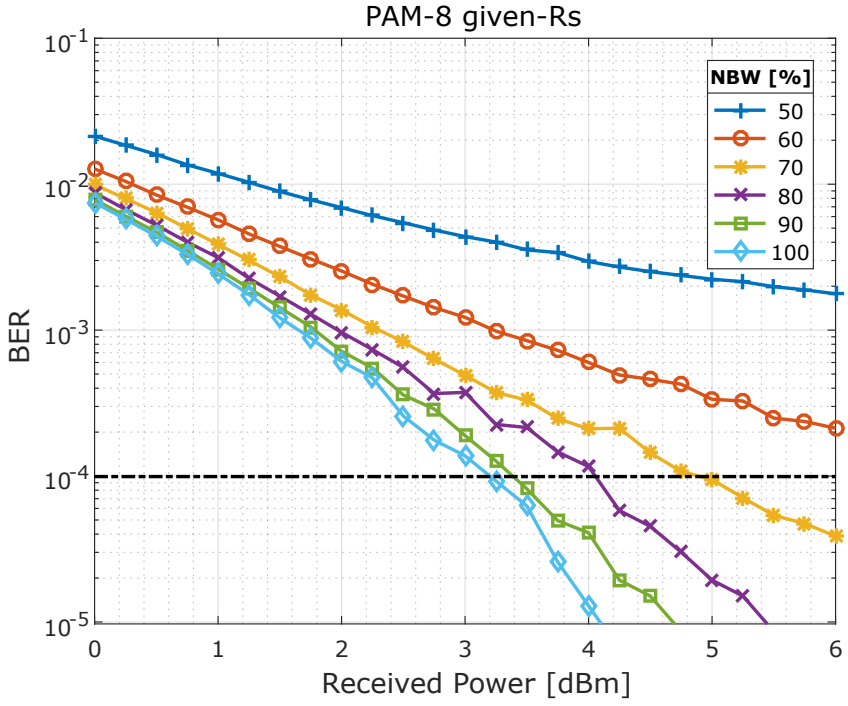

(b) $R_s = 25$ Gbaud

Fig. 4.8 BER vs. the received power for different value of normalized Tx/Rx electric bandwidth, for PAM-8

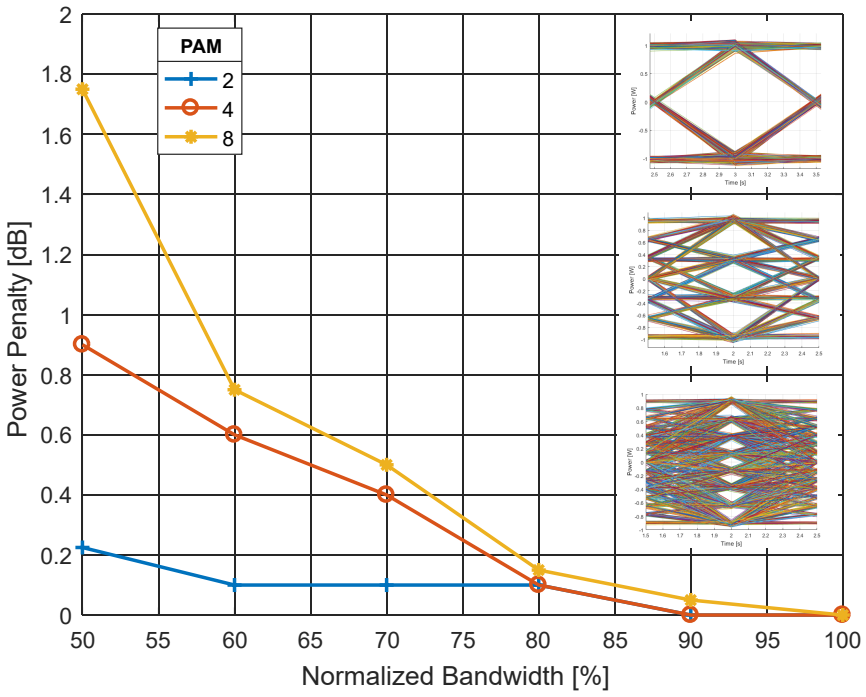

(a) $R_b = 25$ Gbps

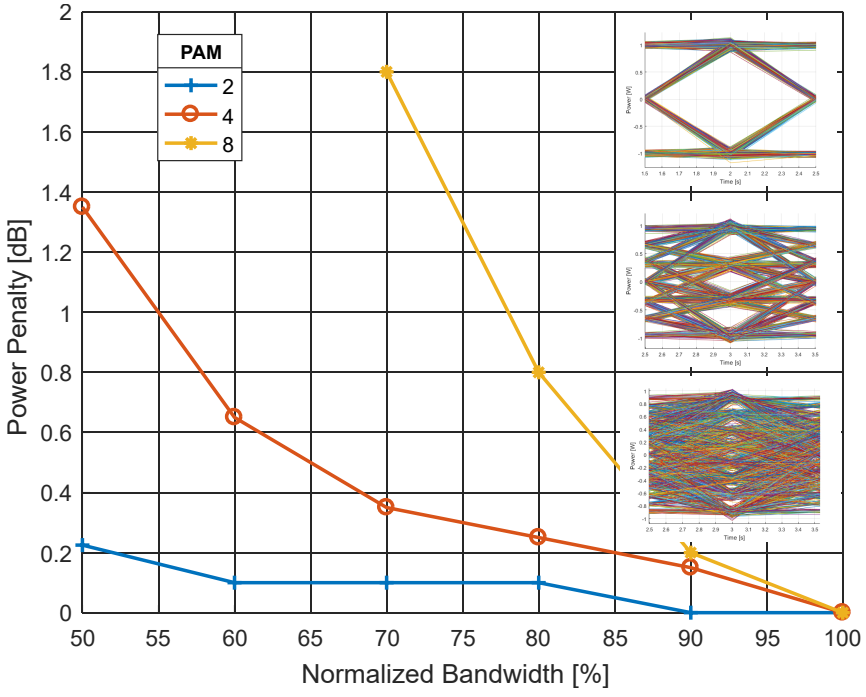

(b) $R_s = 25$ Gbaud

Fig. 4.9 Power Penalty vs. the normalized Tx/Rx electric bandwidth for PAM-n

For the two considered scenarios and three PAM levels, the ideal cases are listed in Sec. 4.3, the sensitivity values is considered as P_{ref} and consequently the power penalty due to the variation of the bandwidth is calculated as $P_{pen} = P_{sens} - P_{ref}$ dB, where P_{sens} is the required received power and is derived from results of Figs. 4.6, 4.7, 4.8

Fig. 4.9a refers to the power penalty for the same-R_b case. It shows that for PAM-2, even reducing NBW down to 50 % we observe a penalty limited only to 0.2 dB thanks to the equalizer. For PAM-4, with the decrease in NBW decrease P_{pen} grows quite regularly, for NBW = 50 % penalty approaches a maximum of 0.9 dB. A similar behavior is seen for the PAM-8 case down to NBW = 60 % while for narrower bandwidths P_{pen} increases more rapidly reaching 1.8 dB for NBW = 50 %. Power penalties for the given-R_s case are shown in Fig. 4.9b. Apart from the PAM-2, for which the two given-R_s and given-R_b cases coincides, the power penalty experienced for given-R_s is larger than the one observed for same-R_b.

Thanks to the equalizer, the impairment is limited for PAM-4 that can operate also at NBW = 50 % with a maximum penalty of 1.4 dB. On the other hand PAM-8 experiencing a BER *flooring*, limits the operation to a minimum tolerable NBW = 70 % corresponding to a penalty of 1.8 dB.

It is observed that PAM with more amplitude levels is more sensitive to bandwidth limitation. A specific case of NBW = 80% for all the considered scenarios under same operating conditions is shown in the inset of Fig.4.9. The eye closure with the increase in PAM level and the increase in the data rate confirms the increase in sensitivity with increasing PAM level due to the bandwidth limitations.

4.5 Results on performance effects of LMS taps

In the previous section, the investigation done was to analyze performance impairments due to the limited bandwidth. Then, the analyses was performed to evaluate the benefits of the equalizer vs. the number of FIR filter taps N_{taps}, i.e. to find the minimum N_{taps} still yielding performance advantages for the specific target BER.

For the bandwidth limitation study, a large number of taps was used for the FIR filter equalizer (N_{taps} = 39). Such a supposition was meant to discover strength of the equalizer, with a large number of N_{taps} ignoring the weaknesses of a limited length

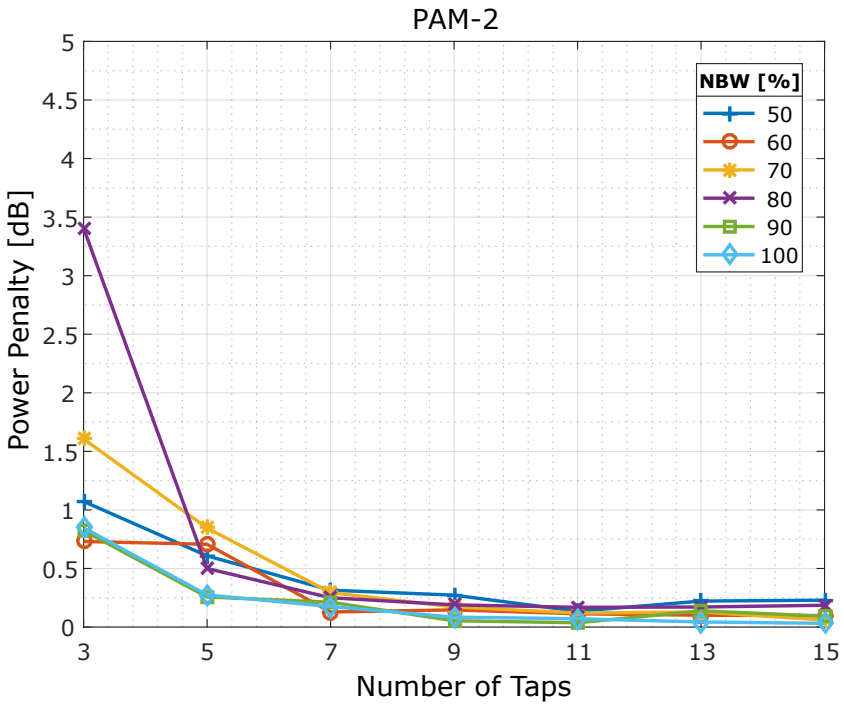

Fig. 4.10 Power Penalty vs. the number of equalizer taps for different value of normalized Tx/Rx electric bandwidth, for PAM-2 for the case of given-R_b $R_b = 25$ Gbps and of given-R_s $R_s = 25$ Gbaud

FIR filter. However, larger number of N_{taps} has some disadvantages, the latency increased with the number of taps – resulting in an increased DSP complexity. Presently latency is not a major issue for the state of the art FEC codes [49] that are largely dominant in terms DSP latency. Whereas with increased DSP complexity and associated power consumption, is certainly a critical issue for the considered scenario of low-cost and low-power equipment. So in this analysis, the power penalty vs. the number of equalizer taps is studied in order to find the minimum N_{taps} required still permitting the benefits shown in previous sections.

Similar to the analysis done for the bandwidth-induced penalties in Sec. 4.4, we refer to the sensitivity values for ideal cases listed in Sec. 4.3 for the evaluation of penalties due to the filter taps. Results are plotted in Figs. 4.10, 4.11 and 4.12 as P_{pen} vs. N_{taps}. Fig. 4.10 shows results for PAM-2 for which given-R_b and given-R_s cases overlap. For PAM-2, it is observed that for all the bandwidths down to NBW = 50 % the penalty is kept controlled under 0.2 dB using only 7 taps for the FIR filter equalizers. Since the DSP operates at 2 sample-per-symbol and N_{taps} = 7, using

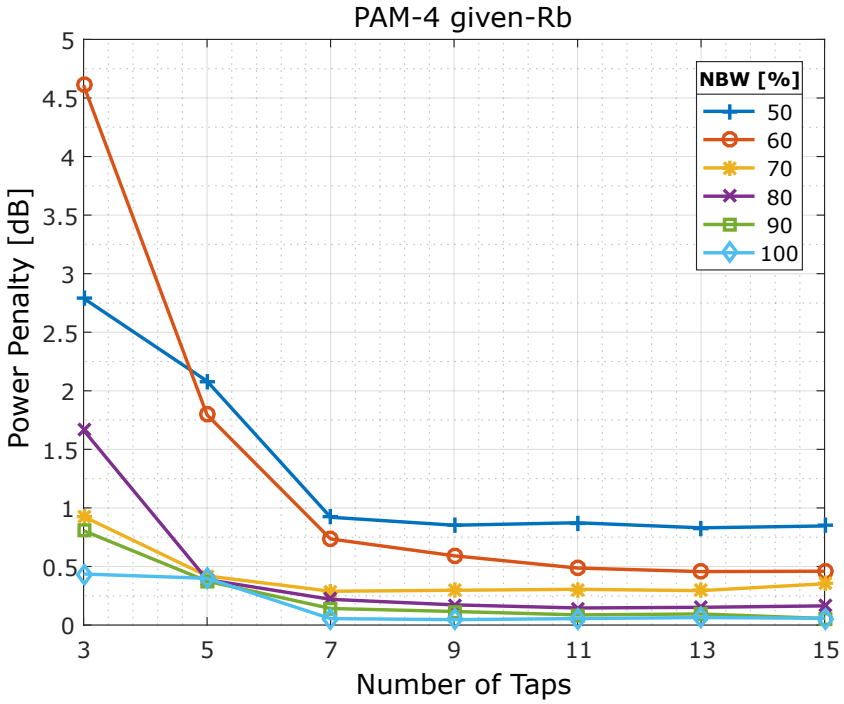

(a) $R_b = 25$ Gbps

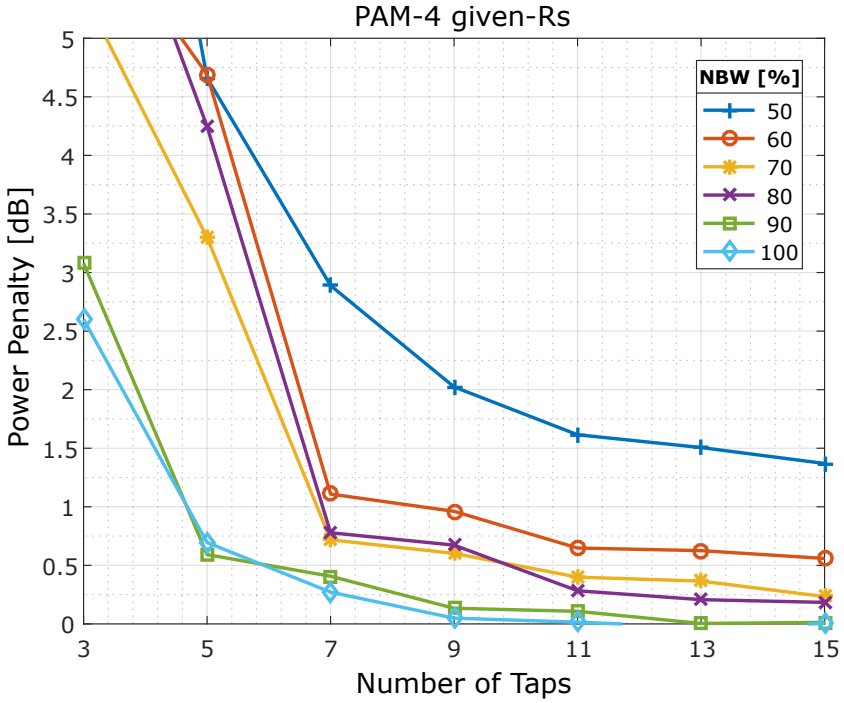

(b) $R_s = 25$ Gbaud

Fig. 4.11 Power Penalty vs. the number of equalizer taps for different value of normalized Tx/Rx electric bandwidth, for PAM-4 for the case of given-R_b $R_b = 25$ Gbps (a) and of given-R_s $R_s = 25$ Gbaud (b)

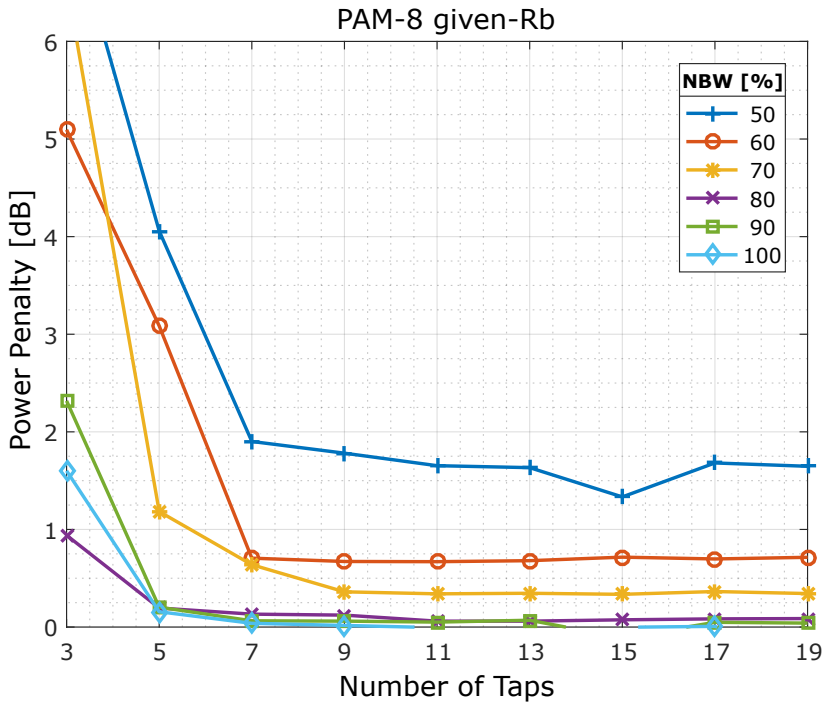

(a)

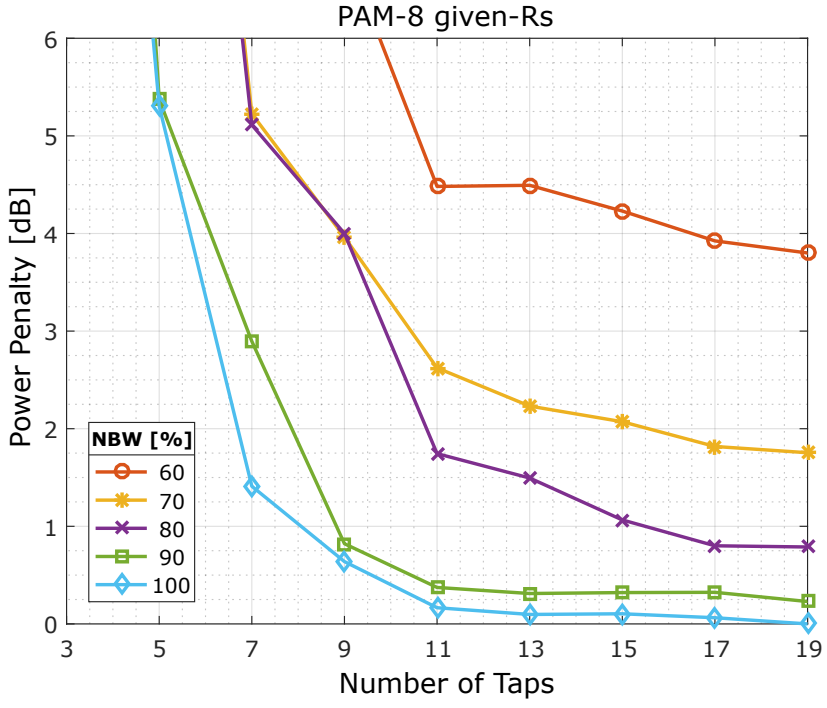

(b)

Fig. 4.12 Power Penalty vs. the number of equalizer taps for different value of normalized Tx/Rx electric bandwidth, for PAM-8 for the case of given-R_b $R_b = 25$ Gbps (a) and of given-R_s $R_s = 25$ Gbaud (b)

equation 4.15 introduces only 3 bits of additional DSP latency and it requires some degree of complexity and power consumption.

Fig. 4.11a and 4.11b displays results for PAM-4 for the same-R_b and same-R_s cases, respectively. With respect to the number of taps required to achieve the benefits of the equalizer, both cases perform alike indeed requiring only 7 taps to have the minimum penalty for each bandwidth limitation. For the PAM-4, from equation 4.15 7 taps results into 6 bits of DSP latency.

Lastly, results for PAM-8 for the same-R_b and same-R_s cases are presented in Fig. 4.12a and 4.12b, respectively. As it has been observed previously, higher number of levels implies a lower resilience to bandwidth limitations, that is more noticeable in the same-R_s case for which we observed also a BER *flooring*. In terms of required N_{taps} permitting the minimum penalty, PAM-8 with given-R_b requires a minimum of 9 taps that results into 12 bits of additional latency, while PAM-8 with given-R_s requires at least 19 taps implying 27 bits of extra latency.

For the hierarchy in families of curves referring to different bandwidth limitation shown in Figs. 4.10, 4.11 and 4.12 an intuitive behavior is observed, i.e. smaller the NBW, the larger the penalty. On the other hand, for some cases with a small number of taps, the observed behavior is not intuitive. More precisely, for some cases the exhibited behaviors of larger NBW is worse than the case with smaller bandwidths. This counter-intuitive behaviors i.e. worse performance for smaller taps with larger NBW can be explained as.

The LMS equalizer, tries to emulate an electric filter that is matched to the reference signal, so the larger NBW, larger the bandwidth of the required matched filter. So for a small number of taps, a matched filter implemented with a wide bandwidth pulse is not suitable resulting into uncontrolled results. e.g. Equalizer filters for PAM-2 using $N_{taps} = 3$ and $N_{taps} = 15$ is shown in Fig. 4.13a and Fig. 4.13b respectively. The proper-behavior case derived for $N_{taps} = 15$ is shown in Fig. 4.13b. It is observed that the equalization requires an appropriate emphasis for high frequency components for NBW upto 80 %. So for small number of taps, the required filter behavior cannot be satisfied which results in to driving the filter to an improper behavior leading to a strong filtering effects on low frequencies, therefore triggering a large penalty. Such a behavior is displayed in Fig. 4.13a and clearly explains results of Fig. 4.10.

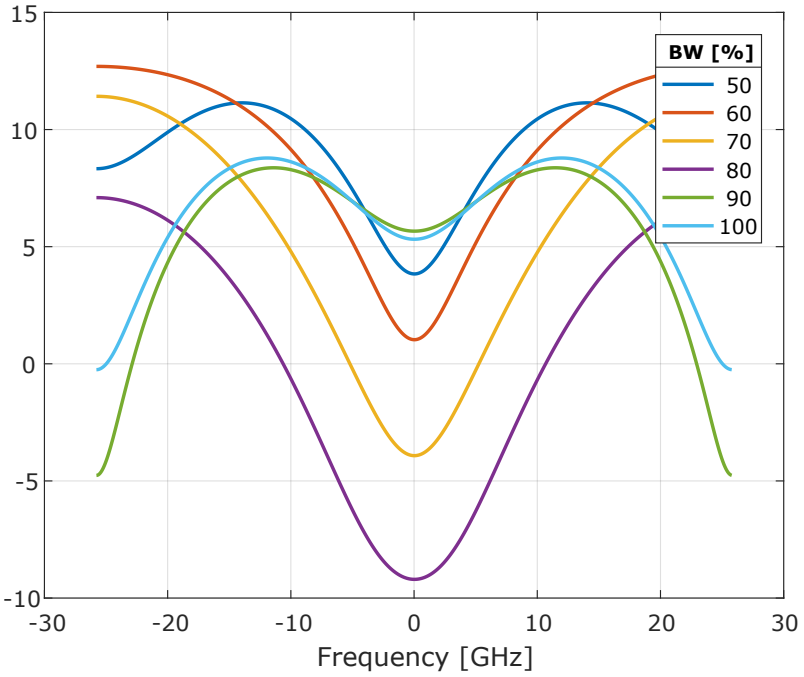

(a) Ntaps = 3

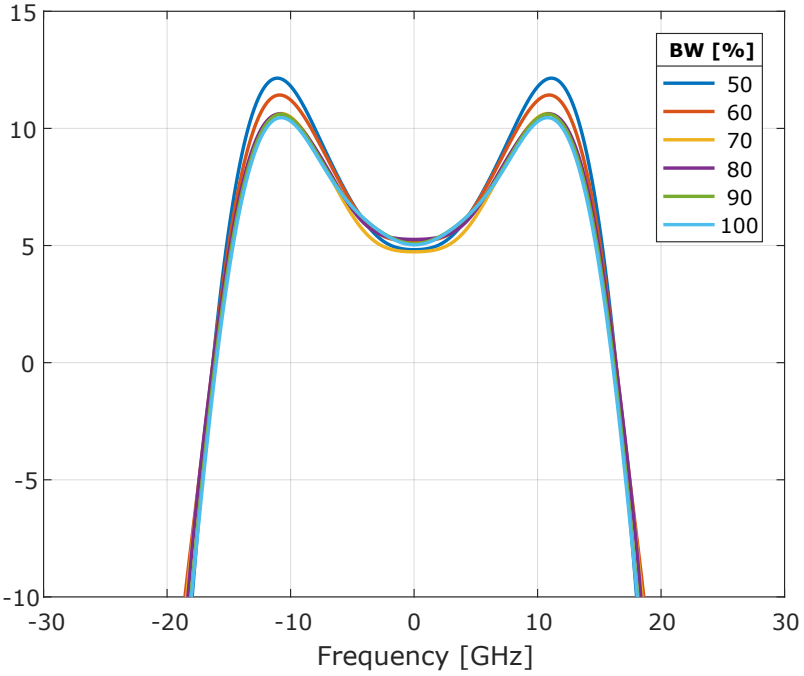

(b) Ntaps = 15

Fig. 4.13 Frequency response of the filter taps for the case of PAM 2

4.6 Conclusions

In this chapter, the performances of PAM-n with n = 2, 4 and 8 is studied, targeting short reach intra data-center transmission links. We used low extinction-ratio (6 dB) Mach-Zehnder modulator that is characterized for a silicon photonics devices at the transmitter. While at the receiver, FIR filter equalizer using training-driven LMS algorithm is used, allowing faster convergence and better BER. Two cases of given-R_b of 25 Gbps and of given-R_s of 25 Gbaud is analyzed. The system resilience to the electrical bandwidth limitations is studied. In the last section benefits of equalizer with respect to latency and system sensitivity is studied.

It is observed that PAM-2 and PAM-4 can operate with normalized bandwidth down to 50% requiring an equalizer of only 7 taps with a penalty of 0.2 dB for PAM-2, while 0.9 dB for the R_b and 1.4 dB for the R_s case of PAM-4. PAM-8 resulted to be the most intolerant to the bandwidth limitations. For the given-R_b case can operate with normalized bandwidth down to 50% using 9-tap FIR filter with a penalty of 1.8 dB. On the other hand for the given-R_s case, a BER *flooring* effect is seen restricting NBW down to 70% .

Chapter 5

Effects of Multipath Interference on PAM 4 Transmission

5.1 Introduction

As discussed in chapter 3 advanced modulation formats such as PAM, DMT and CAP are being studied for the 100G and 400G transmission. Both DMT and PAMn have been extensively investigated in IEEE but PAMn can address the typical optical channel without the need to go with more complex and higher power modulation schemes. To reduce the cost single laser and single receiver technique is being adopted. To reduce the number of fibers, advanced modulation such as 100-Gb/s (51.6-GBd) PAM4 are being considered by the IEEE 400 GbE Task Force [4]. At present, the market place lacks the equipment to generate 100-Gb/s PAM4 signals with sufficient reliability, the alternative is to use 100-Gb/s coherent DAC/ADC, which is designed for operation up to only 32 GBd instead of 51.6 GBd. The current optical links based on advanced modulation cannot rely on the historic IEEE link model spreadsheet [50]. Advanced models needed to account for

- Multi-path interference (*MPI*)
- Laser RIN
- Laser phase noise
- Nonlinear and dispersive fiber effects
- Limited loss budget

Multipath interference due to the connectors is the key limitation to advanced modulation format. A large variation in the penalties has been observed depending on the assumption. Lack of the test equipment and realistic tools to model the impairments are the main obstacles for the standardization process. MPI was the subject of the investigation some years ago. Some of the approaches investigated were

- Gaussian interferometric noise model [51]
- Fully additive interferometric effects [52]
- Etalon Model of cascaded patch cords

Current MPI investigation suggested that the result are closely approximated the Gaussian model [53]. The Gaussian approximation of MPI penalty shows a reasonable match as the number of connectors increases. With the current interest in advanced modulation formats, a detailed analysis is required since multipath interference can significantly increase and is the limitation to advance modulation format.

In the subsequent sections, we have presented the simulation of 100Gbps PAM4 link, using a realistic silicon based transmitter, bidirectional single and double link fiber plants. The study was done to investigate the effect of MPI, RIN, laser phase noise, nonlinear and dispersive fiber effects on the end to end link BER.

5.2 Multipath Interference

Multipath interference is caused by the interference of a multiple reflected signals interfering with the original / direct signal such that the reflected signals have a time delay greater than the bit period. Multiple paths hence MPI is introduced into the transmission path mainly of two reasons

- Discrete reflection sources
  Interference due to discrete reflections from connectors , components and patch panel pairs.

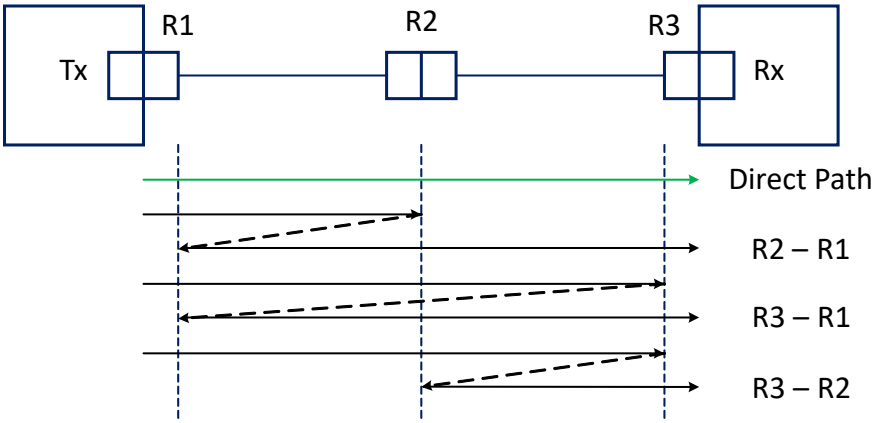

Fig. 5.1 Illustration of MultiPath Interference

- Double Rayleigh scattering
  Interference due to distributed reflections from double Rayleigh scattering (*DRS*).

The receiver receives the sum of all the reflection that combines with the intended signal as shown in Fig. 5.1 and the total MPI is the sum of all the reflectances given by

$$MPI_{total} = \sum_{i=1}^{M} \sum_{j=i+1}^{M} R_i R_k \tag{5.1}$$

The amount of reflected light in an intended signal is given by the ratio of the double reflected power $P_{s,DRS}$ traveling in the direction of the signal, and the power in signal P_s, using the MPI noise ratio

$$MPI_{nr} = \frac{P_{s,DRS}}{P_s} \tag{5.2}$$

The phase relation of the incoming and the reflected signal is important to know as the amplitude of the total signal depends on the phase difference between the two. If the incoming light is not monochromatic or have same frequency, the phase difference will result into time- and frequency-dependent noise source and decide the total amplitude.

5.3 System Design

The architecture of the 100 Gb/s PAM4 link configuration considered for the analysis is shown in Fig. 5.2. The transmitter uses an optical DAC approach, wherein two PAM-2 signal streams are combined into one PAM-4 signal at the optical element. This can be accomplished via parallel weighted electrical drivers or series weighted optical modulation, and is advantageous when compared to an electrical DAC approach as it allows for non-linear optical drivers. The implementation uses a two-input Mach Zehnder Interferometer (*MZI*) to accomplish this, driven by inverter-based CMOS limiting amplifiers. The MZI also has a single optical input, where it receives a non-modulated continuous wave light source. At the output of the transmitter, we have a 1310-nm, 51.6-GBd optical signal with 52,000 bits and an average launch power of approximately -0.5 dBm. The RIN of the laser is set to -142 dB/Hz with a linewidth of 100-MHz.

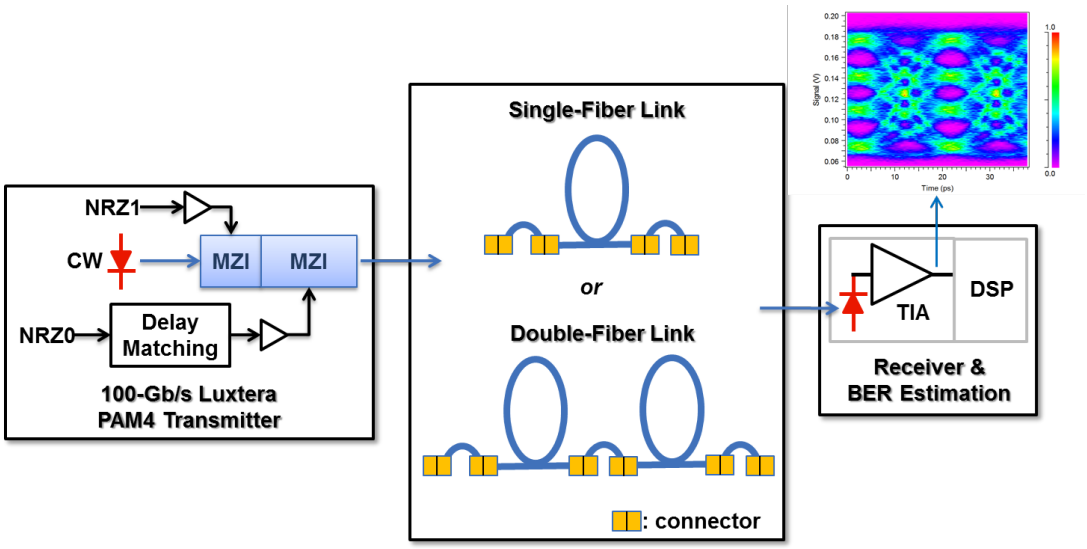

Fig. 5.2 100-Gbps PAM4 link architecture with simulated receiver front-end eye

After the transmitter, the PAM4 signal propagates through the fiber cable plant based on a single link (*SL*) or a double link (*DL*) with Lucent Connector (*LC*) and Multiple Fiber Push-On/ Pull-off (*MPO*) connectors [41], which are the most widely deployed connectors in data centers. The single-link plant includes one transmitter optical sub-assembly (*TOSA*) connector, a pair of 2-m patch cords, two mid-span connectors which can be LC or MPO, and a receiver optical sub-assembly (ROSA) connector. In comparison, the double-link plant includes two additional mid-span

connectors and an additional patch cord between the two links. We assume 20 dB of return loss (*RL*) at the TOSA and 26 dB at the ROSA. As for the mid-span connectors, we assume an LC return loss for legacy installations equal to 26 dB, and 35 dB otherwise. Since all single mode MPO connectors are angled polished, MPO connectors have RL better than 55 dB. In addition, we assume 0.5 dB of insertion loss
cord loss, for the single link this corresponds to a total loss of 2.25 dB and 3 dB for the case of 500 m and 2000 m respectively. While the total loss for the double link corresponds to 3.25 dB and 4 dB at 500 m and 2000 m respectively. Finally, as a worst case, we suppose a standard deviation of 0.25 dB in the connector IL and RL values, an amount typically associated with MPO connectors [41]. A Picometrix (PT-40D/8XMLD) receiver having 32 GHz bandwidth and a sensitivity of -9 dBm at 10^{-12} BER (40-GBd OOK) is used as the PIN/TIA receiver front-end.

The demonstrated front end has a sensitivity of –7.8 dBm AOP at 10^{-12} BER (51.6-GBd OOK) and the sensitivity at the FEC limit of $5 \cdot 10^{-5}$ was -10.8 dBm AOP, Where we assume IEEE 802.3bj KR4 FEC [54] using RS(514, 528) with 3.125 % overhead and a gain of about 5.7 dBe. An example of a simulated eye at the output of the receiver front-end electronics for the case of a 500-m double link with 60-dB of RL per mid-span connector is shown in Fig. 5.2. The output of the receiver front end is passed to the DSP unit that consists of a typical LMS based DSP equalizer applied during the training phase [55]. The DSP is operating at 2 samples per symbol, for the FIR filter 11 taps are used in addition to the optimal decision thresholds. The received signal is characterized using the decision thresholds. The BER is consequently evaluated with a semi-analytical technique. Using such techniques, we can estimate performance down to very low BER values. The combined electrical-optical modeling of this architecture begins with a Luxtera-proven PDK-based simulation of the transmitter. Modeling of the cable plant and front-end receiver electronics is achieved by loading the transmitter waveform into Synopsys' RSoft OptSim and performing a bidirectional time-domain simulation. Laser RIN and phase noise are incorporated into the optical signal waveform, which is then transmitted through the cable plant, incorporating the effects of MPI, nonlinear and dispersive fiber effects and passive loss. The receiver front-end converts the signal to the electrical domain and is passed to MATLAB for the offline processing.

5.4 BER vs Link length

In the first study, we analyzed the effect of total link length (ignoring the patch cords) on the BER for three nominal cases: (i) legacy single link with 26-dB mid-span connector return loss, (ii) double links with 35-dB RL and (iii) double link with 60-dB RL per connector as shown in Fig.5.3. We see that the BER in all three cases is below 10^{-5} even at a 5000 m. Due to high MPI single link case is performing worse when compared to the double link cases for a link shorter than 2000 m. While at longer distances the passive loss of the transmission and thus noise at the receiver, dominates the performance, with the single-link plant and its lower connector count performing better than the double link cases.

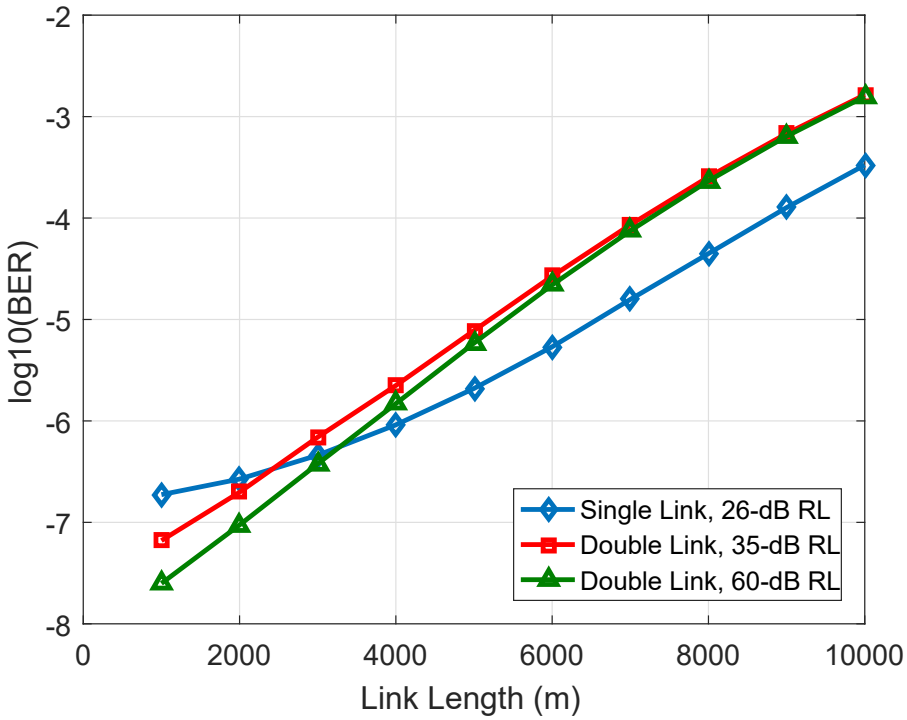

Fig. 5.3 BER vs Link Length

5.5 BER vs Mid-span connector return loss

Fig. 5.4 displays mid-span connector RL effect on BER for both the single and double link plants. The link length considered for the simulation is 500 m and 2000 m. It is observed that for low values of RL the MPI is mainly effecting the performance. Increasing RL reduces the effect of MPI and the dependence of BER increases on total link length and connector count (i.e. passive loss and receiver noise). For the double link in order to perform below a BER of 10^{-5} non legacy connectors are required.

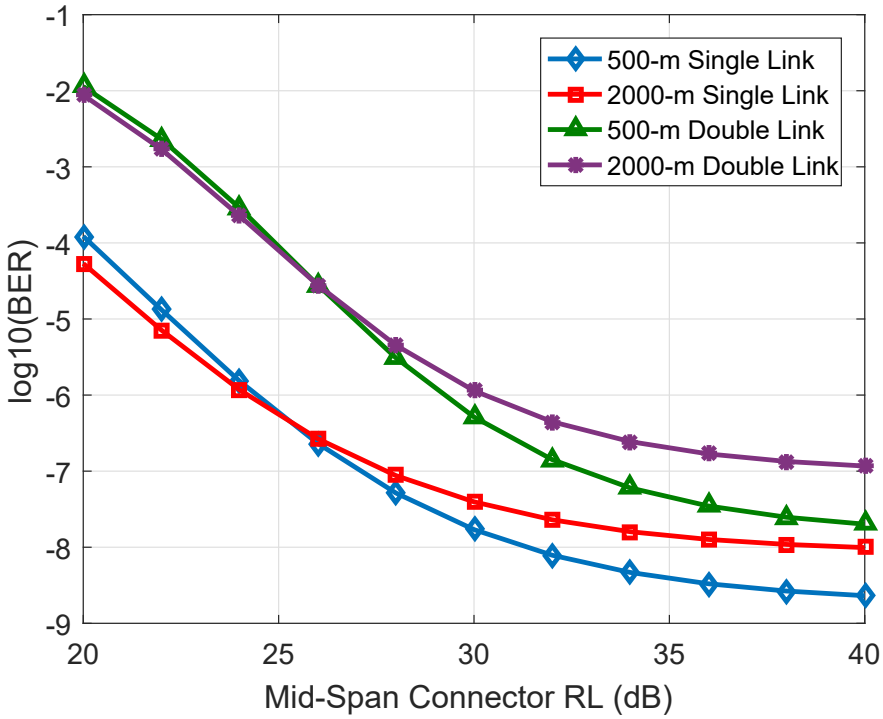

Fig. 5.4 BER vs mid-span connector RL

5.6 BER vs RIN

Fig. 5.5 depicts BER versus laser RIN for the three nominal cases of Fig. 5.3 at 500 m and 2000 m. BER performance converges at large RIN levels, especially above -135 dB/Hz.

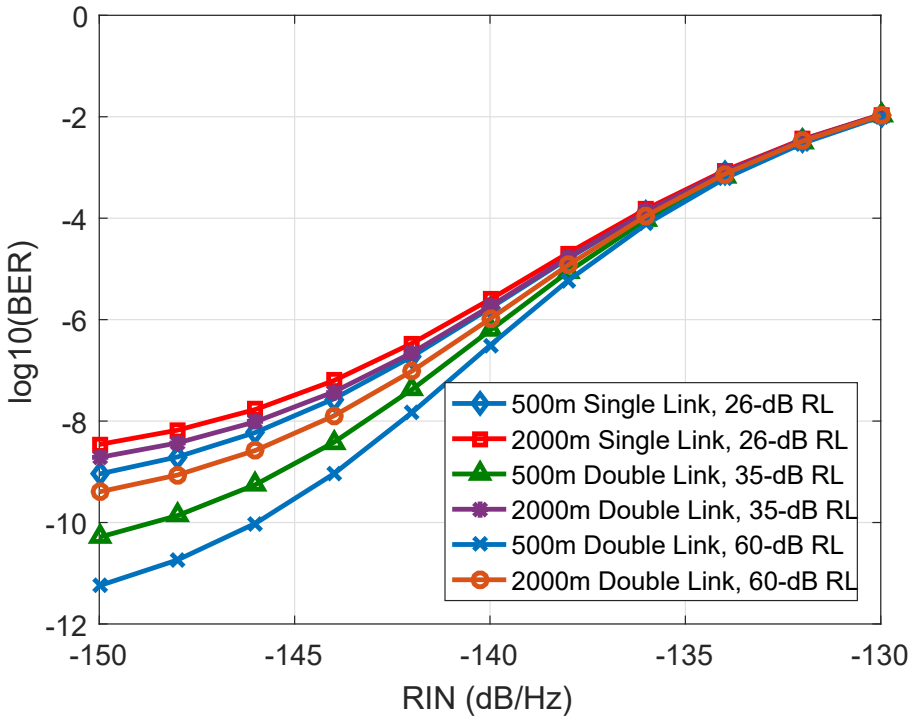

Fig. 5.5 BER vs laser RIN for different cable plants

5.7 BER vs Fiber delay variation

In order to evaluate the impact on MPI of overlapping bits between signal and reflection, the length of the fiber was adjusted such that the propagation delay between adjacent connectors is a multiple of a half bit period. So that the total round trip time is equal to a bit period, maximizing the bits overlapping. The results for the cases considered for 500 m single link and 2000 m double link are shown in Fig. 5.6a and 5.6b respectively. Therefore, by using the conditions described above, the delay can be adjusted, maximizing the MPI. It is observed from the results that the BER is minimized when the patch cord delay offset is set to a quarter of the bit period. For double link case with mid span connector RL of 60 dB the maximum value is not at a multiple of half a bit period. Due to the numerical simulation artifact, a small discrepancy in the BER values is also noted.

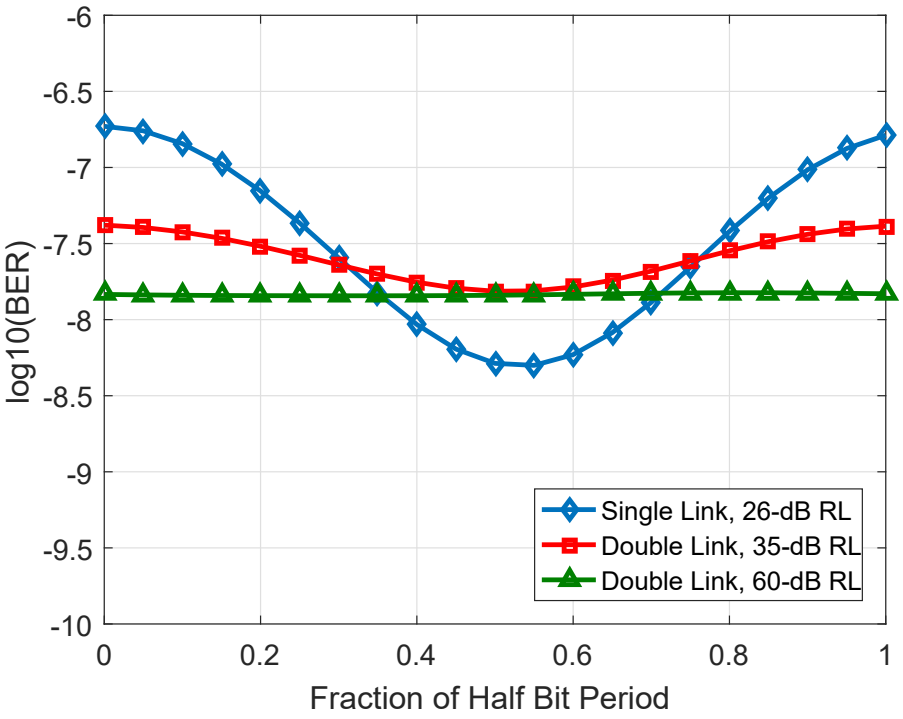

(a) Patch Cord length 500-m

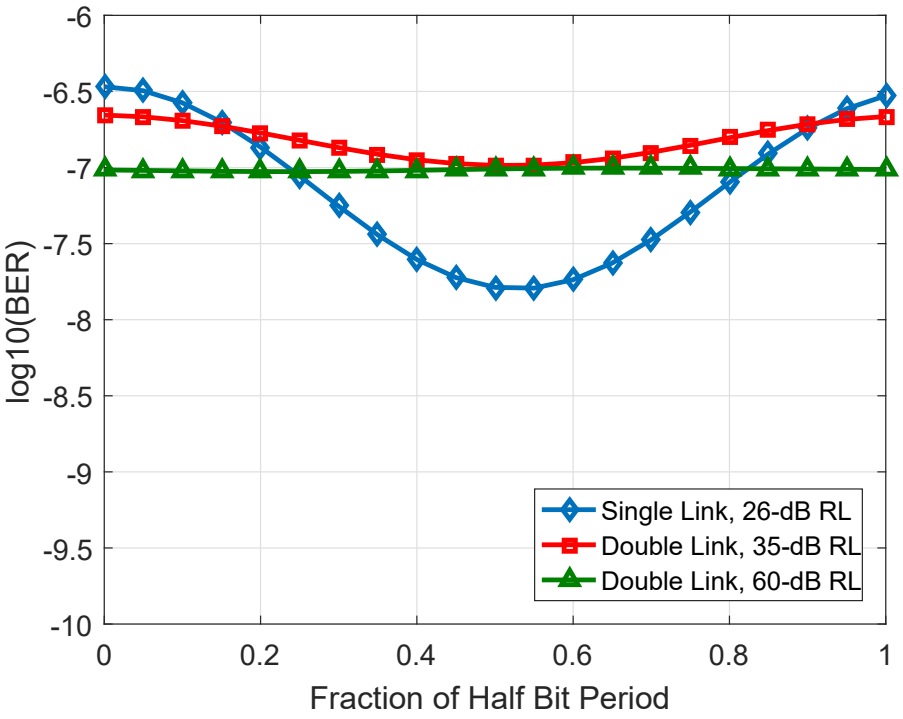

(b) Patch Cord length 2000-m

Fig. 5.6 BER as a function of variations in the delay of the first patch cord over half a bit period

5.8 Monte Carlo Simulation for BER variation

Lastly, we did the Monte Carlo simulations in order to know the effect of statistical variations in connector IL and RL, a total of 50 simulations were performed using the cases (i) single link with 26 dB RL, (ii) double link with 35 dB RL and (iii) double link with 60 dB RL. The result for the link length of 500 and 2000 m are shown in Fig. 5.7, 5.8 and 5.9. It has been observed that the BER for all the considered cases is below 10^{-5}. Secondly, the BER variation for 2000 m is larger than for 500 m. Similarly, the BER variation in double link is more than the single link due to additional connectors in the double link cases.

5.9 Conclusions

We have shown that 100-Gb/s PAM4 transmission based on traditional single-link (26 dB mid-span connector RL) and newer double-link (35 and 60 dB mid-span connector RL) fiber cable plants can achieve a BER below 10^{-5}. We have observed the sensitivity of these implementations to MPI and seen its overall impact on performance in relation to passive loss and RIN. This substantial implementation of PAM4 based on a cascaded Silicon modulator provides tolerable margin to support additional implementation penalties such as clock and data recovery and margin for timing recovery

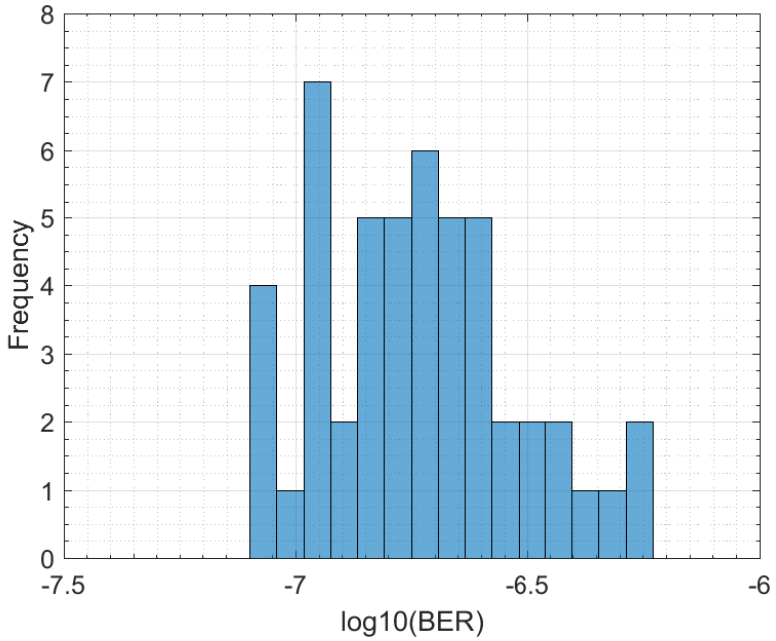

(a) 500-m Single Link, 26 dB RL

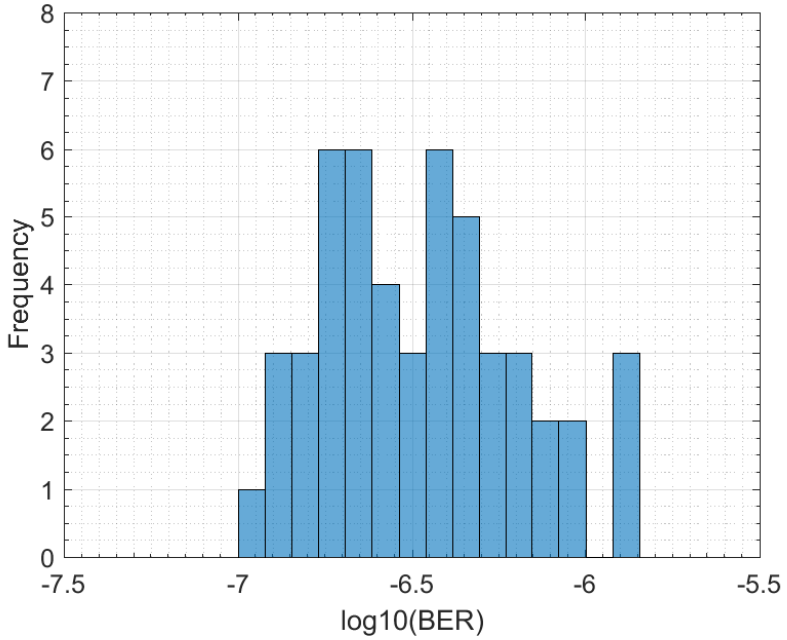

(b) 2000-m Single Link, 26 dB RL

Fig. 5.7 BER distribution during Monte Carlo simulations for single link plant with 26 dB RL

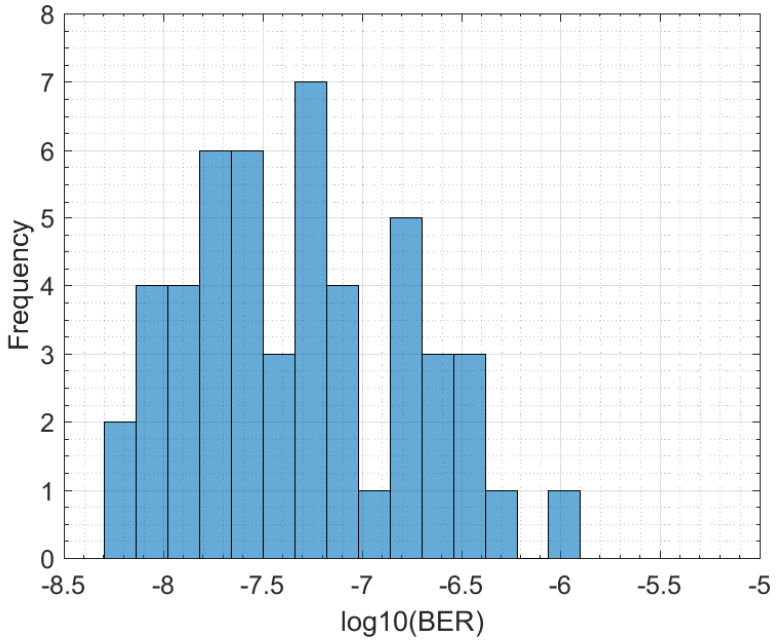

(a) 500-m Double Link, 35 dB RL

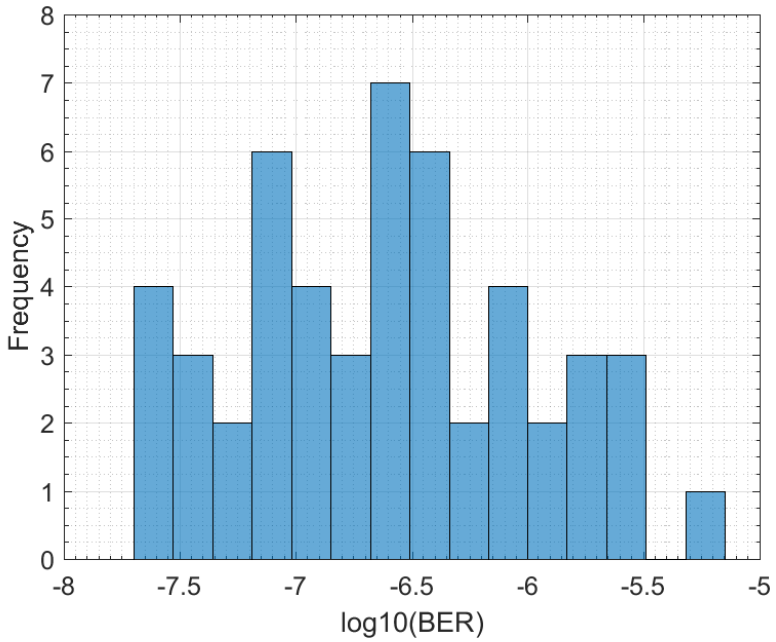

(b) 2000-m Double Link, 35 dB RL

Fig. 5.8 BER distribution during Monte Carlo simulations for Double link plant with 35 dB RL

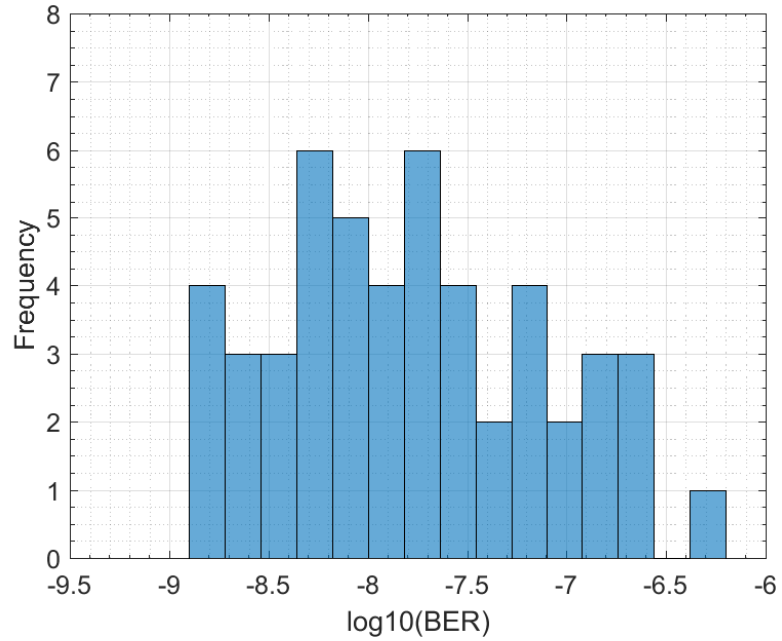

(a) 500-m Double Link, 60 dB RL

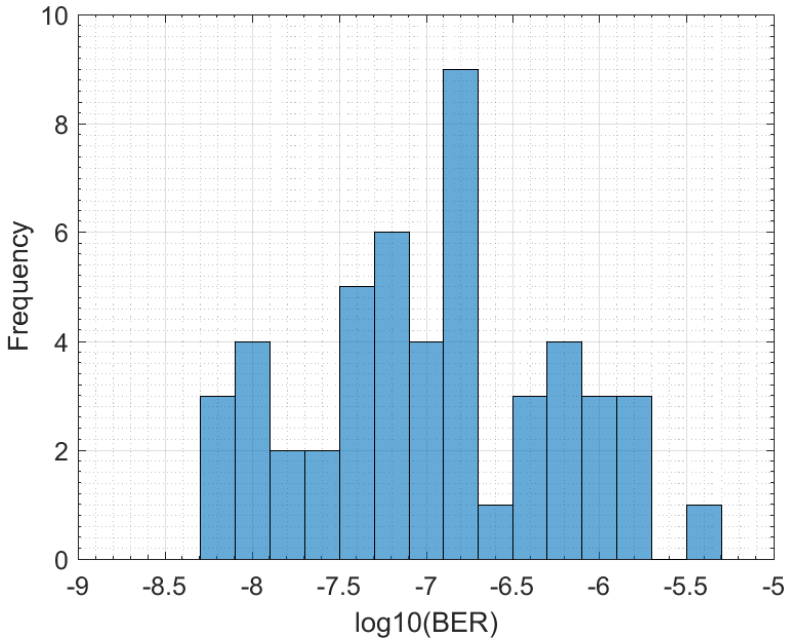

(b) 2000-m Double Link, 60 dB RL

Fig. 5.9 BER distribution during Monte Carlo simulations for Double link plant with 60 dB RL

Chapter 6

Analysis of Forward Error Correction for PAM 4

6.1 Introduction

Over the years the data traffic has increased significantly, due to the ever bandwidth demanding applications like streaming videos, social networks etc.. According to CISCO, the intra data center traffic will grow at a rate of 24% [1]. So it is required to increase the capacity of the optical networks. Due to this dramatic improvement in traffic demand in local area networks, IEEE 802.3bs 400 GbE task force has proposed 100 Gbps and 400 Gbps standards [4]. Contrary to scenarios of high-capacity back-bone networks, cost, complexity and power consumption are the three main issues driving the technological choices for intra data-center transmission. So, the use of coherent receivers based on the need of a local oscillator and quite complex high-speed digital signal processing has been so far discarded and transmission techniques based on direct-detection-based receivers have been taken into account. Some amount of DSP is in any case used, also in this transmission scenario. In particular, forward error correction coding is considered with a limited overhead. Different FEC options have been proposed by the IEEE study groups targeting 100GbE and 400 GbE with the maximum allowed latency [49]. Using FEC codes, implies in any case a large latency of the order of thousands of bits, already introduced by a light code with 3% overhead [49]. Consequently, for intra

data-center transmission simple DSP operations at the receiver are not introducing major excess latency as well as relevant additional power consumption.

6.2 Forward Error Correction

The main concept of Forward Error Correction code is to add extra / redundant code in the original signal to detect and recover the errors added during the transmission at the receiver. Doing so a part of the effective transmission rate is reduced. Based on the presence or absence of memory the FEC codes are divided into two categories

- Block code
  Block codes are memoryless and work on a predefined fixed block size. Since they are memoryless, information about the previous block is not stored, the output depends on the current block only. Some of the example of block codes are Reed–Solomon codes, Reed–Muller codes, Hamming codes etc.
- Convolutional code
  The output of Convolutional coder not only depends on the current input but also on the previous so they have memory. Unlike block code the block size in not fixed. It works on the serial input stream. Since the sample points for processing are less than block code, the encoder has relatively less delay.

6.2.1 Reed–Solomon codes

Reed–Solomon (RS) codes are the linear block codes used to correct the errors. RS codes can be used to correct both random and burst errors. The correction is done by adding redundant symbols with the transmitted sequence. Reed–Solomon codes are represented as $RS(n,k,t,m)$, where n is the code word with k data symbols, $n-k$ redundant / parity symbols and m is number of bits per symbol. The code rate R is given by k/n. The code can correct up to t symbols where $2t = n-k$. RS FEC options currently considered by the IEEE 400GbE Ethernet Standard are shown in Table 6.1.

The performance of a given code is measured by the reduction of optical signal-to-noise ratio for a given bit error rate due to the addition of the extra bits and is

Table 6.1 Summary of RS FEC Options (KR4) [49]

RS FEC (n,k,t,m)	NCG	BERin	Overhead	SerDes Rate	Latency
RS FEC (528,514,7,10)	5.28	3.92e–05	0%	25.78125	87 ns
RS FEC (544,514,15,10)	6.39	3.09e–04	3.03%	26.5625	112 ns
RS FEC (560,514,23,10)	6.93	7.60e–04	6.06%	27.34375	208 ns
RS FEC (576,514,31,10)	7.26	1.30e–03	9.09%	28.125	258 ns

known as the *Coding Gain*. For example from table 6.1 using RS(544,514) a coding gain of 6.39 dB is defined for 100 GBASE-KP4 and 802.3bs 400 GbE. Coding gain can allow additional system margin that can be used to increases the reach or the bit rates etc.

Block codes are usually decoded using *Hard decision* techniques while convolutional codes use *Soft decision* techniques. The hard decision requires single quantization level for decoding the output while in soft decision $2N-1$ thresholds are used for the decision (where N is the number of quantization bits). Increasing the number of thresholds increase the reliability of the decision. But still, they are not very common due to processing complexity and cost of AD converters.

With the increasing data rate, the FEC should also perform in a way to be able to detect and remove the impairments. But all this comes at the cost of extra symbols leading to the latency and additional system complexity. So in short reach optical links power consumption, added latency and the system complexity are the main considerations.

6.3 Setup and analysis

The simulative setup block diagram used for the PAM-4 analysis is shown in Fig.6.1 . At the transmitter (Tx) side, a pseudo random sequence with degree 17 is used to generate the logical data, that are fed to the digital signal processing block. The data are properly mapped and sent to the digital-to-analog converter that drives a Mach-Zehnder modulator with extinction ratio (ER) of 6 dB. The DAC operates using 10 bits to avoid quantization noise. Thus, the only limiting factor at the Tx side is given by electrical bandwidth limitations of the components. The DSP algorithms are working at 2 samples per symbol (SpS). Pre-emphasis filtering is used to neutralize

unwanted DAC effects. Similarly, the sinusoidal electro-optic transfer function of the MZM is pre-compensated. The receiver Rx consists of a PIN photodetector with responsivity R = 0.7 A/W, followed by a trans-impedance amplifier, with transimpedance $Rt = 285\Omega$, and input-referred noise factor of $32pA/(Hz)1/2$. The Optical-to-Electrical conversion performed through the PD introduces shot-noise, whereas thermal noise is generated by the TIA. The bandwidth of the PD for the OE conversion is set to the symbol rate consequently avoiding the need for an anti-aliasing filter

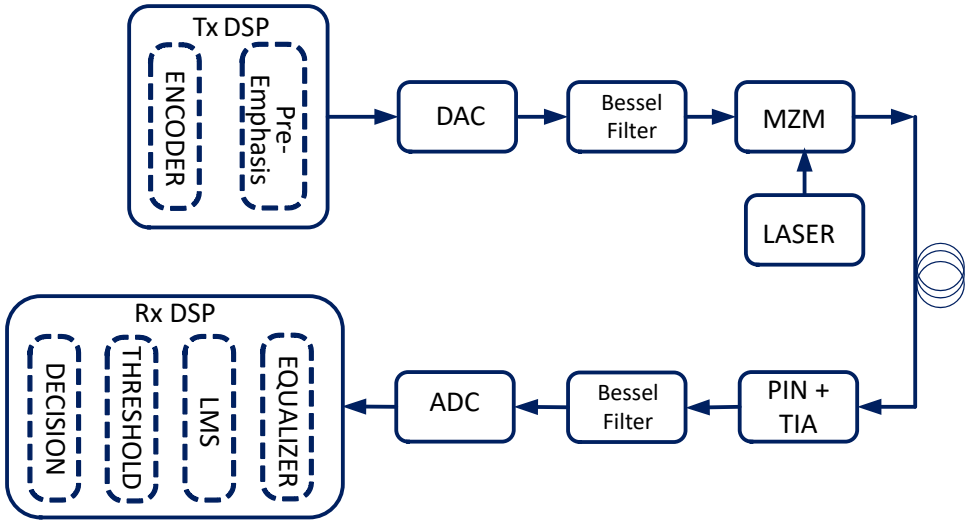

Fig. 6.1 Block Diagram of the Simulative setup

The analog electrical signal after the OE stage is converted to the digital domain by an analog-to-digital converter (ADC) working at 2 SpS and using 10 bits. At the Rx DSP a training-driven feed forward equalizer and a decision thresholds algorithm are used to process and return the data based on hard-decision. The received and the transmitted data sequences are compared and error counting is performed. The equalizer consists of a FIR filter, whose coefficients are defined during the training phase through the least-mean square algorithm. The algorithm introduces a latency of

$$T_L = \frac{1}{SpS} \cdot (N_{taps} - 1) \cdot T_s \tag{6.1}$$

where N_{taps} is the number of equalizer taps and Ts is the symbol duration. The hard-decision algorithm uses the training sequence to calculate the symbol thresholds

starting from the most significant bit to the least-significant bit. After the training phase, the decision is applied to the received bits comparing the equalized signal with the previously defined threshold.

We consider PAM-4 modulation with symbol rate Rs = 50 GBaud, corresponding to a bitrate of 100 Gbps. We consider two different cases with FEC OH = 3 % and 12 % and for three different target pre-FEC BER levels: BER1 = 10^{-2} , BER2 = 10^{-3} and BER3 = 10^{-4}. We study the Rx sensitivities required to achieve these target BER levels for different Tx/Rx BW limitations and number of FFE taps. We used a number of taps ranging from 3 to 15, corresponding to a maximum DSP excess latency of 7.5 bits, requiring limited additional complexity and power consumption. The considered Tx/Rx electrical bandwidth ranges from 30 to 40 GHz.

6.4 System Results

As reference scenario, we consider a Tx/Rx BW-limited at 100 GHz and a DSP FFE made of 39 taps. Fig. 6.2 shows the achievable BER vs received power for this scenario. We use this result to derive reference sensitivities - i.e. the power levels required to achieve the different BER targets – that are then used to understand the impact of the number of taps of the FFE for different bandwidth limitations. The power sensitivities observed are -4.5 dBm, -3 dBm, -2 dBm and -4.25 dBm, -2.9 dBm, -2 dBm for the case of 3 % and 12 % OH case respectively for the three BER targets.

Fig. 6.3 and Fig.6.4 show the sensitivity vs. electric bandwidth BW limitation attainable for the different number of FFE taps for the three considered BER targets for the two cases with FEC OH of 3 % and 12 % respectively. A considerable sensitivity penalty can be observed with respect to the reference scenario, for all the considered Tx/Rx BWs for all the studied BER targets. However, such penalty can be partially mitigated by using a properly sized FFE. Using the largest number of taps considered in this paper (i.e. 15), the smallest BWs that can be used in Tx/Rx are 31.25 GHz, 32.5 GHz and 33.75 for the BER1, BER2 and BER3 respectively for both cases. From Fig. 6.3 the power sensitivities for the target BERs are 1 dBm, 4.25 dBm, and 4.25 dBm respectively, corresponding to sensitivity penalties with respect to the reference BW=100 GHz, 39-taps systems of 5.5 dB, 7.5 dB and 6.25 dB.

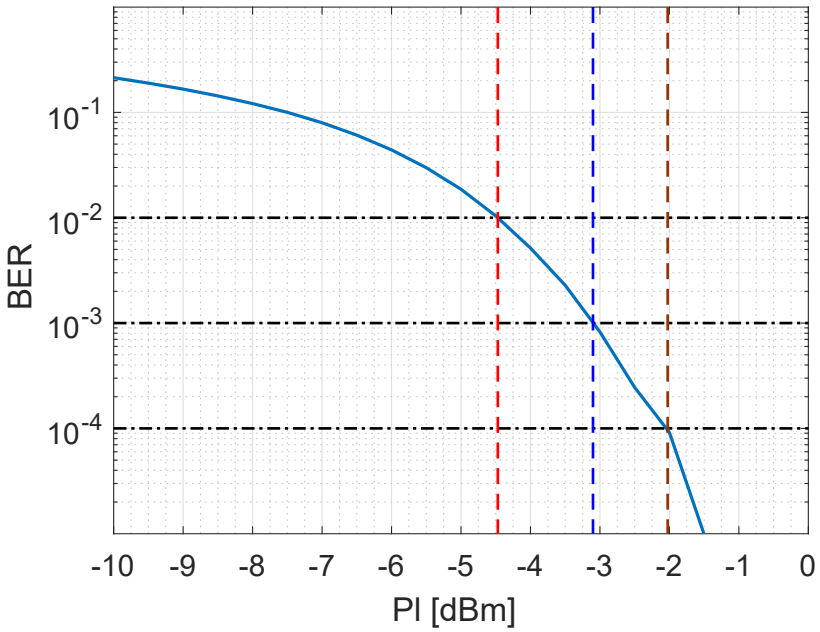

Fig. 6.2 Reference Sensitivity for 100G PAM4

Enlarging the Tx/Rx BW allows decreasing such penalties: having a Tx/Rx with a BW of 40 GHz allows to achieve sensitivity levels of -3.25 dBm, -1.25 dBm, and 0 dBm for target BERs of 10^{-2}, 10^{-3} and 10^{-4}, using a 15-taps FFE. These power sensitivities correspond to a sensitivity penalty with respect to the reference scenario of 1.25 dB, 1.75 dB and 2 dB respectively.

In the BW range between 33.75 GHz and 40 GHz, it is possible to trade-off sensitivity performance with FFE delays. Moreover, it can be also observed that relaxing the BW constraints, the sensitivity variation ranges for different FFE solutions decreases. For example, considering Fig. 6.3a, that refers to a target BER of 10^{-2}, we can observe that using Tx/Rx with a BW of 33.75 GHz, decreasing the FFE size from 15 taps to 7 taps yield a sensitivity variation of 4.25 dB, moving from -1.75 dBm for the 15-taps FFE to 2.5 dBm for the 7-taps FFE. For this BW limitation and relatively modest pre-FEC BER target, a 5-taps FFE cannot be used. Loosening the Tx/Rx BW constraints allow achieving better results. Considering a Tx/Rx BW of 36.25 GHz allows to achieve sensitivities in the range from -3.25 dBm to -2.5 dBm, when using a 15-taps FFE and a 5-taps FFE respectively. For the largest Tx/Rx BW considered in this paper (i.e. 40 GHz), allows achieving sensitivities that are almost independent on the number of FFE taps in the range from 15 to 7 taps.

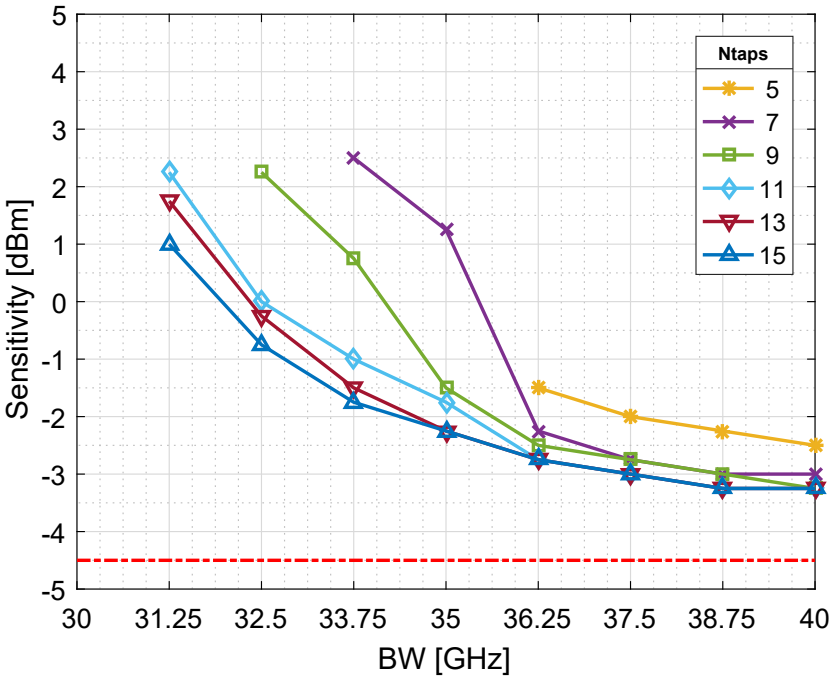

(a) Target BER 1e–2

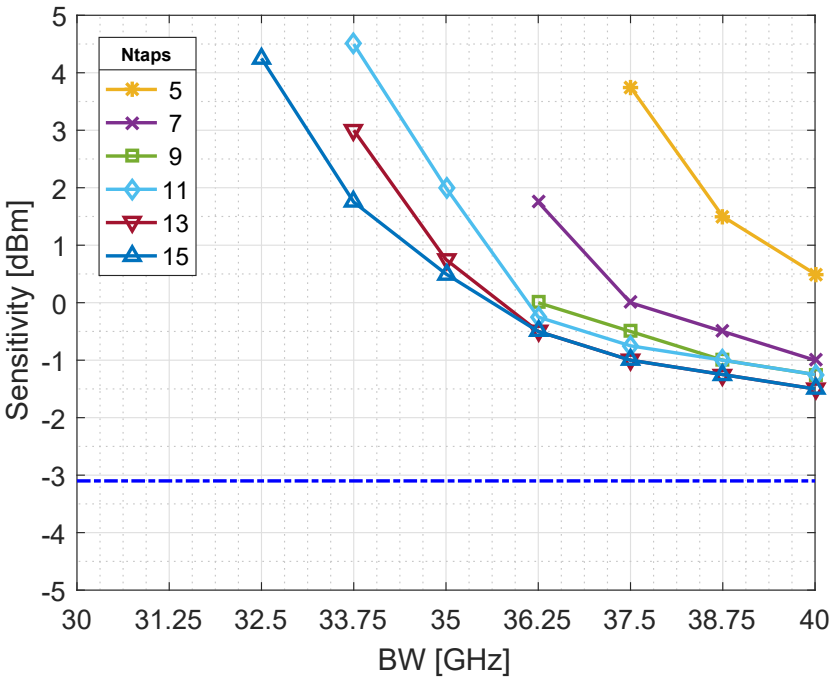

(b) Target BER 1e–3

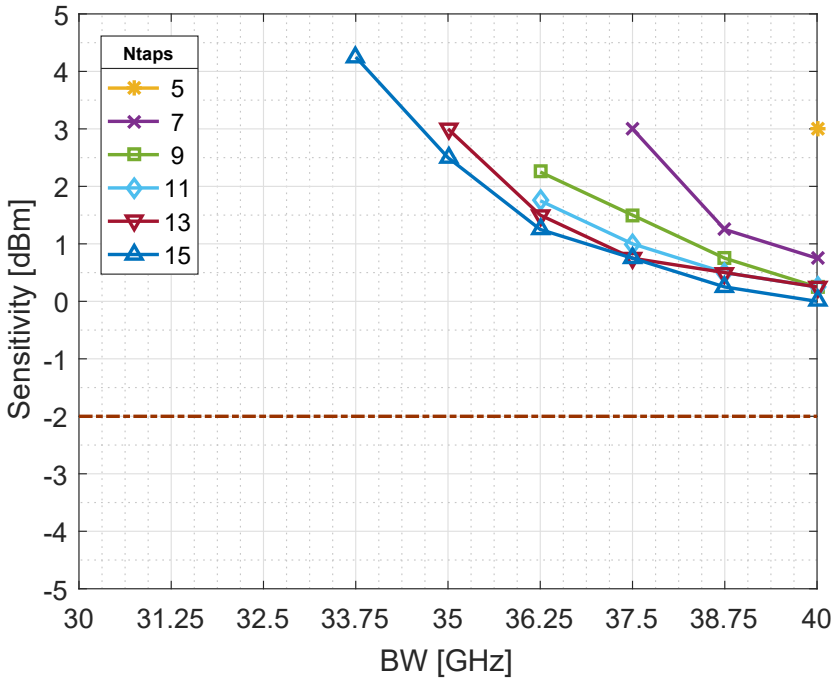

(c) Target BER 1e–4

Fig. 6.3 Sensitivity vs. the Tx/Rx electric bandwidth with 3% FEC OH

Similar results hold also for more demanding BER levels like the one considered in Fig. 6.3b and Fig. 6.3c. Using Tx/Rx with BW limited to 36.25 GHz, requires the adoption of FFE with taps number in the range between 7 to 15 for a BER target of 10^{-3} (Fig. 6.3b) and in the range 9 to 15 for a BER target of 10^{-4} (Fig 6.3c). The corresponding ranges of variation of the power sensitivity are between -1.5 dBm and 1.75 dBm for BER target 10^{-3} and 1.25 dBm and 1.5 dBm for BER target 10^{-4}.

In all the considered BER target scenarios, the BW range in which the lowest delay 5-taps FFE equalizer can be used are quite limited. For a target BER of 10^{-2}, a 5-taps FFE allows working with Tx/Rx with BW limited in the range between 36.25 GHz up to 40 GHz with a sensitivity ranging from -1.5 dBm for 36.25 GHz to -2.5 dBm for BW of 40 GHz. For a BER target of 10^{-3} the acceptable BW range shrinks down to the 37.5 GHz to 40 GHz range, with sensitivity ranging from 3.75 dBm to 0.5 dBm respectively. For a BER target of 10^{-4}, Tx/Rx pair with 40 GHz BW can be used with a 5-taps FFE, however with an unreasonable high sensitivity of 3 dBm.

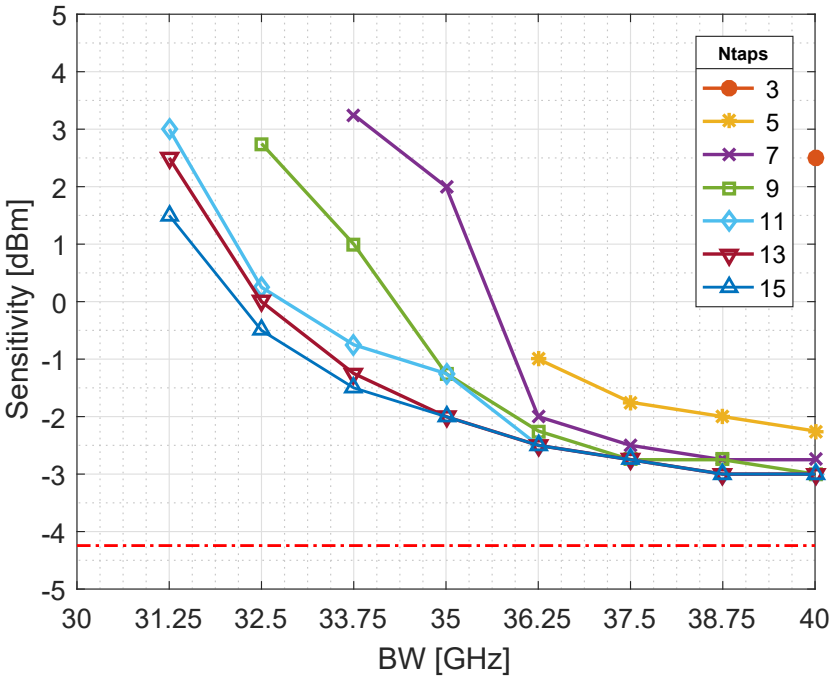

(a) Target BER 1e–2

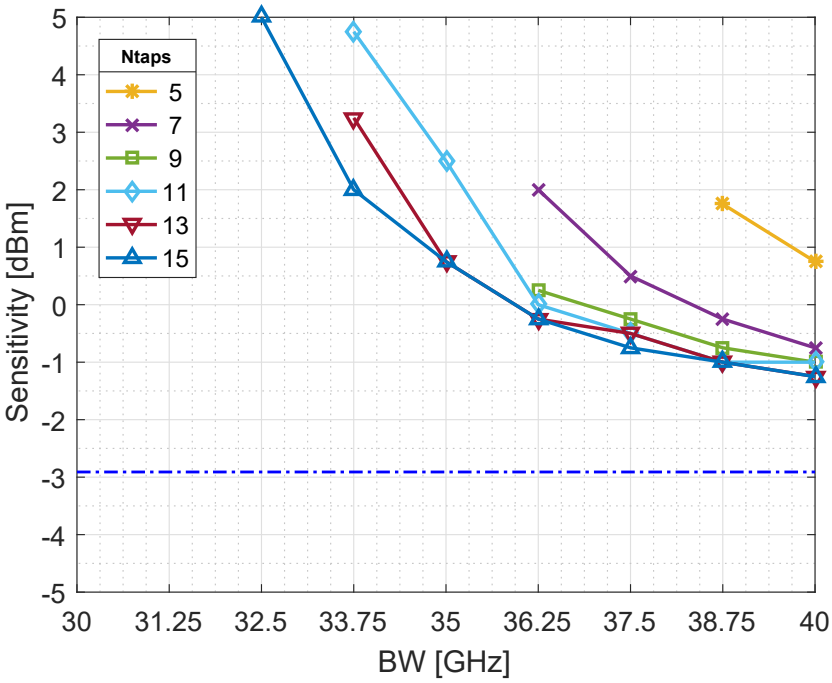

(b) Target BER 1e–3

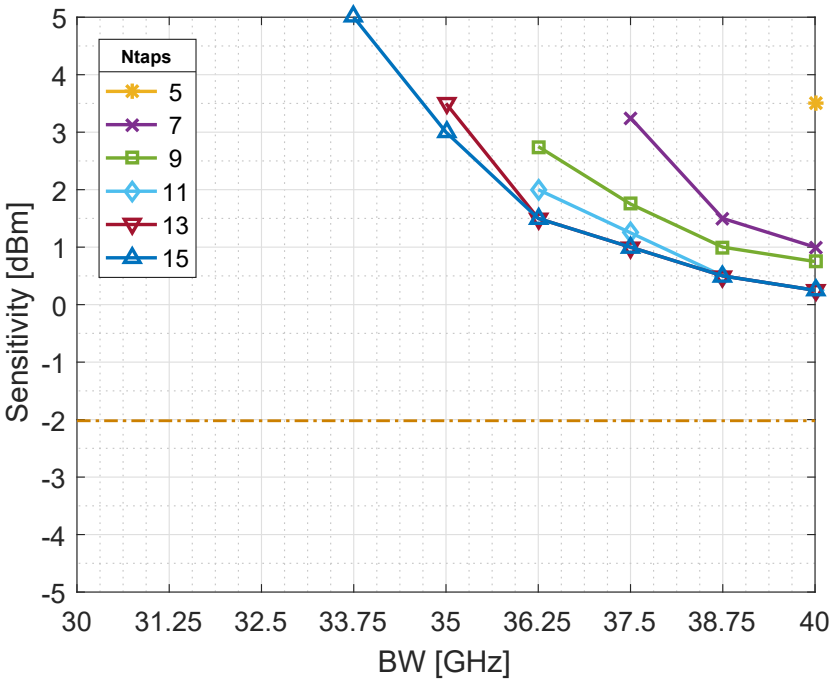

(c) Target BER 1e–4

Fig. 6.4 Sensitivity vs. the Tx/Rx electric bandwidth with 12% FEC OH

Similar analysis was done for the case of 12 % FEC OH because of the fact that increasing the OH by 9 % will provide a coding net coding gain of 7.49 dB [56]. The results are shown in Fig. 6.4. When compared with the 3 % OH case, 12 % OH case is showing an extra penalty of up to 0.75 dB this is due to the increase in the data rate because of the addition of extra bits. For the smallest usable BWs i.e. 31.25 GHz, 31.25 GHz and 32.25 GHz, the power penalties when compared with the reference case having BW=100 GHz and 39-taps are 5.75 dB, 7.9 dB and 7 dB respectively. Working at a larger Tx/Rx BW such 40 GHz (with 15 FFE taps) will decrease the penalties to 1.25 dB, 1.65 dB and 2.25 dB for target BERs of 10^{-2}, 10^{-3} and 10^{-4} respectively.

A trade off between sensitivity performance with FFE delays is also possible in this case. For target BER of 10^{-2} shown in Fig. 6.4a operating at a BW of 31.25 GHz, FFE taps can be reduced from 15 to 11 with a power variation of 1.5 dB. Lowering the BW limitation i.e. working at 36.25 GHz it is possible to use FFE taps down to 7 with a penalty of 0.5 dB as compared to the case for 15 taps while working at 40 GHz the variation is only 0.25 dB. The results for the target BER of 10^{-3} and

10^{-3} shown in Fig. 6.4b and Fig.6.4c respectively. The observation is analogous to the previous discussion. For a low pre-FEC BER target number of taps as low as 3 can be used while for the high demanding BER at least 5 FFE taps are required with a BW of 40 GHz. In general, low BER setups requires relatively large Tx/Rx BWs and FFE with a number of taps larger than 5. Decreasing the number of taps will also shrink the BWs range towards the higher values. However, for these solutions, the excess delay is still limited, therefore their implementation can be considered realistic.

6.5 Conclusions

In this work, we analyze PAM-4 modulation as transmission technique to enable 100G transmission in intra data-center scenarios and focus our investigation on the use of transceivers including some amount of DSP both at the transmitter (Tx) and receiver (Rx) site. We suppose that at the Rx feed-forward equalization equalizer is set using a training sequence through the least mean square algorithm. As previously commented, in the considered transmission scenario, the cost is a primary issue, so impairments due to low-cost components must be considered. Because of this regarding the external modulator we used a very-low extinction ratio Mach- Zehneder modulator, considering the value of ER = 6 dB that is typical for Silicon photonics components.

For Tx and Rx, in general, the main limitation of low-cost components and sub-systems is given by the bandwidth limitation. So, we analyze the effectiveness of the FFE to compensate for such a limitation. Moreover, we take into account power consumption that is another major issue for the considered scenario. To this regard, we focus on reducing the receiver power P_{sens} needed to keep the transmission *in service* the power level commonly defined *sensitivity* thanks to the use of FFE, and present trade-offs between N_{taps} of FFE and the Tx/Rx bandwidth limitation. We show that by using a very-limited number of FFE taps that are not introducing major complexity and giving negligible excess latency, we can save several dBs of sensitivity enabling operation below 35 GHz of electric bandwidth. Furthermore, considering the accepted use of FEC codes, we suppose target pre-FEC bit error rate at different levels, analyzing BER_{target} = 10^{-4}, 10^{-3} and 10^{-2}.

For all the considered scenarios, with the increase of the available electrical Tx/Rx bandwidth we observe the convergence of the sensitivity curves, decreasing the power penalty, so it can be implied that for smaller BW values it is advantageous to use a higher number of taps with relatively small additional latency to achieve the pre-FEC target BER with lower power penalty compared to smaller taps with higher power penalty.

Chapter 7

Master Slave Architecture

7.1 Introduction

Today small size and low power consuming devices are the essential requirements. Due to the same reason, optical interconnects have a great potential and are likely to be built using Photonics integrated circuits (*PIC*). The current status of silicon modulators [57, 58, 26] confirms the possibility to replace the currently deployed transceiver solutions.

In the optical interconnect scenario, lasers are the main source of power consumption. In order to reduce the power and cost effect due to the lasers either we can increase the overall channel capacity i.e. bit rate transmitted by laser or by sharing the laser between different links. To achieve this, multilevel modulation formats can be used to increase the bit rate per link while the laser can be shared as an external element in a top of the rack unit [59].

In current chapter, a novel idea is presented for the optical interconnect that can be efficiently integrated in Silicon Photonics (*SiP*). In contrary to the traditional peer to peer architecture a novel master slave configuration is presented to be used in the optical interconnects environment. The idea is based on wavelength reusability with a view to envision laser less node allowing the possibility to incorporate in silicon photonics. In this approach, the downstream wavelength is reused for the upstream transmission.

7.2 System Architecture

The proposed architecture is no more a traditional peer to peer configuration but is a master-slave architecture. Unlike the traditional architecture, the two nodes are no more symmetrical. The *master node* is characterized by having an optical source (directly or externally modulated) while the *slave node* receive the downstream signal transmitted by the master, it reuses this downstream wavelength by re-modulating it using an optical modulator without requiring an additional laser. Due to the absence of laser at the slave node and using silicon MZM, it is possible to implement the slave architecture completely using silicon photonics.

This master-slave architecture is shown in Fig. 7.1 and can be implemented by two alternative

- Reflective architecture
- Folded architecture

The reflective architecture is derived from the reflective pon architecture [60] and is using a single bidirectional fiber while folded needs two fibers one for the downstream transmission from the master to the slave and one for upstream from slave to the master. Nevertheless, before the production of a proper PIC, for the purpose of testing, verification and parameters definition, discrete components are used for the conducted experiments.

Reflective modulator

The optical field generated by the continuous wave light at the master node is transmitted through the Single Mode Fiber (*SMF*). At the slave node, the light enters the Reflective MZM shown in Fig. 7.2 with a random polarization, a Polarization Beam Splitter (*PBS*) splits the light into the two modes, propagating in clock wise and anti clock wise direction towards the MZM. When the two arms of MZM are perfectly balanced and the MZM work in traveling wave mode, the device implements a 90° polarization rotation in reflection independent of the received input polarization. The reflected light has a polarization orthogonal to the incoming light and this polarization is maintained till the reception at the master node allowing a coherent photodetection between the two polarization.

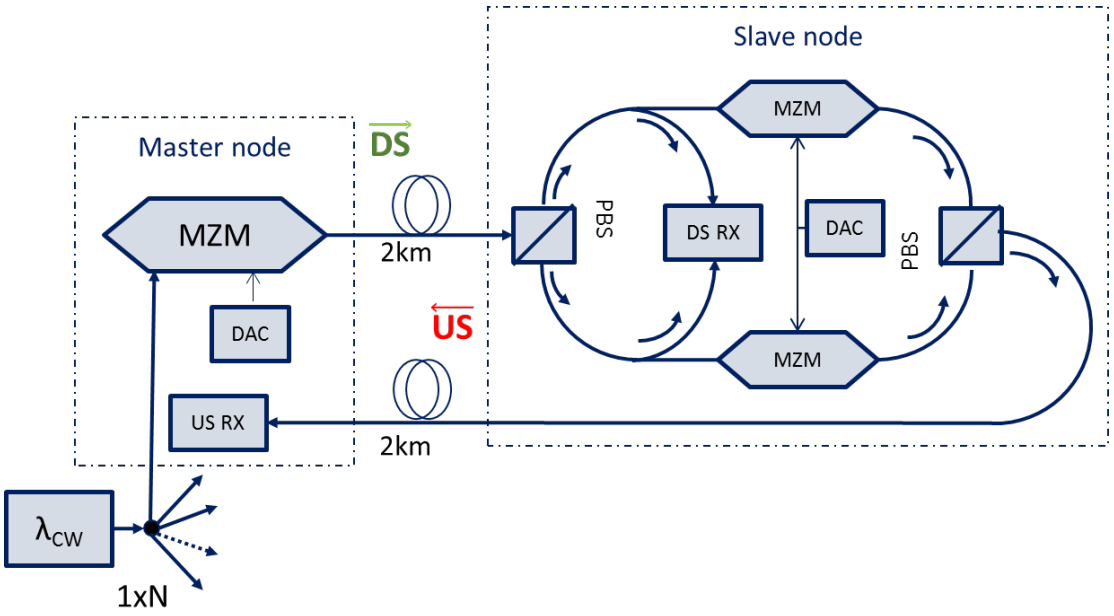

(a) Folded configuration

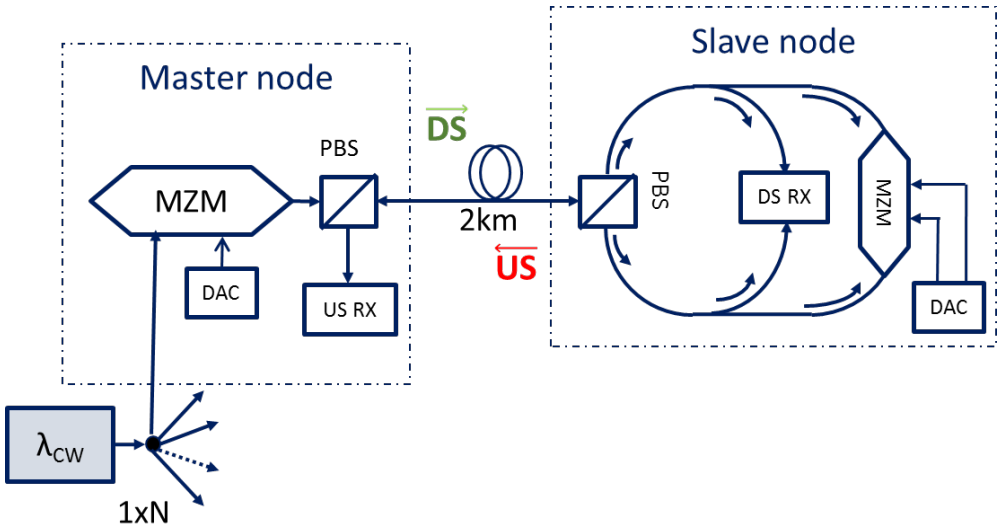

(b) Reflective configuration

Fig. 7.1 Master Slave configuration

7.3 Experimental Setup and Analysis

The purpose of the architecture presented targeted to explore the possibility of using a single laser source for a transmitter receiver pair. The transmission will no more be a peer-to-peer approach used in the optical interconnect.

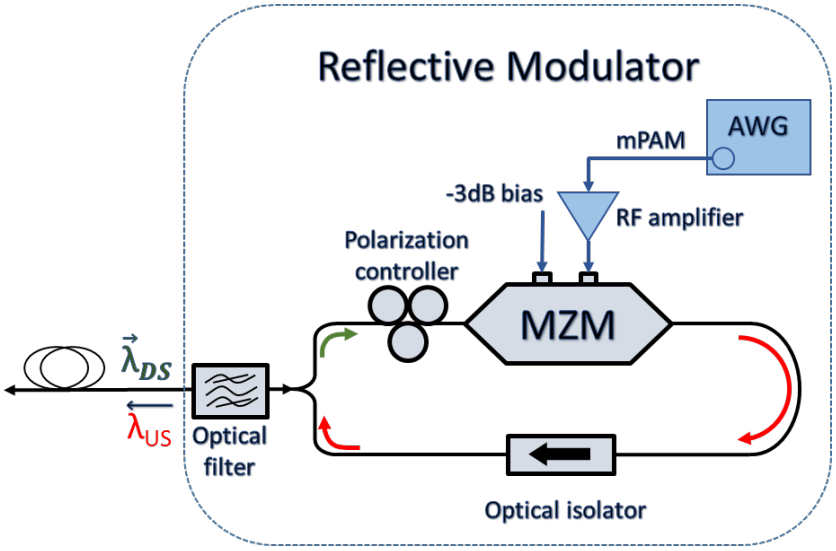

Fig. 7.2 Block Diagram of the Reflective Modulator

For the folded configuration shown in Fig. 7.1a, at the slave node a portion of the signal is received as the downstream signal while the rest is used for the upstream transmission. The incoming light is split to the two optical polarization component using the polarization beam splitter. The two optical polarization component and are modulated at the same time by the two 12 GHz Mach-Zehnder modulators.

Fig. 7.1b shows the Reflective configuration and is built on a 12 GHz Reflective-MZM structure explained in [57, 60]. For the same signal applied to the two arms of the reflective modulator an orthogonal signal is received after the reflection.

Both architecture have been implemented using discrete components. We started the investigation using PAM2 signal with a date rate of 12.5 Gbaud and a transmission distance of 2 Km between the master and the slave node. The transmission from master to the slave is known as the “downstream ” (*DS*) transmission while the transmission from the slave to the master is known as the “upstream” (*US*) transmission.

The investigation is carried out to find a good balance between the modulation amplitudes in both directions, since the modulation amplitude of the master node is affecting the transmission performance of the slave, i.e. the US transmission is effected by the DS modulation amplitude. The effect is shown in Fig.7.3 and Fig.7.4. It is observed that the increasing the modulation depth/amplitude of the DS will improve the DS transmission and is seen by the clear eye opening in Fig.7.3b with

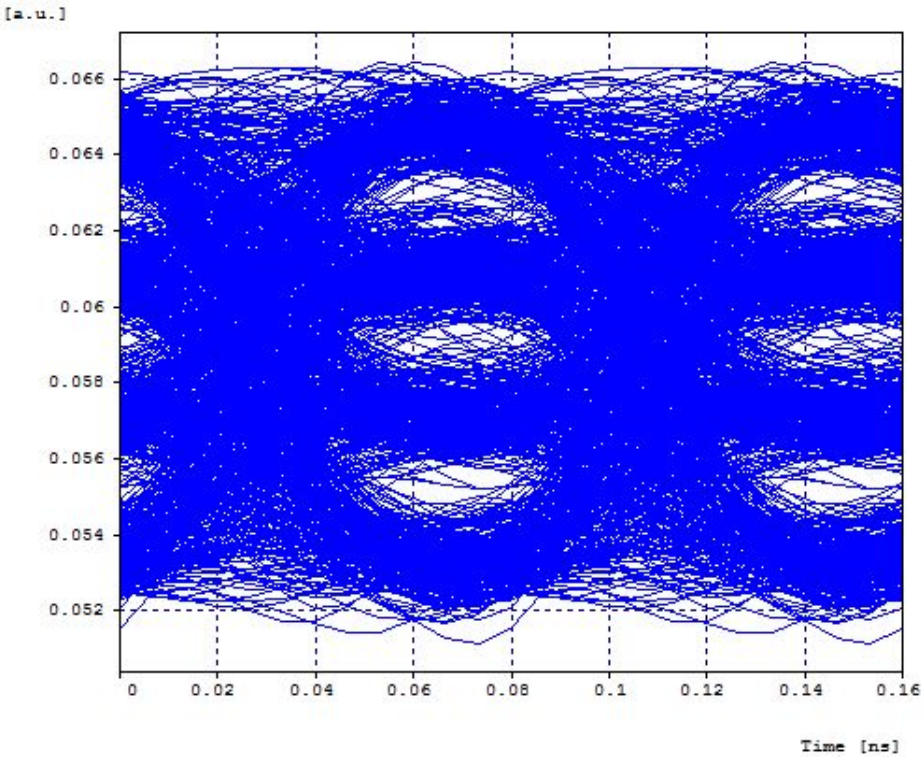

(a) Down Stream MD=10 %

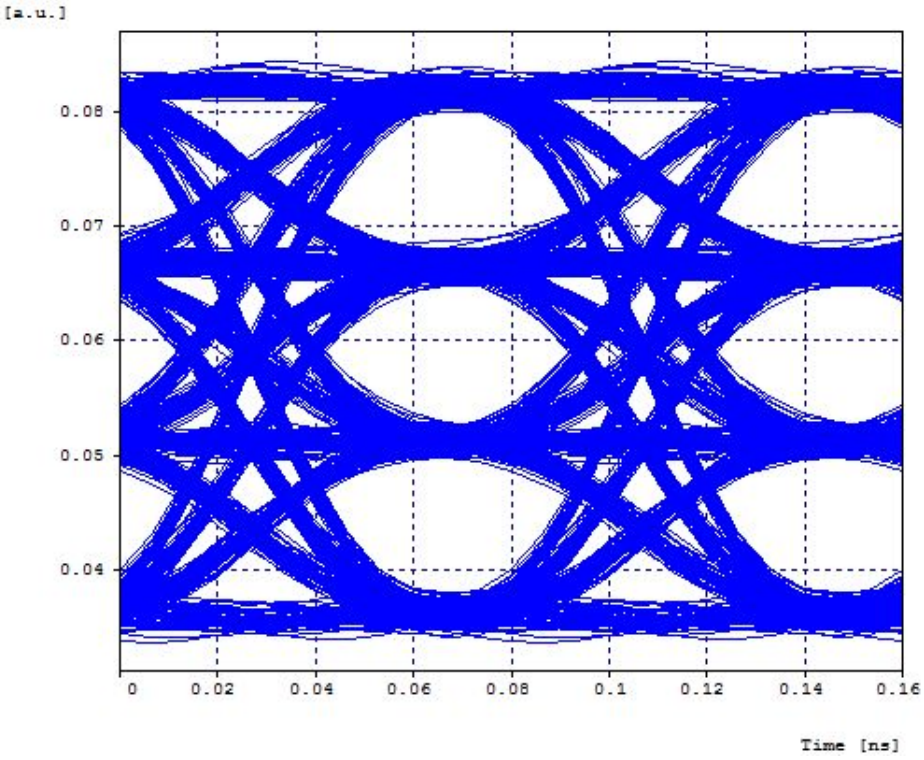

(b) Down Stream MD=40 %

Fig. 7.3 Effect Of Down Stream modulation depth on the received DS signal

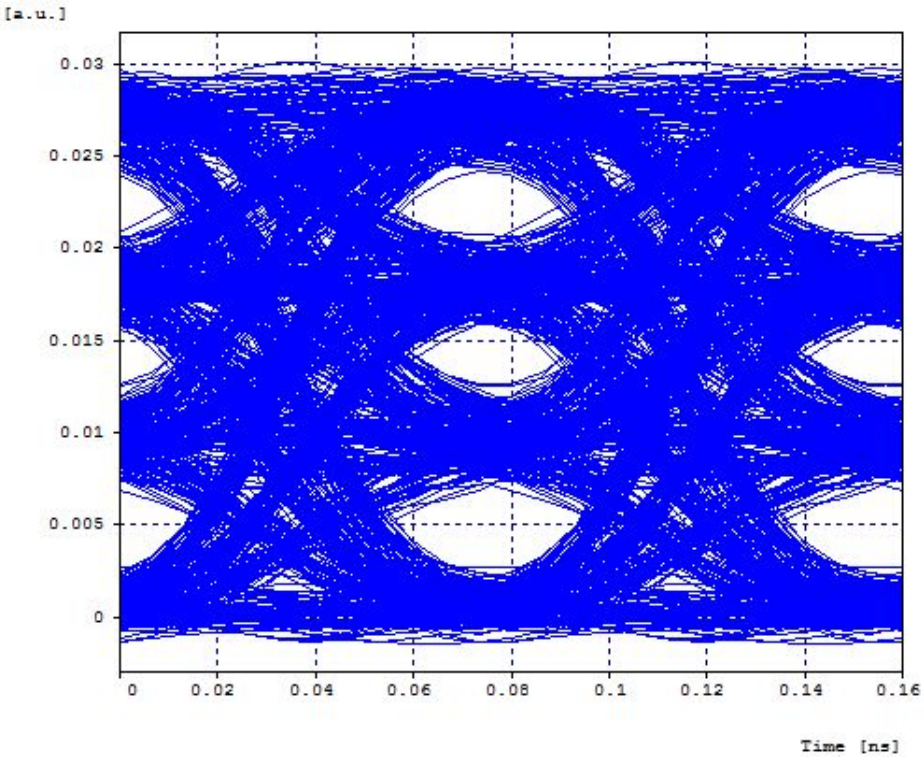

(a) Down Stream MD=10 %

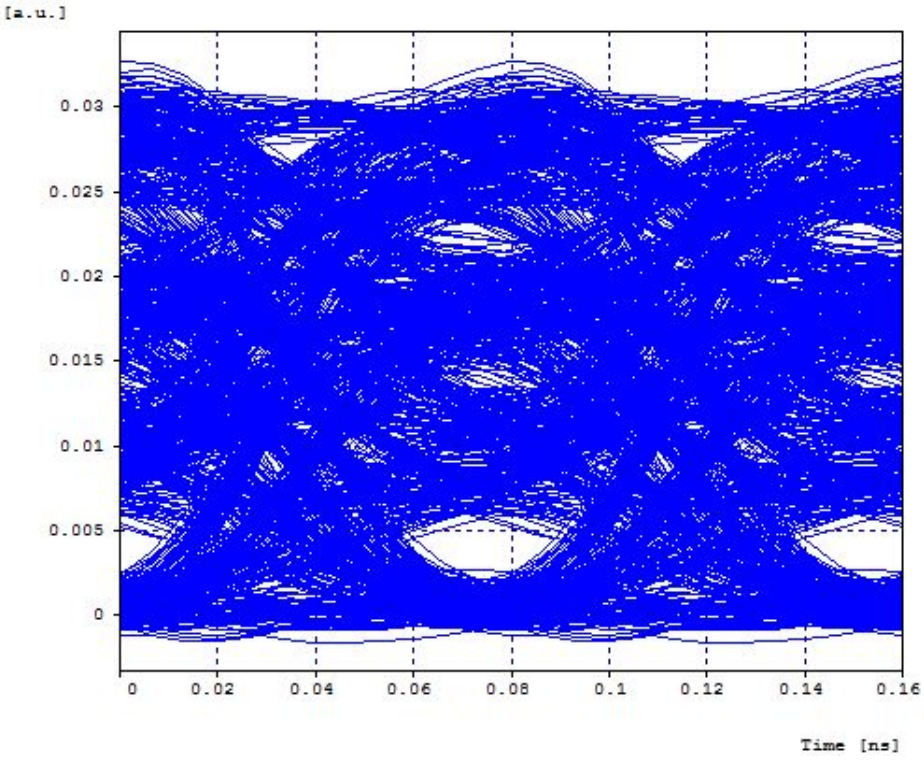

(b) Down Stream MD=25 %

Fig. 7.4 Effect Of Down Stream modulation depth on the received US signal

MD = 40% as compare to the case with MD = 10% shown in Fig.7.3a. While for the US case increasing the DS modulation depth from 10% to MD = 25 % has worsen the performance and the eye is almost closed as shown in Fig. 7.4a and Fig.7.4b respectively. So a working range needs to be defined for a proper transmission in both directions.

A distributed feedback laser is used for the modulation of the downstream PAM2 signal in both configurations. The experiment is carried out at 12.5 Gbaud with the external MZM biased at the quadrature point. The launch power in the fiber was set to 6 dBm. A simple direct detection with 11 GHz bandwidth receiver is used for both the DS and US receiver. Offline processing was done on the received data. In order to improve the sensitivity, some filtering and a decision threshold is applied to enable us to work with low extension ratio. Since both US and DS are working at the same data rate, the received DS signal is remodulated with a 12.5 Gbps NRZ signal using the folded or the reflective MZM to generate the US signal. We assumed to use a hard FEC code RS (1023,1007) BCH(2047,1952) as in G.795.1-I.4, to correct a BER=$2.17 \cdot 10^{-3}$ in both DS and US.

7.3.1 Results for PAM2

The results for the stated experiments at 12.5 Gbaud are shown in Fig. 7.5. We have plotted the BER levels for the DS and US transmission as a function of DS and US modulation amplitude. The wide working range shown by the white area guarantees error free transmission in both directions since the BER level is below the FEC threshold for both DS and US. For the folded case for the error free transmission using FEC threshold a minimum of 0.25 Vpp for DS and 2.0 Vpp for US signal is required (refer to Fig.7.5a) and 0.5 Vpp and 2.0 Vpp of DS and US signal is required for the reflective case shown in Fig. 7.5b. On the other hand, BER=10^{-9} is achievable with using modulation amplitude of 0.75 Vpp and 5 Vpp for DS and US respectively.

We also verified the performance of both configurations using a lower launch power in the fiber i.e. at 0 dBm. It is observed that we can still achieve the error free transmission in both direction and the results are shown in Fig. 7.6. For the folded configuration at least 0.6 Vpp for DS and 2.0 Vpp for US signal is required (Fig. 7.6a) and 0.6 Vpp and 3.0 Vpp of DS and US signal is required for the reflective

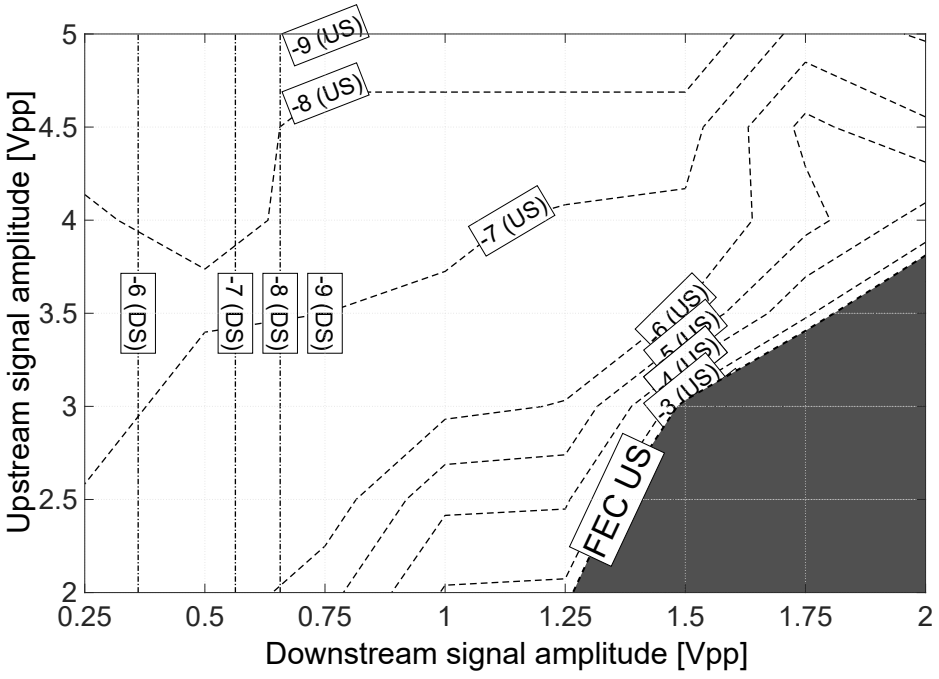

(a) Folded Configuration

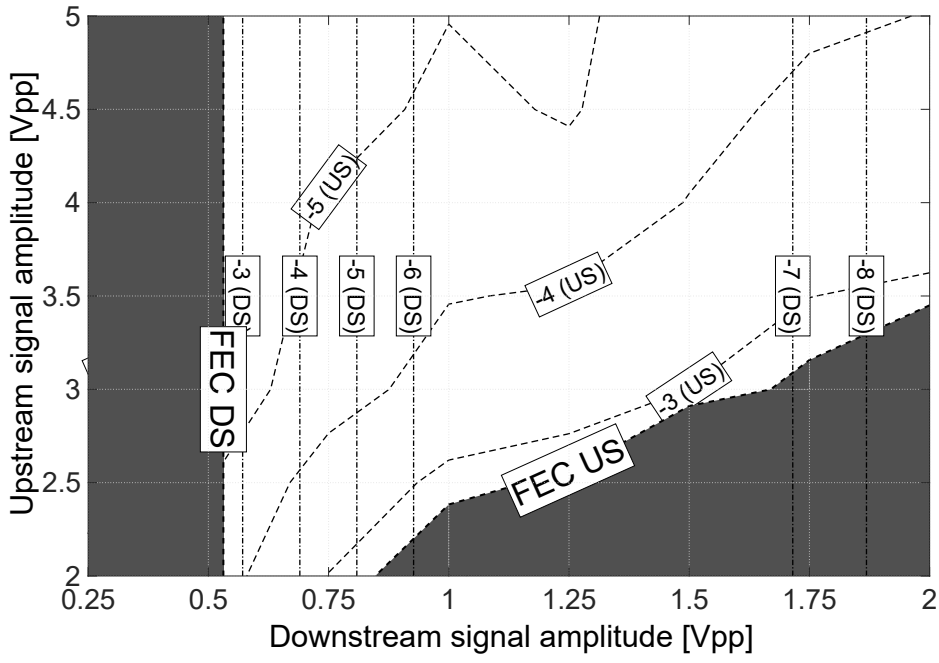

(b) Reflective Configuration

Fig. 7.5 BER vs US and DS signal amplitude for PAM 2 with pf=6 dBm

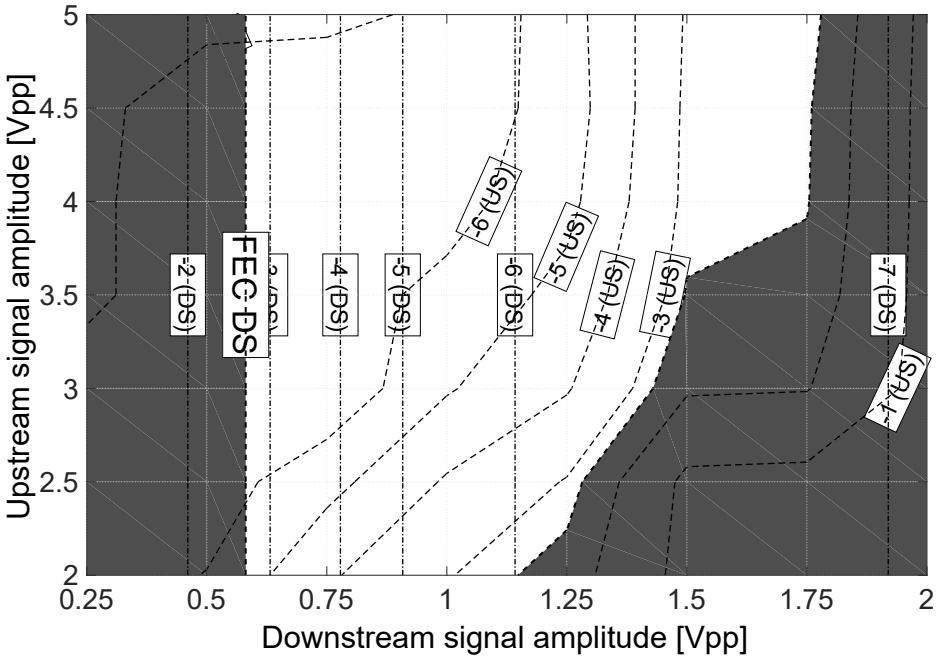

(a) Folded Configuration

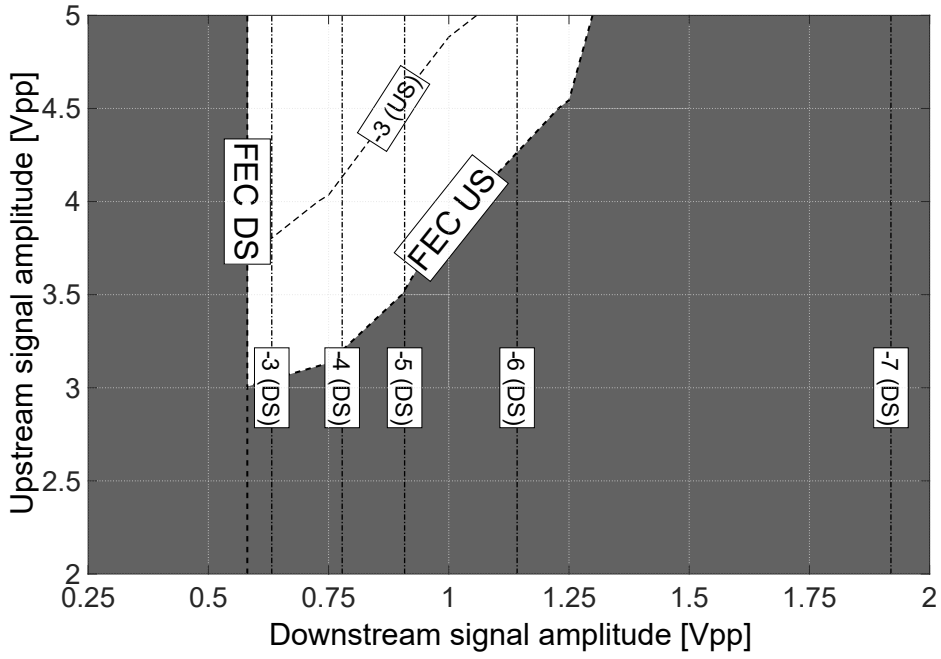

(b) Refective Configuration

Fig. 7.6 BER vs US and DS signal amplitude for PAM 2 with pf=0 dBm

case shown in Fig. 7.6b. Therefore indicating additional 6 dB of system margin that can be used to reduce the laser output power or share among other users.

From Fig.7.6 and Fig.7.5, it is witnessed that the folded configuration is performing better than the reflective configuration so for the rest of the scenarios we focus on folded configuration only.

Once a reference has been set and verified experimentally, we simulated the proposed configurations using Optsim™ + Matlab™ . Since when focusing on higher modulation level and higher data rate the simulation provides many degrees of freedom. The simulation parameters were set in accordance with the experimental values and verified the simulative result with the experimental results. Table 7.1 shows the values used for simulation to match the experimental setup.

Table 7.1 Simulations parameters used to match the experimental setup

Parameter	Value
MZM $V\pi$	5 V
MZM Extinction Ratio	20 dB
MZM Bandwidth	12 GHz
Rx Bandwidth	11 GHz
Rx noise equivalent power	30 $pW/\sqrt{Hz}$
Rx conversion gain	200 V/W

7.3.2 Results for PAM4

After matching the experimental and simulative setup, for the next analysis, we used the folded configuration for PAM4 transmission operating at the same baud rate of 12.5 Gbaud. Fig. 7.7 present the simulations results with and without LMS equalization. It is obvious that for PAM4 transmission FEC is required but LMS is optional for the parameters used for this simulation. Using the LMS equalizer not only the effective operating range has increased but the required operating voltage has also lowered e.g. to meet the minimum FEC threshold value the required modulation amplitude without the LMS equalizer is 0.5 Vpp and 2.7 Vpp for DS and US respectively as shown in Fig.7.7a but using the LMS equalizer the requirement has droped to 0.35 Vpp and 2.25 Vpp for DS and US respectively as displayed in Fig.7.7b.

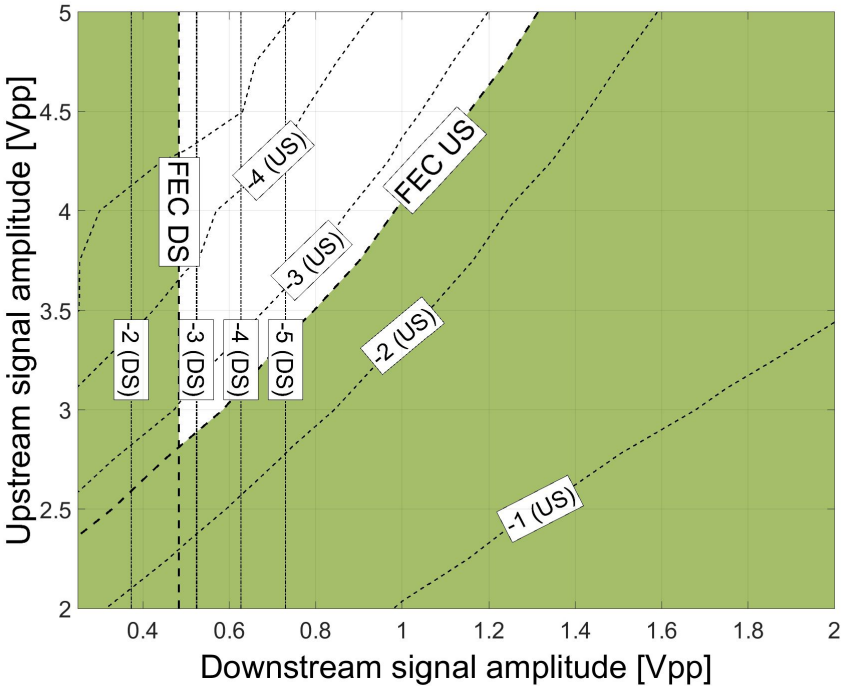

(a) Results without LMS equalization

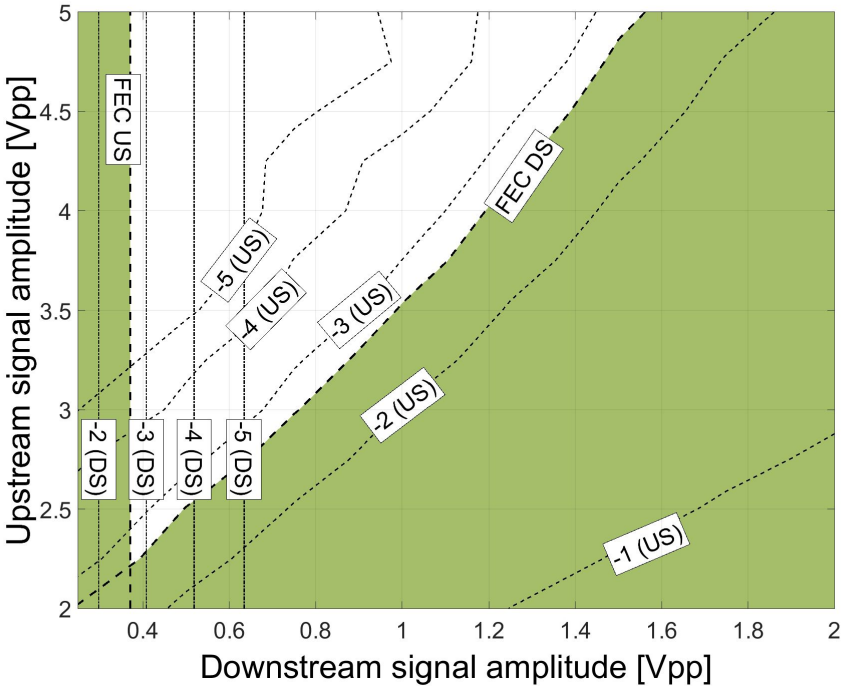

(b) Results using LMS equalization

Fig. 7.7 BER vs US and DS signal amplitude for PAM 4 with and without LMS equalization

7.3.3 Latency due to LMS equalizer

Since both FEC and LMS equalizer leads to additional latency, it is significant to make proper choices to reduce the FEC overhead and to latency due to the equalizer taps. We did an analysis with by signal amplitude of 1 Vpp and 4 Vpp for DS and US respectively to find the number of filter taps required to achieve the pre-FEC BER. The result is shown in Fig. 7.8. It is seen that 13 taps corresponding to 12 bit of DSP latency (using equation 4.15) are sufficient to achieve the best performance for the upstream case.

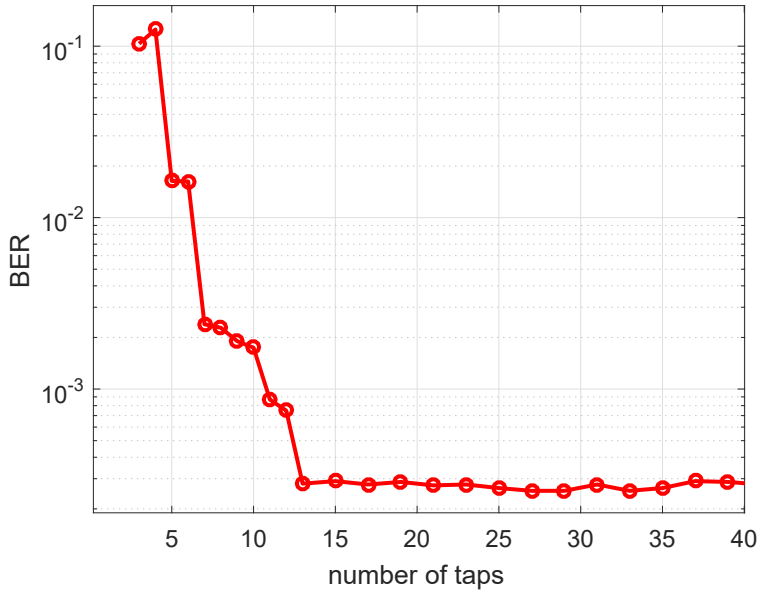

Fig. 7.8 Number of LMS taps vs. pre-FEC BER for US transmission

7.4 Conclusions

We demonstrated in this work a novel idea of using the master-slave architecture for the optical interconnects with the aim to exploit and integrate the silicon modulators. It relies on one laser for a transmitter receiver pair remodulating an already modulated wavelength to obtain a laser less node at one end. The feasibility of the proposed architecture is verified for the PAM2 and PAM4 modulation using FEC and LMS. Adopting this technique will not only reduce the footprint but also the cost and the power consumption is reduced.

Chapter 8

Conclusions

8.1 Conclusions and Future Work

Fiber optic communication is the basis of the modern network. The ability to provide high data rate at a low cost and low loss make it the preferred choice to be used for the telecommunication networks. In this thesis, we study high capacity and short-reach optical communication links. Unlike the long haul links that are mostly using the complex coherent detection with advanced modulation formats, short reach links for the time being depends on the direct detection only with an advantage of a simple implementation.

In this work, we have designed a complete optical communication system with a target to achieve 100G communication over a distance of 2 Km. We analyzed and designed both transmitter and receiver in Matlab, at the receiver we implemented the direct detection using a single photodetector. As a modulation format, we used a simple multilevel modulation format such as Pulse amplitude modulation. We used the single polarity PAM signal i.e. positive pulses only so that it can be detected by the photodetector.

Starting from the back to back system we implemented the system for a distance of up to 2 Km, we analyzed the sensitivity benefits achieved by using the LMS equalizer, the electrical bandwidth limitations due to devices, effect of multipath interference, the effect of FEC code and the corresponding latency is studied. In all the cases the BER is below the hard FEC threshold making PAM as a strong candidate for the short reach and data center application.

Last but not the least a novel idea using reflective MZM is introduced that remodulating an already modulated wavelength to obtain a laser less node at one end of the transmission pair reducing the footprint, cost and the power consumption.

8.1.1 Future work

For short reach optical communication cost and power efficiency are the main requirements. Some of the problems observed during the investigation that needs to be solved in future and some other ideas that need to be investigated in order for a commercial implementation are

- We used an equal spacing PAM signal, most errors are observed in the upper levels, an unequal space PAM signal needs to be investigated to improve the performance.
- The work carried out used a CW laser and a Mach-Zehnder modulator, studies using directly modulated laser (DML) technologies needs to be performed to achieve low power and low cost solution.
- We used an ideal DAC and ADC which cannot be used in the real low cost implementation.
- Further study related to equalizer and FEC codes is required to increase the sensitivity and reach without increasing the latency.
- Modulation formats other than PAM needs to investigated to meet low cost and power requirement of short reach links.
- What will the advantages of using other pulse shaping? especially using Nyquist shaped pulse. Since Nyquist signaling requires half of the bandwidth effectively doubling the efficiency.
- For data center power consumption is the main challenge, a trade off between the performance and the power utilized is necessary.
- The study was focused targeting the data centers but these short reach optical links can be used for multimedia distribution in an automobile, communication in avionics etc.

References

[1] I Cisco. Cisco global cloud index: Forecast and methodology, 2015 –2020. *CISCO White paper*, 2016.

[2] A. Benner. Optical interconnect opportunities in supercomputers and high end computing. In *OFC/NFOEC*, pages 1–60, March 2012.

[3] P Delforge. America's data centers are wasting huge amounts of energy. *National Resources Defense Council, vol. Issue Brief*, pages 14–08, 2014.

[4] J D'Ambrosia. IEEE p802.3bs 400gbe baseline summary, 2015.

[5] Jiangwei Man, Wei Chen, Xiaolu Song, and Li Zeng. A low-cost 4× 25gbps pam4 module for short-reach optical interconnection. In *Optical Interconnects Conference, 2014 IEEE*, pages 127–128. IEEE, 2014.

[6] Evgeny Vanin. Performance evaluation of intensity modulated optical ofdm system with digital baseband distortion. *Opt. Express*, 19(5):4280–4293, Feb 2011.

[7] Gi-Hong Im, Dale D. Harman, Gang Huang, A. V. Mandzik, Mai-Huong Nguyen, and Jean-Jacques Werner. 51.84 mb/s 16 cap atm lan standard. *IEEE Journal on Selected Areas in Communications*, 13(4):620–632, 1995.

[8] Xiaogeng Xu, Enbo Zhou, Gordon Ning Liu, Tianjian Zuo, Qiwen Zhong, Liang Zhang, Yuan Bao, Xuebing Zhang, Jianping Li, and Zhaohui Li. Advanced modulation formats for 400-gbps short-reach optical inter-connection. *Opt. Express*, 23:492–500, Jan 2015.

[9] L. Tao, Y. Ji, J. Liu, A. P. Tao Lau, N. Chi, and C. Lu. Advanced modulation formats for short reach optical communication systems. *IEEE Network*, 27(6):6–13, November 2013.

[10] J. L. Wei, J. D. Ingham, D. G. Cunningham, R. V. Penty, and I. H. White. Performance and power dissipation comparisons between 28 gb/s nrz, pam, cap and optical ofdm systems for data communication applications. *Journal of Lightwave Technology*, 30(20):3273–3280, Oct 2012.

[11] T. Yamamoto. High-speed directly modulated lasers. In *OFC/NFOEC*, pages 1–39, March 2012.

[12] C. Peucheret. Direct and External Modulation of Light. Lecture Notes, Technical University of Denmark,Department of Photonics Engineering, 2009.

[13] Sckinger Eduard. *Broadband Circuits for Optical Fiber Communication*. Wiley, 2005.

[14] M. Cignoli, G. Minoia, M. Repossi, D. Baldi, A. Ghilioni, E. Temporiti, and F. Svelto. 22.9 a 1310nm 3d-integrated silicon photonics mach-zehnder-based transmitter with 275mw multistage cmos driver achieving 6db extinction ratio at 25gb/s. In *2015 IEEE International Solid-State Circuits Conference - (ISSCC) Digest of Technical Papers*, pages 1–3, Feb 2015.

[15] Matthias Seimetz. *High-Order Modulation for Optical Fiber Transmission*. Springer, 2009.

[16] Govind Agrawal. *Fiber-optic communication systems*. Wiley, 2002.

[17] Y. Akage, K. Kawano, S. Oku, R. Iga, H. Okamoto, Y. Miyamoto, and H. Takeuchi. Wide bandwidth of over 50 ghz travelling-wave electrode electroabsorption modulator integrated dfb lasers. *Electronics Letters*, 37(5):299–300, Mar 2001.

[18] Dario Pilori. Discrete-multitone mo dulation for short distance 100 gps optical links. Master's thesis, Politecnico Di Milano, 2015.

[19] Joseph Kahn. Modulation and detection techniques for optical communication systems. In *Optical Society of America*, page CThC1, 2006.

[20] J. M. Kahn and Keang-Po Ho. Spectral efficiency limits and modulation/detection techniques for dwdm systems. *IEEE Journal of Selected Topics in Quantum Electronics*, 10(2):259–272, March 2004.

[21] Kazuro Kikuchi. *Coherent Optical Communications: Historical Perspectives and Future Directions*, pages 11–49. Springer Berlin Heidelberg, Berlin, Heidelberg, 2010.

[22] BELL Labs. Metro network traffic growth: An architecture impact study. *White paper*, 2013.

[23] Wei-Ren Peng, Xiaoxia Wu, Kai-Ming Feng, Vahid R. Arbab, Bishara Shamee, Jeng-Yuan Yang, Louis C. Christen, Alan E. Willner, and Sien Chi. Spectrally efficient direct-detected ofdm transmission employing an iterative estimation and cancellation technique. *Opt. Express*, 17:9099–9111, May 2009.

[24] Scott Feller. New technologies shaping the future of 100G data center interconnects. In *Ethernet Technology Summit*, April 2015.

[25] Gary Nicholl and Chris Fludger. Update on technical feasibility for PAM modulation. *IEEE 802.3 NG100GE PMD study Group*, March 2012.

[26] Mathieu Chagnon, Mohamed Osman, Michel Poulin, Christine Latrasse, Jean-Frédéric Gagné, Yves Painchaud, Carl Paquet, Stéphane Lessard, and David Plant. Experimental study of 112 gb/s short reach transmission employing pam formats and sip intensity modulator at 1.3 μm. *Opt. Express*, 22(17):21018–21036, Aug 2014.

[27] Kangping Zhong, Xian Zhou, Yuliang Gao, Wei Chen, Jiangwei Man, Li Zeng, Alan Pak Tao Lau, and Chao Lu. 140 gbit/s 20km transmission of pam-4 signal at 1.3 μm for short reach communications. *IEEE Photon. Technol. Lett.*, 27(16):1757–1760, 2015.

[28] X. Song and D. Dove. Opportunities for PAM4 modulation. *IEEE 802.3 400 GbE study Group*, January 2014.

[29] Krzysztof Szczerba, Magnus Karlsson, Peter A Andrekson, and Anders Larsson. Intersymbol interference penalties for ook and 4-pam in short-range optical communications. In *Optical Fiber Communication Conference*, pages OW4A–3. Optical Society of America, 2013.

[30] Z. Li, X. Xiao, T. Gui, Q. Yang, R. Hu, Z. He, M. Luo, C. Li, X. Zhang, D. Xue, S. You, and S. Yu. 432-gb/s direct-detection optical ofdm superchannel transmission over 3040-km ssmf. *IEEE Photonics Technology Letters*, 25(15):1524–1526, Aug 2013.

[31] P. S. Chow, J. M. Cioffi, and J. A. C. Bingham. A practical discrete multitone transceiver loading algorithm for data transmission over spectrally shaped channels. *Communications, IEEE Transactions on*, 43(234):773–775, February 1995.

[32] Yutaka Kai, Masato Nishihara, Toshiki Tanaka, Tomoo Takahara, Lei Li, Zhenning Tao, Bo Liu, Jens C Rasmussen, and Tomislav Drenski. Experimental comparison of pulse amplitude modulation (pam) and discrete multi-tone (dmt) for short-reach 400-gbps data communication. In *Optical Communication (ECOC 2013), 39th European Conference and Exhibition on*, pages 1–3. IET, 2013.

[33] Toshiki Tanaka, Masato Nishihara, Tomoo Takahara, Weizhen Yan, Lei Li, Zhenning Tao, Manabu Matsuda, Kazumasa Takabayashi, and Jens Rasmussen. Experimental demonstration of 448-gbps+ dmt transmission over 30-km smf. In *Optical Fiber Communication Conference*, pages M2I–5. Optical Society of America, 2014.

[34] A. Peled and A. Ruiz. Frequency domain data transmission using reduced computational complexity algorithms. In *Acoustics, Speech, and Signal Processing, IEEE International Conference on ICASSP '80.*, volume 5, pages 964–967, Apr 1980.

[35] Seung Hee Han and Jae Hong Lee. An overview of peak-to-average power ratio reduction techniques for multicarrier transmission. *IEEE Wireless Communications*, 12(2):56–65, April 2005.

[36] M. I. Olmedo, T. Zuo, J. B. Jensen, Q. Zhong, X. Xu, S. Popov, and I. T. Monroy. Multiband carrierless amplitude phase modulation for high capacity optical data links. *Journal of Lightwave Technology*, 32(4):798–804, Feb 2014.

[37] J. C. Rasmussen, T. Takahara, T. Tanaka, Y. Kai, M. Nishihara, T. Drenski, L. Li, W. Yan, and Z. Tao. Digital signal processing for short reach optical links. In *2014 The European Conference on Optical Communication (ECOC)*, pages 1–3, Sept 2014.

[38] J. Wei, Q. Cheng, R. V. Penty, I. H. White, and D. G. Cunningham. 400 gigabit ethernet using advanced modulation formats: Performance, complexity, and power dissipation. *IEEE Communications Magazine*, 53(2):182–189, Feb 2015.

[39] Kangping Zhong, Xian Zhou, Tao Gui, Li Tao, Yuliang Gao, Wei Chen, Jiangwei Man, Li Zeng, Alan Pak Tao Lau, and Chao Lu. Experimental study of pam-4, cap-16, and dmt for 100 gb/s short reach optical transmission systems. *Opt. Express*, 23(2):1176–1189, Jan 2015.

[40] C. Cole, I. Lyubomirsky, A. Ghiasi, and V. Telang. Higher-order modulation for client optics. *IEEE Communications Magazine*, 51(3):50–57, March 2013.

[41] Ieee standard for ethernet amendment 2: Physical layer specifications and management parameters for 100 gb/s operation over backplanes and copper cables, Sept 2014.

[42] Stephen M Rumble, Diego Ongaro, Ryan Stutsman, Mendel Rosenblum, and John K Ousterhout. It's time for low latency. In *HotOS*, volume 13, 2011.

[43] S. U. H. Qureshi. Adaptive equalization. *Proceedings of the IEEE*, 73(9):1349–1387, 1985.

[44] David Smalley. Equalization concepts: a tutorial. *Atlanta Regional Technology Center, Texas Instruments*, pages 1–29, 1994.

[45] Zhensheng Jia, Hung-Chang Chien, Junwen Zhang, Ze Dong, and Yi Cai. Performance analysis of pre-and post-compensation for bandwidth-constrained signal in high-spectral-efficiency optical coherent systems. In *Optical Fiber Communications Conference and Exhibition (OFC), 2014*, pages 1–3. IEEE, 2014.

[46] Danish Rafique, Antonio Napoli, Stefano Calabro, and Bernhard Spinnler. Digital preemphasis in optical communication systems: On the dac requirements for terabit transmission applications. *Journal of Lightwave Technology*, 32(19):3247–3256, 2014.

[47] Pablo V Mena, Enrico Ghillino, Ali Ghiasi, Brian Welch, Muhammad Shoaib Khaliq, and Dwight Richards. 100-gb/s pam4 link modeling incorporating mpi. In *Optical Interconnects Conference (OI), 2015 IEEE*, pages 14–15. IEEE, 2015.

[48] A Ghiasi and B Welch. Investigation of 100gbe based on pam-4 and pam-8. *IEEE 802.3 bm Task Force*, 2012.

[49] M Gustlin, M Langhammer, D Ofelt, and ZF Wang. Investigation on technical feasibility of stronger rs fec for 400gbe. In *IEEE P802. 3bs 400GbE Task Force, Interim Meeting*, 2015.

[50] IEEE P802.3ae 10Gb/s Ethernet Task Force. 10 gb/s link budget spreadsheet (version 3.1.16a). In *IEEE P802.3ae 10Gb/s Ethernet Task Force*, 2001.

[51] James L Gimlett and Nim K Cheung. Effects of phase-to-intensity noise conversion by multiple reflections on gigabit-per-second dfb laser transmission systems. *Journal of Lightwave Technology*, 7(6):888–895, 1989.

[52] Daniel A Fishman, Donald G Duff, and Jonathan A Nagel. Measurements and simulation of multipath interference for 1.7-gb/s lightwave transmission systems using single-and multifrequency lasers. *Journal of Lightwave Technology*, 8(6):894–905, 1990.

[53] Chris R Fludger, Marco Mazzini, Theo Kupfer, and Matt Traverso. Experimental measurements of the impact of multi-path interference on pam signals. In *Optical Fiber Communication Conference*, pages W1F–6. Optical Society of America, 2014.

[54] Paul Kolesar. Loss budgeting for 400ge channels. In *IEEE P802. 3bs 400GbE Task Force, Interim Meeting*, 2014.

[55] Gabriella Bosco, Vittorio Curri, Andrea Carena, Pierluigi Poggiolini, and Fabrizio Forghieri. On the performance of nyquist-wdm terabit superchannels based on pm-bpsk, pm-qpsk, pm-8qam or pm-16qam subcarriers. *Journal of Lightwave Technology*, 29(1):53–61, 2011.

[56] Wenbin Yang Xinyuan Wang, Yu Xu. Some consideration of stronger fec in 400gbe. In *IEEE P802. 3bs 400GbE Task Force, Interim Meeting*, 2015.

[57] Sylvie Menezo, Benoit Charbonnier, G Beninca De Farias, David Thomson, Philippe Grosse, André Myko, Jean-Marc Fedeli, B Ben Bakir, GT Reed, and Aurélien Lebreton. Reflective silicon mach zehnder modulator with faraday rotator mirror effect for self-coherent transmission. In *Optical Fiber Communication Conference and Exposition and the National Fiber Optic Engineers Conference (OFC/NFOEC), 2013*, pages 1–3. IEEE, 2013.

[58] David Patel, Samir Ghosh, Mathieu Chagnon, Alireza Samani, Venkat Veerasubramanian, Mohamed Osman, and David V Plant. Design, analysis, and transmission system performance of a 41 ghz silicon photonic modulator. *Optics express*, 23(11):14263–14287, 2015.

[59] S Straullu, S Abrate, V Ferrero, and R Gaudino. Laser-sharing in pon. In *Photonics Conference (IPC), 2016 IEEE*, pages 295–296. IEEE, 2016.

[60] Stefano Straullu, Paolo Savio, Joana Chang, Valter Ferrero, Antonino Nespola, Roberto Gaudino, and Silivo Abrate. Optimization of reflective fdma-pon architecture to achieve 32 gb/s per upstream wavelength over 31 db odn loss. *Journal of Lightwave Technology*, 33(2):474–480, 2015.